

ISSN 1881-7815    Online ISSN 1881-7823

# **BST**

## **BioScience Trends**

Volume 7, Number 5  
October, 2013



[www.biosciencetrends.com](http://www.biosciencetrends.com)



# BST

## BioScience Trends



ISSN: 1881-7815  
Online ISSN: 1881-7823  
CODEN: BTIRCZ  
Issues/Year: 6  
Language: English  
Publisher: IACMHR Co., Ltd.

**BioScience Trends** is one of a series of peer-reviewed journals of the International Research and Cooperation Association for Bio & Socio-Sciences Advancement (IRCA-BSSA) Group and is published bimonthly by the International Advancement Center for Medicine & Health Research Co., Ltd. (IACMHR Co., Ltd.) and supported by the IRCA-BSSA and Shandong University China-Japan Cooperation Center for Drug Discovery & Screening (SDU-DDSC).

**BioScience Trends** devotes to publishing the latest and most exciting advances in scientific research. Articles cover fields of life science such as biochemistry, molecular biology, clinical research, public health, medical care system, and social science in order to encourage cooperation and exchange among scientists and clinical researchers.

**BioScience Trends** publishes Original Articles, Brief Reports, Reviews, Policy Forum articles, Case Reports, News, and Letters on all aspects of the field of life science. All contributions should seek to promote international collaboration.

## Editorial Board

### Editor-in-Chief:

Masatoshi MAKUUCHI  
*Japanese Red Cross Medical Center, Tokyo, Japan*

### Co-Editors-in-Chief:

Xue-Tao CAO  
*Chinese Academy of Medical Sciences, Beijing, China*  
Rajendra PRASAD  
*UP Rural Institute of Medical Sciences & Research, Uttar Pradesh, India*  
Arthur D. RIGGS  
*Beckman Research Institute of the City of Hope, Duarte, CA, USA*

### Chief Director & Executive Editor:

Wei TANG  
*The University of Tokyo, Tokyo, Japan*

### Managing Editor:

Munehiro NAKATA  
*Tokai University, Hiratsuka, Japan*

### Senior Editors:

Xunjia CHENG  
*Fudan University, Shanghai, China*  
Yoko FUJITA-YAMAGUCHI  
*Tokai University, Hiratsuka, Japan*  
Na HE  
*Fudan University, Shanghai, China*  
Kiyoshi KITAMURA  
*The University of Tokyo, Tokyo, Japan*

Misao MATSUSHITA  
*Tokai University, Hiratsuka, Japan*  
Takashi SEKINE  
*The University of Tokyo, Tokyo, Japan*  
Yasuhiko SUGAWARA  
*The University of Tokyo, Tokyo, Japan*

### Web Editor:

Yu CHEN  
*The University of Tokyo, Tokyo, Japan*

### Proofreaders:

Curtis BENTLEY  
*Roswell, GA, USA*  
Christopher HOLMES  
*The University of Tokyo, Tokyo, Japan*  
Thomas R. LEBON  
*Los Angeles Trade Technical College, Los Angeles, CA, USA*

### Editorial Office

Pearl City Koishikawa 603,  
2-4-5 Kasuga, Bunkyo-ku,  
Tokyo 112-0003, Japan  
Tel: +81-3-5840-8764  
Fax: +81-3-5840-8765  
E-mail: office@biosciencetrends.com

# BioScience Trends

## Editorial and Head Office

Pearl City Koishikawa 603, 2-4-5 Kasuga, Bunkyo-ku,  
Tokyo 112-0003, Japan

Tel: +81-3-5840-8764, Fax: +81-3-5840-8765  
E-mail: office@biosciencetrends.com  
URL: www.biosciencetrends.com

## Editorial Board Members

Girdhar G. AGARWAL (Lucknow, India)	David M. HELFMAN (Daejeon, Korea)	Qingyue MENG (Beijing, China)	Sumihito TAMURA (Tokyo, Japan)
Hirotsugu AIGA (Geneva, Switzerland)	Takahiro HIGASHI (Tokyo, Japan)	Mark MEUTH (Sheffield, UK)	Puay Hoon TAN (Singapore, Singapore)
Hidechika AKASHI (Tokyo, Japan)	De-Xing HOU (Kagoshima, Japan)	Satoko NAGATA (Tokyo, Japan)	Koji TANAKA (Tsu, Japan)
Moazzam ALI (Geneva, Switzerland)	Sheng-Tao HOU (Ottawa, Canada)	Miho OBA (Odawara, Japan)	John TERMINI (Duarte, CA, USA)
Ping AO (Shanghai, China)	Yong HUANG (Ji'ning, China)	Xianjun QU (Ji'nan, China)	Usa C. THISYAKORN (Bangkok, Thailand)
Hisao ASAMURA (Tokyo, Japan)	Hirofumi INAGAKI (Tokyo, Japan)	John J. ROSSI (Duarte, CA, USA)	Toshifumi TSUKAHARA (Nomi, Japan)
Michael E. BARISH (Duarte, CA, USA)	Masamine JIMBA (Tokyo, Japan)	Carlos SAINZ-FERNANDEZ (Santander, Spain)	Kohjiro UEKI (Tokyo, Japan)
Boon-Huat BAY (Singapore, Singapore)	Kimitaka KAGA (Tokyo, Japan)	Yoshihiro SAKAMOTO (Tokyo, Japan)	Masahiro UMEZAKI (Tokyo, Japan)
Yasumasa BESSHO (Nara, Japan)	Ichiro KAI (Tokyo, Japan)	Erin SATO (Shizuoka, Japan)	Junming WANG (Jackson, MS, USA)
Generoso BEVILACQUA (Pisa, Italy)	Kazuhiro KAKIMOTO (Osaka, Japan)	Takehito SATO (Isehara, Japan)	Ling WANG (Shanghai, China)
Shiuan CHEN (Duarte, CA, USA)	Kiyoko KAMIBEPPU (Tokyo, Japan)	Akihito SHIMAZU (Tokyo, Japan)	Xiang-Dong Wang (Boston, MA, USA)
Yuan CHEN (Duarte, CA, USA)	Haidong KAN (Shanghai, China)	Zhifeng SHAO (Shanghai, China)	Hisashi WATANABE (Tokyo, Japan)
Naoshi DOHMAE (Wako, Japan)	Bok-Luel LEE (Busan, Korea)	Ri SHO (Yamagata, Japan)	Lingzhong XU (Ji'nan, China)
Zhen FAN (Houston, TX, USA)	Mingjie LI (St. Louis, MO, USA)	Judith SINGER-SAM (Duarte, CA, USA)	Masatake YAMAUCHI (Chiba, Japan)
Ding-Zhi FANG (Chengdu, China)	Ren-Jang LIN (Duarte, CA, USA)	Raj K. SINGH (Dehradun, India)	Aitian YIN (Ji'nan, China)
Yoshiharu FUKUDA (Ube, Japan)	Daru LU (Shanghai, China)	Junko SUGAMA (Kanazawa, Japan)	George W-C. YIP (Singapore, Singapore)
Rajiv GARG (Lucknow, India)	Hongzhou LU (Shanghai, China)	Hiroshi TACHIBANA (Isehara, Japan)	Benny C-Y ZEE (Hong Kong, China)
Ravindra K. GARG (Lucknow, India)	Duan MA (Shanghai, China)	Tomoko TAKAMURA (Tokyo, Japan)	Yong ZENG (Chengdu, China)
Makoto GOTO (Tokyo, Japan)	Francesco MAROTTA (Milano, Italy)	Tadatoshi TAKAYAMA (Tokyo, Japan)	Xiaomei ZHU (Seattle, WA, USA)
Demin HAN (Beijing, China)	Yutaka MATSUYAMA (Tokyo, Japan)	Shin'ichi TAKEDA (Tokyo, Japan)	

(as of October 2013)

**Review**

---

- 202 - 208     **Genetic modification of mesenchymal stem cells in spinal cord injury repair strategies.**  
*Xiaoyan Cui, Lei Chen, Yilong Ren, Yazhong Ji, Wei Liu, Jie Liu, Qiao Yan, Liming Cheng, Yi E. Sun*

**Original Articles**

---

- 209 - 220     **Insights on the structural characteristics of Vim-TBS (58-81) peptide for future applications as a cell penetrating peptide.**  
*Avneet Saini, Radhika R. Jaswal, Riteshwari Negi, Fateh S. Nandel*
- 221 - 229     **Characterization of anti-Tn-antigen MLS128 binding proteins involved in inhibiting the growth of human colorectal cancer cells.**  
*Normaiza Zamri, Naoya Masuda, Fumie Oura, Kazuya Kabayama, Yukiko Yajima, Hiroshi Nakada, Kazuo Yamamoto, Yoko Fujita-Yamaguchi*
- 230 - 236     **A novel semi-synthetic andrographolide analogue A5 inhibits tumor angiogenesis via blocking the VEGFR2-p38/ERK1/2 signal pathway.**  
*Chenyuan Gong, Chong Xu, Lili Ji, Zhengtao Wang*
- 237 - 244     **SL1122-37, a novel derivative of sorafenib, has greater effects than sorafenib on the inhibition of human hepatocellular carcinoma (HCC) growth and prevention of angiogenesis.**  
*Yizhuo Qin, Yuyin Lu, Ruiqi Wang, Wenbao Li, Xianjun Qu*

**Commentary**

---

- 245 - 249     **Japan's advanced medicine.**  
*Ri Sho, Hiroto Narimatsu, Masayasu Murakami*
- 250 - 252     **Standardizing management of hepatocellular carcinoma in China: Devising evidence-based clinical practice guidelines.**  
*Peipei Song*

## CONTENTS

(Continued)

---

- 253 - 256      **Complementary and alternative medicine is expected to make greater contribution in controlling the prevalence of influenza.**  
*Zhengang Tao, Yuxiu Yang, Wenna Shi, Mingming Xue, Weiqiang Yang, Zhenju Song, Chenling Yao, Jun Yin, Dongwei Shi, Yaping Zhang, Yingyun Cai, Chaoyang Tong, Ying Yuan*

### Letter

---

- 257 - 258      **Combat with emerging infectious diseases: Clinicians should do better.**  
*Hongzhou Lu*

### Guide for Authors

---

### Copyright

---

# Genetic modification of mesenchymal stem cells in spinal cord injury repair strategies

Xiaoyan Cui<sup>1,\*</sup>, Lei Chen<sup>2</sup>, Yilong Ren<sup>2</sup>, Yazhong Ji<sup>3</sup>, Wei Liu<sup>3</sup>, Jie Liu<sup>1</sup>, Qiao Yan<sup>1</sup>, Liming Cheng<sup>2</sup>, Yi E. Sun<sup>1,\*</sup>

<sup>1</sup> Translational Center for Stem Cell Research, Tongji Hospital, Department of Regenerative Medicine, Tongji University School of Medicine, Shanghai, China;

<sup>2</sup> Department of Spine Surgery, Tongji Hospital, Tongji University School of Medicine, Shanghai, China;

<sup>3</sup> Department of Obstetrics and Gynecology, Tongji Hospital, Tongji University School of Medicine, Shanghai, China.

## Summary

Spinal cord injury (SCI) is a serious injury of the central nervous system and up until now there is no evident effective treatment for SCI. Axonal regeneration is the only way to restore functions after serious SCI that interrupt the long tracts mediating motor and sensory function. The hurdles for axonal regeneration in SCI include: glial scar tissue and molecular barriers, the inhibiting microenvironment, and the lack of sufficient neurotrophic support. Therefore, the key point of applying stem cells to treat SCI is to build a microenvironment conducive to the survival and differentiation of stem cells and regulate neurotrophic factor expression. Adult mesenchymal stem cells (MSCs) have been applied in experimental animal models and clinical trials of SCI. Genetic modification of MSCs can increase secretion of peptides or total length proteins with potential to repair SCI and promote survival of themselves and survival or regeneration of neurons. There are many proteins that have been applied to modified MSCs, such as neurotrophic factors (neurotrophin 3, brain-derived neurotrophic factor, glial cell line-derived neurotrophic factor, nerve growth factor, and MNTS1), receptor tyrosine kinases (tropomyosin-related kinase C), and hepatocyte growth factor. In the future, there will be more molecules acting as transgenes in MSCs for treatment of SCI.

**Keywords:** Spinal cord injury, mesenchymal stem cells, neurotrophic factors, neurotrophin 3, brain-derived neurotrophic factor

## 1. Introduction

Spinal cord injury (SCI) is a serious injury of the central nervous system and its main clinical manifestations include movement, sensory, and sphincter dysfunction below the level of injury, which lead to a consequent reduction of the quality of life. The injury mainly results from contusion, compression or stretch of the spinal cord. An epidemiological study based on a nationwide database reported that SCI accounted

for 16.87% of spinal trauma in Mainland China and the incidence of SCI increased annually during the study period (1). Operative treatment and conservative treatment are employed in the management of SCI. However, up until now there is no evident effective treatment for SCI due to this injury's complicated pathophysiology (2). The focal mechanical insult disrupts tissue homeostasis during the acute phase that induces secondary injury processes. Multiple destructive cascades in the secondary injury processes cause the necrotic and apoptotic death of neurons, astrocytes, and oligodendrocytes, which spreads beyond the initial injury site and leads to irreversible axonal damage and demyelination (3). It has been recognized that axonal regeneration is the only way to restore functions for decades after serious SCI that interrupt the long tracts mediating motor and sensory function

\*Address correspondence to:

Dr. Xiaoyan Cui and Dr. Yi E. Sun, translational Center for Stem Cell Research, Tongji Hospital, Department of Regenerative Medicine, Tongji University School of Medicine, 389 Xincun road Shanghai 200065, China.  
E-mail: cuixiaoyan.tu@gmail.com

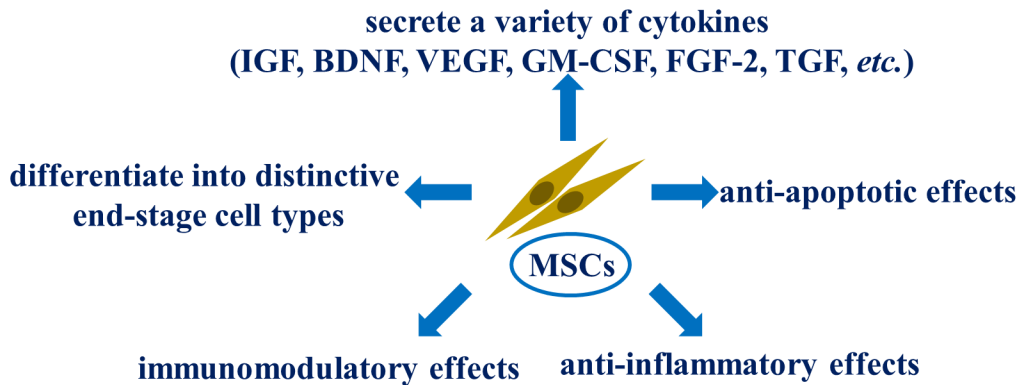


**Figure 1.** MSCs possess properties directed to the hurdle for axonal regeneration in SCI.

(4). The hurdle for axonal regeneration in SCI include: glial scar tissue and molecular barriers, inhibiting microenvironment (such as chondroitin sulphate proteoglycans and myelin-associated inhibitors), and the lack of sufficient neurotrophic support (5,6). Therefore, the key point of applying stem cells to treat SCI is to build a microenvironment conducive to the survival and differentiation of stem cells and regulate neurotrophic factor expression. Genetic modification of adult mesenchymal stem cells (MSCs) is expected to overcome the hurdle for axonal regeneration and has been applied in experimental animal models of SCI.

## 2. Mesenchymal stem cells

Embryonic stem cells (ESCs) and neural stem cells (NSCs) have been used to repair SCI. These stem cells survived, differentiated into astrocytes, oligodendrocytes, and neurons, and promoted neural functional recovery (7). However, these stem cells can also differentiate into inappropriate cells, resulting in tumor formation (8). Moreover, NSCs have a tendency to differentiate into glial cells after they are transplanted into an impaired central nervous system. Therefore, NSCs could promote astrogliosis and the extension of a glial scar (9).

At present, adult MSCs have been applied in experimental animal models and clinical trials of SCI (10). MSCs are multipotent nonhematopoietic cells with the potential to differentiate into osteoblasts, chondrocytes, adipocytes, as well as myogenic and neuronal cells (11). MSCs are a heterogeneous population that can be isolated from several tissues, such as bone marrow, adipose, umbilical cord blood, Whartons jelly, amnion, *etc.* MSCs possess many properties directed to the hurdle for axonal regeneration in SCI (Figure 1). Once MSCs arrive at an injury, they can secrete a variety of cytokines, such as insulin-like growth factor (IGF), brain-derived neurotrophic factor (BDNF), vascular endothelial growth factor (VEGF), granulocyte-macrophage colony stimulating factor (GM-CSF), fibroblast growth factor (FGF)-2, and

transforming growth factor (TGF) (12). MSCs down-regulate apoptotic molecules and up-regulate anti-apoptotic molecules in SCI animal models. In addition, MSCs increase serum interleukin (IL)-10 and decrease tumor necrosis factor (TNF)- $\alpha$ . T cells change from pro-inflammatory Th1 cells to anti-inflammatory Th2 cells and macrophage phenotypes change from M1 (immune surveillance) to M2 (down-regulating immune response) in the presence of MSCs. The immunophenotype of MSCs are major histocompatibility (MHC) I positive and MHC II negative and MSCs also lack costimulatory molecules CD40, CD80, and CD86. Therefore, MSCs have an immunomodulatory effect (13).

Multifunctional therapies seem to be extremely promising because they counteract multiple injury mechanisms and combine both neuroprotective and neuroregenerative agents (14). Although MSCs secrete some cytokines, the levels of these cytokines are not enough for SCI repair. Genetic modification of MSCs can increase secretion of peptides or total length proteins with potential to repair SCI and promote the survival of themselves and the survival or regeneration of neurons. There are many proteins that have been applied to modified MSCs, such as neurotrophic factors (neurotrophin 3, brain-derived neurotrophic factor, glial cell line-derived neurotrophic factor, nerve growth factor, and MNTS1), receptor tyrosine kinases (tropomyosin-related kinase C), and hepatocyte growth factor (Table 1).

## 3. Proteins with potential to repair SCI

### 3.1. Neurotrophic factors

#### 3.1.1. Neurotrophin 3 (NT-3)

NT-3 has been shown to act as a neuroprotective agent (15). NT-3 can promote axonal growth and the differentiation of sensory neurons, motor neurons, dopaminergic neurons, and other neurons. The effect of NT-3 promoting neuron growth is due largely to activating tropomyosin-related kinase (Trk) C (16). The co-expression of NT-3 and BDNF had an anti-apoptotic

**Table 1. Activities of Genetic modification of MSCs in SCI animal models**

Transduced genes	Animals	SCI models	Modified MSCs	Time point and dose	Gene carriers	Outcome	Ref.
NT-3	60 female SD rats	Compression of at L1 level	HUMSCs	Seven days after injury, $1 \times 10^6$ per rat	Adenovirus vector	Significant improvement of locomotor function	19
NT-3	36 female SD rats	Complete transection at T10 level	Rat BMSCs	Immediately, $5 \times 10^5$ per rat	Adenovirus vector	Some improvement (both functionally and structurally)	20
NT-3	25 female SD rats	1 $\mu$ L EB (0.1 mg/mL) into the T10 thoracic cord	Rat BMSCs	Three days after EB injection, $1 \times 10^5$ per rat	Adenovirus vector	Significant improvement of locomotor function and restoration of electrophysiological properties	21
BDNF	66 female SD rats	Transection at T9 level	Human BMSCs	Immediately, $1.2 \times 10^5$ cells per rat	Adenovirus vector	Locomotor recovery improvement	26
GDNF	18 female SD rats	Contusion injury at T9 level	Rat BMSCs	Seven days after surgery, $2 \times 10^5$ cells per rat	Retrovirus vector	Limited capacity for the replacement of neural cells lost	32
MNTS1	48 female Fischer rats	Moderate contusion at T8 level	Rat BMSCs	Seven days after injury, $4 \times 10^5$ cells per rat	Lentivirus vector	Axonal growth increase and cutaneous hypersensitivity prevention	39
TrkC	80 female SD rats	Complete transection of the spinal cord at T10	Rat BMSCs	Immediately, $5 \times 10^5$ cells per rat	Adenovirus vector	Improvement in conduction of cortical MEPs and hindlimb locomotor function	43
HGF	51 female SD rats	Hemisection injury at C4 level	Human BMSCs	Immediately, $2.0 \times 10^5$ cells per rat	Lentivirus vector	Anti-gliar scar, axonal growth increase and improvement in recovery of forepaw function	47

effect in a cellular SCI model of rat spinal cord neurons (17). Moreover, transduction of spinal motoneurons with adenoviral vector (Adv) carrying the NT-3 gene induced growth of axons from the intact corticospinal tract (CST) across the midline to the denervated side in animals with a CST lesion (18).

Implantation of genetically modified MSCs with NT-3 can improve locomotor function, structure, and electrophysiological properties. Sprague–Dawley (SD) rats in a NT-3-human umbilical cord MSCs (HUMSCs) group had significantly improved locomotor function recovery and more than the control group in a rat model for clipped SCI (19). The NT-3-HUMSCs group achieved better functional recovery, more intensive 5-HT fibers, a larger volume of spared myelination, and a smaller area of cystic cavity than the HUMSCs group at the end of 12 weeks after SCI. Bone marrow-derived MSCs (BMSCs) overexpressing NT-3 also can promote locomotor function and structure recovery. After NT-3 modified BMSCs were implanted into the transected spinal cord of rats, the animals obtained some improvement (both functionally and structurally), including the recovery of hindlimb locomotor function, dramatically reduced cavity volume, clear axonal regeneration, and more neuronal survival (20). In contrast, simple MSC implantation was not a very effective therapy for spinal transection. Moreover, implantation of NT-3 gene-modified BMSCs resulted

in significant improvement of locomotor function and restoration of electrophysiological properties in rats via a recombinant adenoviral vector (Adv) into a region of ethidium bromide (EB)-induced demyelination in the spinal cord (21). The morphological basis of this recovery was evidenced by robust myelin basic protein (MBP) expression and extensive remyelination and these results may be due to participating directly in myelination of the endogenous remyelinating cells.

### 3.1.2. BDNF

BDNF was discovered in the early 1980's (22). An intensive interest in exploring BDNF's potential in treating SCI have been spurred because of its role as a promoter of cell survival and neurite outgrowth. BDNF can enhance plasticity and regenerative growth in tracts, such as the CST (23). It can specifically interact with the high affinity TrkB receptor inducing most of the desirable effects of BDNF in SCI. Furthermore, BDNF can also interact with the low-affinity pan-neurotrophin receptor p75, leading to signaling effects that often counteract TrkB activation (24).

Although MSCs continuously produce BDNF and significantly rescue avulsed motoneurons (25), gene-modified human BMSCs overexpressing BDNF can further increase the potential therapeutic effect of BDNF in SCI (26). At 5 weeks after transplantation of modified

BMSCs for SCI, locomotor recovery improvement was observed for the BDNF-BMSC group, but not in the BMSC group. Structurally there was increased sprouting of the injured corticospinal tract and an increased cell survival of corticospinal tract neurons in the primary motor cortex.

### 3.1.3. Glial cell line -derived neurotrophic factor (GDNF)

GDNF exists in embryonic limb and muscle at high levels at the time of innervation and is necessary for normal neuromuscular development (27). It has been shown to protect motor neurons in a number of different animal models (28). GDNF can increase neural sprouting and prevent cell death (29). The heterodimer receptor system of GDNF includes GDNF receptor alpha (GFR $\alpha$ ) and c-Ret expressed by healthy motor neurons. These neurons can bind, internalize, and transport GDNF in both antero- and retrograde directions in a receptor-dependent manner (30). GDNF administration may stimulate the survival of injured motor neurons and promote axonal regeneration (31). GDNF-transduced MSCs can survive and express the therapeutic gene after 6 weeks of transplantation to the site of SCI, while maintaining an undifferentiated phenotype. However, they provide excellent opportunities for local delivery of neurotrophic factors into the injured spinal cord (32).

### 3.1.4. Nerve growth factor (NGF)

NGF can promote survival and axonal growth of sensory and sympathetic neurons. The functions of NGF are mediated by its binding to TrkA and the p75 neurotrophin receptor (p75 NTR) (33). This NGF-receptor complex undergoes endocytosis and retrograde transport to the neuronal soma where it regulates gene expression (34).

NGF expression significantly increased in the spinal cord injured tissue 3 days after MSC graft (35). Moreover, secreted NGF from genetically modified MSCs induced neurite outgrowth from PC12 cells (36). Combination of MSC transplantation with NGF promoted axonal regeneration and further functional improvement compared with single MSC transplantation or NGF on the repair of SCI in adult rats (37).

### 3.1.5. MNTS1

MNTS1 contains only seven amino acid changes from multineurotrophin NT-3/D15A. It can bind all receptors of the Trk family and induce autophosphorylation of TrkA, TrkB, and TrkC (38). MSCs transduced with a multineurotrophin are effective in cell growth promotion and sensory function improvement after SCI. Kumagai *et al.* reported that transplantation with MSC-MNTS1 and MSC-MNTS1/p75<sup>-</sup> enhanced axonal growth and significantly prevented cutaneous hypersensitivity after SCI (39). Furthermore, transplantation with MSC-

MNTS1/p75<sup>-</sup> increased angiogenesis and decreased glial scar formation.

### 3.2. TrkC

The effects of mature neurotrophins on neuronal survival are mediated by members of the Trk family of receptor tyrosine kinases (40) and are modulated by the common neurotrophin receptor p75 NTR (also known as NGFR) (41). The Trk family of receptor tyrosine kinases which neurotrophins bind to includes TrkA (NGF), TrkB (BDNF and NT-4/5) and TrkC (NT-3).

Chen *et al.* showed that *in vivo* transplanted MSCs overexpressing TrkC migrated into the NT-3 enriched area. Moreover, the migrating incidence as well as migration distance of MSCs was significantly higher than the control (42). The results indicated that TrkC acts as a chemokine receptor with its high affinity for NT-3 and may play a role in MSC homing. TrkC gene-modified MSCs transplantation combined with electroacupuncture treatment not only increased MSC survival and differentiation into neuron-like cells but also promoted CST regeneration across injured sites to the caudal cord and functional improvement in SCI (43). In addition, the conduction of cortical motorevoked potentials (MEPs) and hindlimb locomotor function increased as compared to controls. These results are perhaps due to an increase of NT-3 levels, upregulation of laminin and GAP-43, and downregulation of GFAP and chondroitin sulphate proteoglycan (CSPG) proteins.

### 3.3. Hepatocyte growth factor (HGF)

HGF is primarily produced by cells of mesenchymal origin. It is a pleiotropic cytokine which promotes angiogenesis and cell survival (44). Injection of HGF has been demonstrated to enhance kidney and liver regeneration (45). In addition, systemic treatment with HGF significantly accelerated remyelination in lysolecithin-induced rat dorsal spinal cord lesions and in slice cultures (46). Moreover, HGF has anti-glial scar effects and could be used to ameliorate functional deficits following SCI. Transplantation of HGF overexpressing MSCs (HGF-MSCs) into hemisection spinal cord lesions at C4 markedly decreased TGF $\beta$  isoform and neurocan levels and reduced the extent of astrocytic activation and glycosaminoglycan chain deposition around hemisection lesions. Furthermore, animals treated with HGF-MSCs showed axonal growth promotion beyond glial scars and recovery improvement of forepaw function (47).

## 4. Gene carriers

Effective gene transduction is the basis of genetic modification of MSCs in SCI repair. Viral vectors are characterized by high transduction efficiency and stable transgene expression. Viral vectors mediating genetic

modification of MSCs include retroviral, adeno-associated viral, adenoviral, and lentiviral vectors. They have their own advantages and disadvantages (48). Lentiviral vectors have the unique ability to integrate into the genome of non-dividing cells and enable their relatively long and stable transgene expression. On the contrary, other retroviral vectors only transduce dividing cells. Moreover, the immunogenicity of lentiviral vectors is significantly reduced (49,50). Adenoviral vectors are able to transduce dividing and non-dividing cells (51). They are relatively safe to the host due to no integration function. Meanwhile, adeno-associated virus is also considered non-pathogenic to humans because it is a defective virus (52).

Non-viral vector systems have many advantages compared to viral vector systems, including, significantly lower toxicity/immunogenicity and potential tumorigenicity, unlimited transgene size (range is from oligonucleotides to artificial chromosomes), simple quality control, and simple requirements for drugs and management (53). Non-viral vectors may be applied to transduce exogenous genes into MSCs in SCI repair.

## 5. Conclusions

Continuous development of new strategies to treat SCI is urgently needed because, to date, there is no evident effective treatment for SCI. More information is needed regarding genetic modification of MSCs, including transgene expression level and stabilization, elaborate gene regulation, and safety. Further experimental and clinical investigations will allow a better understanding of mechanisms of action, therapeutic effects, and the safety profile. Many molecules have been recognized for their promising and potent activities of rescuing SCI. Besides the above-mentioned neurotrophic factors, TrkC, and HGF, other cytokines and anti-apoptosis molecules can also be used to modify MSCs, such as D15A (with NT-3 and BDNF activity) (54), ciliary neurotrophic factor (CNTF) (55), and survivin (56). In the future, more molecules acting as overexpressing genes in MSCs and treating SCI will be recognized.

## Acknowledgements

This project was supported by a grant (2012M520933) from the National Science Foundation for Post-doctoral Scientists of China, a grant (20124y147) from the Shanghai Municipal Health Bureau Youth Projects, a grant (2012KJ016) from the Scientific Research Foundation for Training Excellent Youth Teacher of Tongji University.

## References

- Liu P, Yao Y, Liu MY, Fan WL, Chao R, Wang ZG, Liu YC, Zhou JH, Zhao JH. Spinal trauma in mainland China from 2001 to 2007: An epidemiological study based on a nationwide database. *Spine (Phila Pa 1976)*. 2012; 37:1310-1315.
- Sakai K, Yamamoto A, Matsubara K, Nakamura S, Naruse M, Yamagata M, Sakamoto K, Tauchi R, Wakao N, Imagama S, Hibi H, Kadomatsu K, Ishiguro N, Ueda M. Human dental pulp-derived stem cells promote locomotor recovery after complete transection of the rat spinal cord by multiple neuro-regenerative mechanisms. *J Clin Invest*. 2012; 122:80-90.
- Rowland JW, Hawryluk GW, Kwon B, Fehlings MG. Current status of acute spinal cord injury pathophysiology and emerging therapies: promise on the horizon. *Neurosurg Focus*. 2008; 25:E2.
- Tuszynski MH, Steward O. Concepts and methods for the study of axonal regeneration in the CNS. *Neuron*. 2012; 74:777-791.
- Blits B, Kitay BM, Farahvar A, Caperton CV, Dietrich WD, Bunge MB. Lentiviral vector-mediated transduction of neural progenitor cells before implantation into injured spinal cord and brain to detect their migration, deliver neurotrophic factors and repair tissue. *Restor Neurol Neurosci*. 2005; 23:313-324.
- Löw K, Blesch A, Herrmann J, Tuszynski MH. A dual promoter lentiviral vector for the *in vivo* evaluation of gene therapeutic approaches to axon regeneration after spinal cord injury. *Gene Ther*. 2010; 17:577-591.
- Karimi-Abdolrezaee S, Eftekharpour E, Wang J, Morshead CM, Fehlings MG. Delayed transplantation of adult neural precursor cells promotes remyelination and functional neurological recovery after spinal cord injury. *J Neurosci*. 2006; 26:3377-3389.
- Erdö F, Bührle C, Blunk J, Hoehn M, Xia Y, Fleischmann B, Föcking M, Küstermann E, Kolossov E, Hescheler J, Hossmann KA, Trapp T. Host-dependent tumorigenesis of embryonic stem cell transplantation in experimental stroke. *J Cereb Blood Flow Metab*. 2003; 23:780-785.
- Vroemen M, Aigner L, Winkler J, Weidner N. Adult neural progenitor cell grafts survive after acute spinal cord injury and integrate along axonal pathways. *Eur J Neurosci*. 2003; 18:743-751.
- Caplan AI. Adult mesenchymal stem cells for tissue engineering versus regenerative medicine. *J Cell Physiol*. 2007; 213:341-347.
- Sun T, Ma QH. Repairing neural injuries using human umbilical cord blood. *Mol Neurobiol*. 2013; 47:938-945.
- Azari MF, Mathias L, Ozturk E, Cram DS, Boyd RL, Petratos S. Mesenchymal stem cells for treatment of CNS injury. *Curr Neuropharmacol*. 2010; 8:316-323.
- Chidgey AP, Layton D, Trounson A, Boyd RL. Tolerance strategies for stem-cell-based therapies. *Nature*. 2008; 453:330-337.
- Rossi F, Ferrari R, Papa S, Moscatelli D, Casalini T, Forloni G, Perale G, Veglianesi P. Tunable hydrogel-nanoparticles release system for sustained combination therapies in the spinal cord. *Colloids Surf B Biointerfaces*. 2013; 108:169-177.
- Beutner C, Lepperhof V, Dann A, Linnartz-Gerlach B, Litwak S, Napoli I, Prinz M, Neumann H. Engineered stem cell-derived microglia as therapeutic vehicle for experimental autoimmune encephalomyelitis. *Gene Ther*. 2013; 20:797-806.
- Novikova LN, Novikov LN, Kellerth JO. Survival effects of BDNF and NT-3 on axotomized rubrospinal neurons depend on the temporal pattern of neurotrophin

- administration. *Eur J Neurosci.* 2000; 12:776-780.
17. Wang Y, Gu J, Wang J, Feng X, Tao Y, Jiang B, He J, Wang Q, Yang J, Zhang S, Cai J, Sun Y. BDNF and NT-3 expression by using glucocorticoid-induced bicistronic expression vector pGC-BDNF-IRES-NT3 protects apoptotic cells in a cellular injury model. *Brain Res.* 2012; 1448:137-143.
  18. Zhou L, Baumgartner BJ, Hill-Felberg SJ, McGowen LR, Shine HD. Neurotrophin-3 expressed in situ induces axonal plasticity in the adult injured spinal cord. *J Neurosci.* 2003; 23: 1424-1431.
  19. Shang AJ, Hong SQ, Xu Q, Wang HY, Yang Y, Wang ZF, Xu BN, Jiang XD, Xu RX. NT-3-secreting human umbilical cord mesenchymal stromal cell transplantation for the treatment of acute spinal cord injury in rats. *Brain Res.* 2011; 1391:102-113.
  20. Zhang W, Yan Q, Zeng YS, Zhang XB, Xiong Y, Wang JM, Chen SJ, Li Y, Bruce IC, Wu W. Implantation of adult bone marrow-derived mesenchymal stem cells transfected with the neurotrophin-3 gene and pretreated with retinoic acid in completely transected spinal cord. *Brain Res.* 2010; 1359:256-271.
  21. Zhang YJ, Zhang W, Lin CG, Ding Y, Huang SF, Wu JL, Li Y, Dong H, Zeng YS. Neurotrophin-3 gene modified mesenchymal stem cells promote remyelination and functional recovery in the demyelinated spinal cord of rats. *J Neurol Sci.* 2012; 313:64-74.
  22. Barde YA, Edgar D, Thoenen H. Purification of a new neurotrophic factor from mammalian brain. *EMBO J.* 1982; 1:549-553.
  23. Hiebert GW, Khodarahmi K, McGraw J, Steeves JD, Tetzlaff W. Brain-derived neurotrophic factor applied to the motor cortex promotes sprouting of corticospinal fibers but not regeneration into a peripheral nerve transplant. *J Neurosci Res.* 2002; 69:160-168.
  24. Weishaupt N, Blesch A, Fouad K. BDNF: the career of a multifaceted neurotrophin in spinal cord injury. *Exp Neurol.* 2012; 238:254-264.
  25. Rodrigues Hell RC, Silva Costa MM, Goes AM, Oliveira AL. Local injection of BDNF producing mesenchymal stem cells increases neuronal survival and synaptic stability following ventral root avulsion. *Neurobiol Dis.* 2009; 33:290-300.
  26. Sasaki M, Radtke C, Tan AM, Zhao P, Hamada H, Houkin K, Honmou O, Kocsis JD. BDNF-hypersecreting human mesenchymal stem cells promote functional recovery, axonal sprouting, and protection of corticospinal neurons after spinal cord injury. *J Neurosci.* 2009; 29:14932-14941.
  27. Wang CY, Yang F, He XP, Je HS, Zhou JZ, Eckermann K, Kawamura D, Feng L, Shen L, Lu B. Regulation of neuromuscular synapse development by glial cell line-derived neurotrophic factor and neurturin. *J Biol Chem.* 2002; 277:10614-10625.
  28. Acsadi G, Anguelov RA, Yang H, Toth G, Thomas R, Jani A, Wang Y, Ianakova E, Mohammad S, Lewis RA, Shy ME. Increased survival and function of SOD1 mice after glial cell-derived neurotrophic factor gene therapy. *Hum Gene Ther.* 2002; 13:1047-1059.
  29. Deshpande DM, Kim YS, Martinez T, Carmen J, Dike S, Shats I, Rubin LL, Drummond J, Krishnan C, Hoke A, Maragakis N, Shefner J, Rothstein JD, Kerr DA. Recovery from paralysis in adult rats using embryonic stem cells. *Ann Neurol.* 2006; 60:32-44.
  30. von Bartheld CS, Wang X, Butowt R. Anterograde axonal transport, transcytosis, and recycling of neurotrophic factors: The concept of trophic currencies in neural networks. *Mol Neurobiol.* 2001; 24:1-28.
  31. Henderson CE, Camu W, Mettling C, Gouin A, Poulsen K, Karihaloo M, Rullamas J, Evans T, McMahon SB, Armanini MP, Berkemeier L, Phillips HS, Rosenthal A. Neurotrophins promote motor neuron survival and are present in embryonic limb bud. *Nature.* 1993; 363:266-270.
  32. Rooney GE, McMahon SS, Ritter T, Garcia Y, Moran C, Madigan NN, Flügel A, Dockery P, O'Brien T, Howard L, Windebank AJ, Barry FP. Neurotrophic factor-expressing mesenchymal stem cells survive transplantation into the contused spinal cord without differentiating into neural cells. *Tissue Eng Part A.* 2009; 15:3049-3059.
  33. Schor NF. The p75 neurotrophin receptor in human development and disease. *Prog Neurobiol.* 2005; 77:201-214.
  34. Ginty DD, Segal RA. Retrograde neurotrophin signaling: Trk-ing along the axon. *Curr Opin Neurobiol.* 2002; 12:268-274.
  35. Quertainmont R, Cantinieaux D, Botman O, Sid S, Schoenen J, Franzen R. Mesenchymal stem cell graft improves recovery after spinal cord injury in adult rats through neurotrophic and pro-angiogenic actions. *PLoS One.* 2012; 7:e39500.
  36. Rooney GE, Moran C, McMahon SS, Ritter T, Maenz M, Flügel A, Dockery P, O'Brien T, Howard L, Windebank AJ, Barry FP. Gene-modified mesenchymal stem cells express functionally active nerve growth factor on an engineered poly lactic glycolic acid (PLGA) substrate. *Tissue Eng Part A.* 2008; 14:681-690.
  37. Huang F, Wang J, Chen A. Effects of co-grafts mesenchymal stem cells and nerve growth factor suspension in the repair of spinal cord injury. *J Huazhong Univ Sci Technolog Med Sci.* 2006; 26:206-210.
  38. Urfer R, Tsoulfas P, Soppet D, Escandón E, Parada LF, Presta LG. The binding epitopes of neurotrophin-3 to its receptors trkC and gp75 and the design of a multifunctional human neurotrophin. *EMBO J.* 1994; 13:5896-5909.
  39. Kumagai G, Tsoulfas P, Toh S, McNiece I, Bramlett HM, Dietrich WD. Genetically modified mesenchymal stem cells (MSCs) promote axonal regeneration and prevent hypersensitivity after spinal cord injury. *Exp Neurol.* 2013; 248:369-380.
  40. Huang EJ, Reichardt LF. Neurotrophins: roles in neuronal development and function. *Annu Rev Neurosci.* 2001; 24:677-736.
  41. Lee KF, Davies AM, Jaenisch R. p75-deficient embryonic dorsal root sensory and neonatal sympathetic neurons display a decreased sensitivity to NGF. *Development.* 1994; 120:1027-1033.
  42. Chen YF, Zeng X, Zhang K, Lai BQ, Ling EA, Zeng YS. Neurotrophin-3 stimulates migration of mesenchymal stem cells overexpressing TrkC. *Curr Med Chem.* 2013; 20:3022-3033.
  43. Ding Y, Yan Q, Ruan JW, Zhang YQ, Li WJ, Zeng X, Huang SF, Zhang YJ, Wu JL, Fisher D, Dong H, Zeng YS. Electroacupuncture promotes the differentiation of transplanted bone marrow mesenchymal stem cells overexpressing TrkC into neuron-like cells in transected spinal cord of rats. *Cell Transplant.* 2013; 22:65-86.
  44. Sulpice E, Ding S, Muscatelli-Groux B, Bergé M, Han ZC, Plouet J, Tobelem G, Merkulova-Rainon T. Cross-

- talk between the VEGF-A and HGF signalling pathways in endothelial cells. *Biol Cell*. 2009; 101:525-539.
45. Anan F, Shimomura T, Imagawa M, Masaki T, Nawata T, Takahashi N, Yonemochi H, Eshima N, Saikawa T, Yoshimatsu H. Predictors for silent cerebral infarction in patients with chronic renal failure undergoing hemodialysis. *Metabolism*. 2007; 56:593-598.
  46. Bai L, Lennon DP, Caplan AI, DeChant A, Hecker J, Kranso J, Zaremba A, Miller RH. Hepatocyte growth factor mediates mesenchymal stem cell-induced recovery in multiple sclerosis models. *Nat Neurosci*. 2012; 15:862-870.
  47. Jeong SR, Kwon MJ, Lee HG, Joe EH, Lee JH, Kim SS, Suh-Kim H, Kim BG. Hepatocyte growth factor reduces astrocytic scar formation and promotes axonal growth beyond glial scars after spinal cord injury. *Exp Neurol*. 2012; 233:312-322.
  48. Hendriks WT, Ruitenber MJ, Blits B, Boer GJ, Verhaagen J. Viral vector-mediated gene transfer of neurotrophins to promote regeneration of the injured spinal cord. *Prog Brain Res*. 2004; 146:451-476.
  49. Naldini L, Blömer U, Gage FH, Trono D, Verma IM. Efficient transfer, integration, and sustained long-term expression of the transgene in adult rat brains injected with a lentiviral vector. *Proc Natl Acad Sci U S A*. 1996; 93:11382-11388.
  50. Schambach A, Baum C. Clinical application of lentiviral vectors – concepts and practice. *Curr Gene Ther*. 2008; 8:474-482.
  51. Lu CH, Chang YH, Lin SY, Li KC, Hu YC. Recent progresses in gene delivery-based bone tissue engineering. *Biotechnol Adv*. 2013; pii: S0734-9750(13)00149-3.
  52. Ke J, Zheng LW, Cheung LK. Orthopaedic gene therapy using recombinant adeno-associated virus vectors. *Arch Oral Biol*. 2011; 56:619-628.
  53. Kostarelos K, Miller AD. Synthetic, self-assembly ABCD nanoparticles; a structural paradigm for viable synthetic non-viral vectors. *Chem Soc Rev*. 2005; 34:970-994.
  54. Hurtado A, Moon LD, Maquet V, Blits B, Jérôme R, Oudega M. Poly (D,L-lactic acid) macroporous guidance scaffolds seeded with Schwann cells genetically modified to secrete a bi-functional neurotrophin implanted in the completely transected adult rat thoracic spinal cord. *Biomaterials*. 2006; 27:430-442.
  55. Lu Z, Hu X, Zhu C, Wang D, Zheng X, Liu Q. Overexpression of CNTF in Mesenchymal Stem Cells reduces demyelination and induces clinical recovery in experimental autoimmune encephalomyelitis mice. *J Neuroimmunol*. 2009; 206:58-69.
  56. Liu N, Zhang Y, Fan L, Yuan M, Du H, Cheng R, Liu D, Lin F. Effects of transplantation with bone marrow-derived mesenchymal stem cells modified by Survivin on experimental stroke in rats. *J Transl Med*. 2011; 9:105.

(Received September 22, 2013; Revised October 24, 2013; Accepted October 26, 2013)

## Insights on the structural characteristics of Vim-TBS (58-81) peptide for future applications as a cell penetrating peptide

Avneet Saini\*, Radhika R. Jaswal, Riteshwari Negi, Fateh S. Nandel

Department of Biophysics, Panjab University, Chandigarh, India.

### Summary

The plasma membrane presents a remarkable barrier for the delivery of peptide and nucleic acid based drugs to the inside of cells. This restraint in the path of their development as therapeutic agents can be offset by their conjugation to cell penetrating peptides (CPPs) that can lead to an improved pharmacological profile. In this context, conformational behavior of Vimentin Tubulin Binding Site (TBS) peptide, Vim-TBS (58-81), was investigated for its acknowledged cell penetrating properties along with Trans-activating Tat (48-60) peptide and a pro-apoptogenic peptide of p21/WAF1 protein (p10). Also, the fusion peptides Vim-TBS (58-81)-p10 & Tat (48-60)-p10 were studied using molecular mechanics (MM) and molecular dynamics (MD) based strategies. MM results revealed formation of stable  $\alpha$ -helix like secondary structures in Vim-TBS (58-81), Tat (48-60) and p10 peptides. In water, three peptides adopted either a helical structure or a random conformation; the stability of either of the two states being governed by the formation of polar contacts with the solvent. The fusion peptides formed helical structures after MD simulations but the structure obtained for the fusion peptide, Vim-TBS-p10 is relatively better characterized in terms of its amphipathic nature with a hydrophilic face formed by the positively charged residues facilitating a better interaction of this fusion peptide with the membrane as compared to that of Tat-p10 peptide. This is the first report on the conformational characteristics of the Vim-TBS (58-81) peptide and the fusion peptide, Vim-TBS (58-81)-p10. The results presented here are significant for their potential role in guiding and facilitating the future efforts of designing peptide based cell penetrating drugs.

**Keywords:** CPPs, Vim-TBS, Tat, p10, peptides, molecular mechanics, molecular dynamics

### 1. Introduction

Living cells are protected from their surrounding environment by cell membranes that only allow movement of small molecular size compounds across their barrier. During the last two decades, a number of peptides presenting the ability to be translocated across biological membranes have been identified and thoroughly studied, resulting in the characterization of a new family of peptides known as cell-penetrating peptides, in some cases also frequently referred to as protein transduction domains (PTDs) (1). CPPs are short (~35 amino acids) water soluble, partly hydrophobic

or polybasic peptides that are capable of entering most mammalian cells at low molecular concentrations *in vivo* and *in vitro* without using any chiral receptors and without causing significant membrane damage (2). Many CPPs are highly cationic, usually rich in arginine and lysine amino acids and hydrophilic, exhibiting no or relatively low amphipathicity when compared to other peptides that are known to interact with and permeabilize phospholipid membranes. The mechanism of penetration of CPPs is ambiguous, but ample evidence prevails for multiple mechanisms, including direct translocation across the plasma membrane and endocytosis (3).

The profound interest that CPPs evoked among the scientific community was associated not only with their ability to cross cellular membranes by a non-toxic process, apparently independent of membrane receptors and energy consumption, but mainly due to the capacity

\*Address correspondence to:

Dr. Avneet Saini, Department of Biophysics, Panjab University, Chandigarh 160014, India.  
E-mail: avneet@pu.ac.in

to promote the efficient cellular internalization of bio-molecules/drugs conjugated to these peptides (4-11). Since, the lack of permeability of the cellular membranes to hydrophilic bio-molecules constitutes one of the most important barriers to the delivery of therapeutic agents; this discovery has been regarded as an important step towards the development of novel strategies to increase the intracellular availability of molecules with high therapeutic interest but with low membrane permeability. Furthermore, CPPs are capable of carrying cargoes of a wide range of molecular size such as proteins (12,13), oligonucleotides (14) and even 200 nm liposomes (15,16) into different cellular compartments. Therefore, they are extremely attractive candidates to transport drugs to the interior of the cell. These peptides are also of profound interest in imaging processes, specifically in case of cancerous cells (17). The penetration of CPPs into cells is usually rapid and of first-order, with half-times from 5 to 20 minutes (18).

Among all CPPs, which include protein transduction domains (19), chimeric peptides and peptides of synthetic origin, the peptides derived from the HIV-1 Tat protein (1), from the homeodomain of the Antennapedia protein of *Drosophila* (Tat and Penetratin peptides, respectively), as well as the synthetic Pep-1 peptide (20), are the best characterized. These peptides have been successfully used for the intracellular delivery of different cargoes (21), including nanoparticles, full-length proteins, liposomes and nucleic acids, both *in vitro* and *in vivo*, thus resulting in successful transduction in animal tissues, including the brain.

Intermediate filaments (IFs) by binding to unpolymerized tubulin at discrete tubulin binding sites, provides flexible intracellular scaffolding which imparts structure to cytoskeleton hence, providing resistance to the cell from external stresses (22). In a recent report, a peptide Vim-TBS 58-81 corresponding to the tubulin

binding site of the type III IF protein Vimentin, has been shown to enter cells (23) using well-established cell biology techniques (24). Furthermore, the inhibition of cell proliferation through nucleus localization of Vim-TBS 58-81 coupled to p10 (a pro-apoptogenic peptide of p21/WAF1 protein, an established model peptide to evaluate the translocation efficiency of CPPs) has been reported (25).

To the best of our knowledge, no work has been done on the conformational characterization of the vimentin-tubulin binding site peptide, Vim-TBS (58-81), for its cell penetrating properties. Therefore, the primary aim of this project is to evaluate its conformational preferences in terms of various interactions that tend to guide and stabilize its structure. To have an in depth knowledge of its structural characteristics, structural properties of Tat (48-60) and p10 peptides were also studied. Tat (48-60) and p10 were particularly selected as the former is a well studied CPP and the later is a pro-apoptogenic fragment of p21/WAF1 protein that is often used as a model cargo to evaluate cell penetrating properties. As structural versatility has been described as an important factor to be considered for deciphering cellular uptake properties by CPPs (26-28) the present work supports the hypothesis that structural plasticity could have a crucial role on its properties and functionality. Therefore, we examined the conformational aspects in a step by step approach that begins by the identification of intrinsic properties of the peptides through refined systematic fragmentation as shown in Table 1 and 2. The structural states and conformational plasticity of peptides in distinct environmental models was studied using molecular mechanics and molecular dynamics approaches. Finally, conformational preferences of the fusion peptides Vim-TBS (58-81)-p10 and Tat (48-60)-p10 were analyzed by MD simulations in explicit water as solvent.

**Table 1. Amino acid sequence of different peptides investigated**

Peptide	Sequence
Tat 48-60	GRKKRRQRRPPQ
Vim-TBS 58-81	GGAYVTRSSAVRLRSSVPGVRLQ
p10	RQTSMTDFYHSKRRLIFS
Vim-TBS 58-81-p10	GGAYVTRSSAVRLRSSVPGVRLQ-RQTSMTDFYHSKRRLIFS
Tat 48-60-p10	GRKKRRQRRPPQ -RQTSMTDFYHSKRRLIFS

**Table 2. Model oligopeptide fragments of Tat (48- 60), Vim-TBS (58-81), p10 peptides**

Tat. (48- 60) peptide				Vim-TBS (58-81) peptide					p10 peptide			
I	II	III	IV	I	II	III	IV	V	I	II	III	IV
G <sup>48</sup>	K <sup>51</sup>	Q <sup>54</sup>	R <sup>57</sup>	G <sup>58</sup>	V <sup>62</sup>	A <sup>67</sup>	S <sup>73</sup>	V <sup>77</sup>	R <sup>1</sup>	M <sup>5</sup>	Y <sup>9</sup>	K <sup>12</sup>
R	R	R	P	G	T	V	V	R	Q	T	H	R
K	R	R	P	A	R	R	P	L	T	D	S	R
K	Q	R	Q	Y	S	L	G	L	S	F	K	L
R <sup>52</sup>	R <sup>55</sup>	P <sup>58</sup>	Q <sup>60</sup>	V	S	R	V	Q <sup>81</sup>	M	Y	R	I
				T	A	S	R <sup>78</sup>		T <sup>6</sup>	H	R <sup>14</sup>	F
				R <sup>64</sup>	V <sup>68</sup>	S				S <sup>11</sup>		S <sup>18</sup>
						V <sup>74</sup>						

## 2. Methods

To gain insights on the  $\Phi$ ,  $\Psi$ ,  $\omega$ , &  $\chi$  values and thus, on the potential energy space explored by each amino acid residue, the peptide sequences were divided into short overlapping model oligopeptide fragments, each containing five to seven amino acid residues (Table 2). Understanding secondary structure of peptides is a prerequisite for functional characterization. Since, most of the peptide secondary and tertiary structures are not available in Protein Data Bank (PDB) secondary structure prediction methods are used to obtain crucial knowledge about the structure and function of the peptides. PSIPRED, a web server (29) based on such prediction methods, was used to gain valuable insights into the type of secondary structure these peptides may possibly adopt. These prediction results (results not shown) provided the initial background on the various possible starting conformations for energy minimization studies. Hence, different starting conformations were taken along with a linear starting geometry. Every oligopeptide fragment was then minimized by MM based software- Swiss pdb Viewer (30), using a steepest descent and conjugate gradient method with a cut-off of 0.05 kJ/mol. MM energy minimization calculations were then performed on the full length peptides *i.e.* Vim-TBS (58-81), Tat (48-60) and p10 at a dielectric constant of 4, using different starting conformations based on the minimization results of model oligopeptides together with the conformations obtained from the secondary structure prediction results. The results thus obtained were analyzed in terms of the various stabilizing interactions.

Simulations provide a great deal of information with respect to the stability of non-covalent interactions in water and gain insight on the dynamic characteristics of the peptides in solvent. GROMACS software was used for the MD studies (31). Interaction parameters for the simulations were taken from GROMOS-96 force field (31). Energy of the system was minimized with the convergence value (emtol) of 1000 kJ mol<sup>-1</sup> nm<sup>-1</sup>. In order to allow equilibration of solvent around the model sequence, the position of all residues was restrained for 20ps at the desired temperature. MD simulations were performed for 1ns in an NVT ensemble with water (32) as solvent at a constant temperature of 300K *i.e.* at constant volume, temperature, and mass. The run was carried out with a time step of 2fs using the Leap Frog Algorithm (33) and temperature was controlled through weak coupling to a constant temperature bath (34) using a coupling time constant;  $\tau_p$  of 0.1ps and a reference temperature;  $T_0$  of 300, 313 & 343 K. LINCS algorithm (35) was used to restrict all bonds to their equilibrium lengths and the center of mass motion of the system was removed at every step to maintain the effective simulation temperature at 300 K. Pressure was controlled using weak coupling with a time constant of 0.5 ps and a reference pressure of 1 Bar. For the

evaluation of coulomb interactions and Van der Waals interaction a cut off of 0.9 and 1.0 nm respectively was applied. Long range forces were updated every 10fs during generation of the neighbor list. Long Range Electrostatic Interactions were calculated using a Particle Mesh Ewald Summation (36). Initial velocities of all atoms were taken from a Maxwellian distribution at the desired initial temperature. Because we aim to establish the conformational characteristics of vimentin tubulin binding peptide for its potent applications as a cell penetrating peptide, MD simulations of this peptide in conjunction with p10 (fusion peptide) were also carried out along with the simulations of the fusion peptide Tat 48-60-p10 (acting as control for the study) at 300 K with the same MD parameters (31) for 1 ns under NVT conditions. The results obtained were analyzed using VMD software (37). Detailed analysis will help in the understanding of the interactions playing key roles in the mechanism of cell penetration. All simulations were carried out using the GROMACS Molecular Dynamics Package on the Desktop FUJITSU Workstation R570-2.

## 3. Results

### 3.1. MM energy minimizations

#### 3.1.1. Model oligopeptides

In order to best explore the potential energy surface, three different starting geometries were taken (based on the PSIPRED Prediction results) for minimization of the various model oligopeptides of Vim-TBS 58-81 with  $\Phi$ ,  $\Psi$  values of  $-57^\circ$ ,  $-47^\circ$ ;  $-139^\circ$ ,  $135^\circ$  &  $180^\circ$ ,  $180^\circ$  corresponding to  $\alpha$ -helix,  $\beta$ -strand and linear conformations respectively. This preference of  $\Phi$ ,  $\Psi$  values is also based on extensive study of previous work on usual and unusual peptides/peptoids (38-40). On the basis of energy, the most stable conformations obtained after steepest descent minimization followed by a conjugate gradient method for various model oligopeptides of Vim-TBS 58-81, Tat 48-60 and p10 peptides are discussed in Table 3. It is evident from the results that the most stable conformation in all model oligopeptides of Vim-TBS (58-81) populated the second quadrant of the Ramachandran map with  $\Phi$ ,  $\Psi$  values of  $\sim -100^\circ$ ,  $110^\circ$  ( $\pm 30^\circ$ ) except for model oligopeptide IV. Such structures are particularly stabilized by minimization of steric constraints imposed by the lengthy and/or bulky aromatic and/or charged side chains. Also, CH $\cdots$  $\pi$  interactions and hydrophobic interactions lend stability to such conformations. In model oligopeptide IV no regular secondary structure was observed as large deviations in the  $\Phi$ ,  $\Psi$  values of particularly the centrally placed proline and glycine residues were observed. Proline is a known and most efficient helix breaking residue in natural proteins and peptides because its nitrogen cannot form hydrogen bonds (41). On the other

hand, glycine is the simplest least restricted amino acid and thus, can explore a larger conformational region favoring a larger number of possible combinations of  $\Phi$ ,  $\Psi$  values on the Ramachandran map (42,43). Therefore, the consecutively positioned proline and glycine residues (with contrasting conformational behavior) are argued

to be responsible for the non-regular/random secondary structure in oligopeptide IV.

The peptide Tat (48-60) is highly positively charged and is predicted by PSIPRED to adopt a helical structure (except residues 57-60 that are predicted to adopt a coil like structure). Keeping these observations

**Table 3. Molecular mechanics results for the most stable conformational states of various model oligopeptides**

Vim-TBS 58-81								
Fragment I	G	G	A	Y	V	T	R	
$\Phi$	-	-175.4	-119.4	-126.0	-76.4	-68.6	-118.6	
$\Psi$	146.6	152.7	148.8	143.0	88.1	86.3	-	
$\omega$	-	-178.3	-177.9	-171.2	178.1	-177.7	175.2	
Fragment II	V	T	R	S	S	A	Y	V
$\Phi$	-	-69.6	-115.0	-117.1	-114.5	-115.1	-116.9	-116.2
$\Psi$	139.7	87.4	99.6	148.3	149.2	138.9	-	-
$\omega$	-	177.4	-178.0	179.6	178.8	178.9	-178.3	-179.4
Fragment III	A	V	R	L	R	S	S	
$\Phi$	-	-76.5	-68.8	-71.4	-123.0	-116.7	-110.4	
$\Psi$	143.2	88.4	85.2	81.3	145.1	149.3	143.8	
$\omega$	-	178.3	-179.4	175.5	-175.3	179.4	178.8	
Fragment IV	S	V	P	G	V	R		
$\Phi$	-	-103.9	-60.5	62.8	-130.4	-111.6		
$\Psi$	96.2	126.4	132.5	-148.5	82.8	-		
$\omega$	-	-175.9	176.2		179.0	-179.8		
Fragment V	V	R	L	L	Q			
$\Phi$	-	-70.6	-69.0	-74.3	-120.2			
$\Psi$	103.1	86.4	81.3	77.4	-			
$\omega$	-	177.8	177.4	178.0	-175.8			
Tat 48-60								
Fragment I	G	R	K	K	R			
$\Phi$	-	55.6	-63.2	-81.1	-127.9			
$\Psi$	-152.6	-95.5	35.7	39.9	-			
$\omega$	-	-178.5	172.7	-179.7	-179.1			
Fragment II	K	R	R	Q	R			
$\Phi$	-	-50.8	-57.4	-90.3	-72.5			
$\Psi$	-91.1	-47.8	-26.3	-32.2	-			
$\omega$	-	-176.2	178.2	179.7	-174.1			
Fragment III	Q	R	R	R	P			
$\Phi$	-	-73.4	-79.2	-114.0	-57.3			
$\Psi$	-154.3	72.6	81.8	106.0	-			
$\omega$	-	172.6	176.5	-173.6	178.2			
Fragment IV	R	P	P	Q				
$\Phi$	-	-48.1	-58.6	-66.6				
$\Psi$	-39.8	-32.2	-29.8	-				
$\omega$	-	-179.9	170.2	-177.3				
P10								
Fragment I	R	Q	T	S	M	T		
$\Phi$	-	49.9	-59.5	-64.1	-70.5	-68.7		
$\Psi$	-28.6	-45.6	-55.9	-28.7	-44.3	-	S	
$\omega$	-	176.5	178.0	176.5	171.4	-175.4	-65.4	
Fragment II	M	T	D	F	Y	H		
$\Phi$	-	-55.5	-50.4	-64.8	-61.5	-69.7	178.1	
$\Psi$	-32.2	42.1	-41.4	-46.6	-35.7	-42.7		
$\omega$	-	-177.9	176.1	177.7	175.6	175.1		
Fragment III	Y	H	S	K	R	R	S	
$\Phi$	-	-58.0	-59.7	-58.0	-65.4	-70.8	-63.3	
$\Psi$	-29.3	-40.5	-46.0	-35.3	-29.5	-	-	
$\omega$	-	-177.8	172.6	177.4	176.9	172.0	178.8	
Fragment IV	K	R	R	L	I	F		
$\Phi$	-	-47.0	56.2	-64.8	-60.1	-64.6		
$\Psi$	146.6	-50.1	-39.5	-45.3	-42.5	-42.6		
$\omega$	-	178.5	175.3	176.5	175.2	175.3		

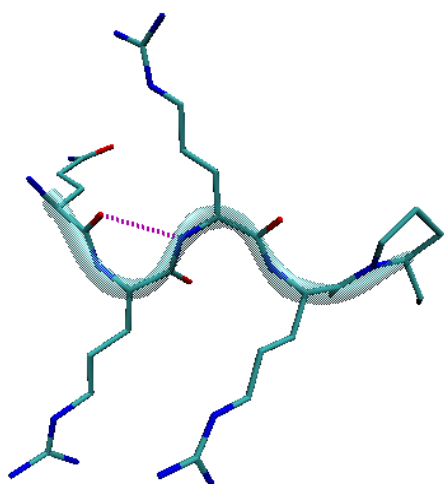


**Figure 1.** Characteristic  $2_7$  ribbon structure is observed in Vim-TBS model oligopeptide III, where arginine residues are placed consecutively.

in consideration along with the properties and functionalities of the consecutively placed residues, various model oligopeptides were designed in such a manner that each fragment was not more than 5 residues in length. As it is clear from the results in Table 3, these model oligopeptides showed variable conformations contrary to the prediction results for the peptide thus signifying the importance of length and nature of the amino acid residues. A careful and critical analysis of these results particularly in the case of model oligopeptides I & III revealed that whenever lysine and arginine are placed consecutively (model oligopeptide I) no uniform structure is formed, while a uniform helical structure was observed when only arginine residues were positioned consecutively (model oligopeptide III), as apparent from the graphical view in Figure 1. This can be explained on the basis of formation of seven membered hydrogen bonds between the carbonyl-oxygen of the  $i$ th residue and amide hydrogen of the  $i^{th}+2$  residue *i.e.*  $d_{COi...HNi+2} = 2.03, 2.27 \text{ \AA}$  and carbonyl-carbonyl interactions resulting in the formation of the  $2_7$  ribbon structure (Figure 1) (44). Thus, it would not be wrong to say that the type of positively charged residue plays a crucial role in designing a helical secondary structure of short length cationic oligopeptides like in the protamine family of cationic peptides (mainly composed of arginine 70%) (45,46). Further, a short model oligopeptide IV corresponding to residues 57-60 of Tat (48-60) (that were predicted to adopt a coiled structure) is designed specifically to contain two consecutively placed proline residues in the center. Contrary to the well known fact that proline facilitates formation of protein secondary structure elements such as turns and the polyproline II helix, but typically disfavors  $\alpha$ -helix and  $\beta$ -strand conformations (47). It was observed that in this model oligopeptide both proline residues adopt  $\Phi, \Psi$  values characteristic of  $3_{10}$  helices and further results in the formation of a strong ten membered hydrogen bond

**Table 4a.** Molecular mechanics results for Vim-TBS (58-81) peptide

Seq ↓	State I	State II	State III
G	-,141.6	-,90.1	-,146.7
G	54.2,-107.8 178.6	-49.4,-37.7 -177.8	-175.4,153.6 -178.4
A	-55.9,-38.6 177.2	-51,-41.6 175.8	-118.6,146.8 -178.9
Y	-64.5,-29.1 176.4	-66.3,-38.7 -179.6	-112.2,94 -169.8
V	-64,-49 175.5	-59.8,-55.4 175.4	-70.6,89.6 -179.6
T	-73.9,16.7 -171.5	-58.6,-35.1 175.1	-69.2,83.7 178.4
R	125.3,142.7 -174.5	-62.2,-52.9 172.2	-73.7,85.7 179.3
S	-56.3,96 -174.5	-60.2,-41.8 178.1	-121,148.1 177.4
S	-153.1,-176.1 -171.9	-66.9,-38.8 175.2	-113.5,142.8 178.2
A	-72.5,74.8 179.5	-58.5,-43.5 169.5	-72.3,83.9 176.1
V	-123.6,137.7 178.1	-58.4,-45.2 -172.8	-72.5,81.5 177.4
R	-45.68,-38.8 -178.1	-57.9,-46.1 175	-72.5,82.1 -178
L	-44.4,-39.3 176.6	-57.9,-44.6 174.8	-73.1,78.9 175
R	-81.5,46 -179	-58.7,-60.5 174.6	-117.3,99 -175.2
S	-169.1,-157 178.8	-61.2,-29.5 -177.6	-115,144.4 179.3
S	-161.6,89.3 173.5	-54.1,-34.8 173.8	-119.1,148.2 179
V	-118.9,91.3 165.9	-68.7,-48.3 179.3	-113,103.9 177.3
P	-57.9,108.1 -171.1	-54.2,-39.6 165.7	-64.6,92.6 175.4
G	64.9,164.9 -7	-54.9,-50.4 172.2	-68.6,78.8 176
V	-122.6,89.2 170.3	-56.4,-47.6 174.1	-73.7,86.6 179.5
R	-121.3,160.9 179.2	-55.8,-45.6 176.3	-69.1,84.2 177.8
L	-40.1,-46.3 -176.6	-62.7,-38.4 175.6	-69.2,80.2 176.9
L	-104.7,29.5 -177.8	-66.7,-36.6 172.6	-74.2,77 177.6
Q	-125.5,- 176.7	-63.1,- 177.7	-119.3,- -175.7
$\Delta E$ kcal/mol	29.7	0.0	96.4

between the carbonyl oxygen of the first arginine residue and the amide hydrogen of the fourth amino acid residue,  $d_{COi...HNi+3} = 1.86 \text{ \AA}$ . Energy minimization results of the various model oligopeptides of p10 revealed the formation of helical secondary structures stabilized by strong carbonyl...carbonyl interactions and a strong hydrogen bond network (Table 3).

### 3.1.2. Full-length peptides

Molecular mechanics energy minimization results of

**Table 4b. Molecular mechanics results for different conformational states of Tat (48-60) peptide and p10 peptide**

Tat (48-60) peptide			p10 peptide		
Seq.↓	I	II	Seq.↓	I	II
G	-94.6	-, -149.3	R	-, -24.6	-, -99.1
R	-62.2, -83.5	49.7, -94	Q	-48.2, -43.3	-123.5, 146.1
K	-118, -3.9	-55.4, -41.1	T	-60.1, -64.5	-69.7, 90.9
K	171.3	176.1	S	176	178.5
K	-99.9, 119.9	-58, -44.9	S	-56.9, -44.7	-67.8, 84.4
R	-169.7	176.6	M	179.3	175
R	-173.5, 153.4	-64.7, -45.2	M	-60.7, -49.4	-72.6, 85.7
R	173.5	178.7	T	177.5	-177.2
R	-49.8, -39.9	-58.7, -45.4	T	-63.8, -40.9	-70.1, 23.3
Q	169.3	175.6	D	175	-178.9
Q	-90.6, 36	-58.7, -45.2	D	-55.7, -44.5	-84.9, 34.7
R	174.8	174.1	F	172	-158.8
R	-171.4, -152.9	-60.3, -40	F	-58.6, -51.6	-88.6, 39.9
R	173.6	174.9	Y	173.2	-177.3
R	-81.9, 91.6	-63.2, -31	Y	-56, -47.4	-82.2, 81.6
R	-176.3	175.9	H	177.5	-174
R	-122, 100.3	-59, -41.5	H	-59.1, -46.2	-121.3, 100
P	163.6	-175.2	S	174.3	-172.2
P	-58.9, 135.1	-62.8, -37.7	S	-61.4, -38.7	-70.4, 82.1
P	177	172	K	174.7	176.7
P	-599, -41.7	-64.8, 41.3	K	-61.3, -46.5	-69, 80.9
Q	174.9	163.9	R	173.2	179.6
Q	-75.8, -	-61.9, -	R	-57.2, -46.3	-72.6, 76.5
	173.1	177.3	R	173.6	178.6
			R	-58.1, -42.9	-73.4, 79.4
			L	174.9	-178.6
			L	-59.2, -45.8	-75.8, 74.7
			I	173.1	-179
			I	-59.6, -43.7	-78.1, 88.7
			F	174.3	-177.2
			F	-64.1, -36.7	-122.9, 143.1
			S	176.9	176.3
			S	-60.8, -	-113.9, -
				-178.8	179.8
$\Delta E$ kcal/mol	33	0.0	$\Delta E$ kcal/mol	0.0	61.8

the full length peptides *i.e.* Vim-TBS (58-81), Tat (48-60) and p10 are as summarized in Table 4a & b.

### 3.1.3. Vim-TBS (58-81)

Three different starting conformations were taken for minimization studies based on the prediction server results as well as the model oligopeptide minimization results. The first conformation called 'State I' corresponds to a state with starting geometry obtained after model oligopeptide fragment minimization calculations. The prediction server results have shown the propensity of both  $\beta$ -strand and coil type secondary structure throughout the sequence, and therefore  $\Phi$ ,  $\Psi$  values of the other two starting conformations correspond to  $\beta$ -strand *i.e.*  $-139^\circ$ ,  $135^\circ$  (State III) and  $\alpha$ -helix *i.e.*  $-57^\circ$ ,  $-47^\circ$  (State II). It is evident from the results in Table 4a that the energetically most stable conformation is State II with  $\Phi$ ,  $\Psi$  values of  $\sim -59.3^\circ$ ,  $-45.3^\circ$  forming a characteristic  $\alpha$ -helix like secondary

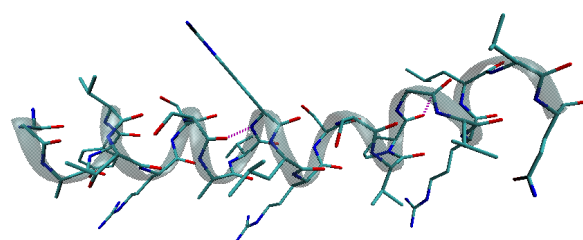


**Figure 2. Intra-strand hydrogen bond network and carbonyl-carbonyl interactions stabilize Vim-TBS (58-81) peptide in the  $\alpha$ -helical conformation.**

structure. A molecular view of this conformation given in Figure 2 depicts the typical intra-strand hydrogen bonding network along with strong carbon-carbonyl interactions. The torsion angles of various residues of State I were found to lie in the second and third quadrant of the Ramachandran plot. Consequently, both the carbonyl-carbonyl interactions and formation of hydrogen bonds lack uniformity and regularity. It

is worth mentioning that smaller model oligopeptides of Vim-TBS (58-81) (Table 3) revealed the stability of  $\beta$ -strand structure while in the full length peptide the  $\alpha$ -helical structure was observed highlighting the critical relation between peptide length and secondary structure. Consequently, future design paradigms for this peptide need to emphasize and explore this vital relation in order to achieve the best design. This is the first report on the structural characterization of Vim-TBS (58-81) peptide.

#### 3.1.4. Tat (48-60) peptide

Two different starting conformations were taken to carry out energy minimization studies viz., State I with starting conformation corresponding to  $\Phi$ ,  $\Psi$  values obtained after model oligopeptide minimization and State II with  $\Phi$ ,  $\Psi$  values corresponding to the  $\alpha$ -helical region ( $-57^\circ$ ,  $-47^\circ$ ). State II that adopted a uniform  $\alpha$ -helix type secondary structure (Table 4b) except terminal residues, was found to be energetically most stable. Helical secondary structures have already been highlighted in the literature as being necessary for cell penetration properties (48,49) because such structures seem essential particularly within the lipid phase of the membrane for its cellular uptake and stabilization. Minimization studies (at a dielectric constant of 4) have revealed that Vim-TBS (58-81) adopts a secondary structure similar to that observed in Tat (48-60), and the same mechanism of cell penetration can be attributed to Vim-TBS (58-81) based on the structure-function and activity relationships (50,51).

#### 3.1.5. p10 peptide

Similarly, two different starting conformations were selected for energy minimization studies *i.e.*, with  $\alpha$ -helix like torsion angles (State I, Table 4b) and with  $\beta$  strand like torsion angles (State II, Table 4b). On the basis of steepest descent and conjugate gradient energy minimization studies, the  $\alpha$ -helix secondary structure (State I) was found to be more stable by  $\sim 62$  kcal mol<sup>-1</sup>.

### 3.2. MD simulations

In general, conformations adopted by proteins/peptides are significantly influenced by local environmental conditions that refer to the solvation interface which communicates bulk properties of the solvent (like temperature, pressure *etc.*) to the peptide and determines localized effects about the proteins/peptides due to specific solute-solvent interactions (52). For a better understanding about conformational behavior, dynamic structure, interactions and stability of these peptides in aqueous environment, MD simulation studies were performed in explicit water. Simulation results in terms of  $\Phi$ ,  $\Psi$  and  $\omega$  values for the various

starting conformations of Tat (48-60), Vim-TBS (58-81) and p10 peptides are given in Table 5. Conformation I, II, and III of Vim-TBS (58-81) correspond to the starting geometry with  $\Phi$ ,  $\Psi$ ,  $\omega$  values obtained after MM energy minimization studies. Similarly, final conformations obtained after MM studies for Tat (48-60) and p10 peptides were the starting conformations for MD simulation studies.

Simulations in water revealed that all three peptides, Tat (48-60), Vim-TBS (58-81) and p10, adopt either a helical structure or a random conformation in water (Table 5). The energy difference between these two states is  $\sim 5$ -6 kcal/mol and is not such that it allows/favors exclusive population of any state especially when one considers the energy contribution of a single hydrogen bond *i.e.*  $\sim 2$ -5 kcal/mol (53,54). In Vim-TBS (58-81), Conformation II with average  $\Phi$ ,  $\Psi$  values of  $\sim -63^\circ$ ,  $-54^\circ$  was energetically more stable with respect to conformation I and III by 6.2 and 11.5 kcal/mol respectively. On the other hand such a helical structure (Conformation II) was energetically less stable by 5 kcal/mol in Tat (48-60) peptide. The stability of these two states is governed by the dominance or contribution of polar contacts between the solvent water molecules and the various backbone and side chain functionalities (intermolecular interactions) of the peptide. Because these two conformations are labile on the energy scale it is argued that in water both helical and random coil like structures co-exist in a dynamic state and moreover, this energy gap can be compensated by the choice of the solvent *i.e.*, in protic or aprotic environment (55). It is worth mentioning here that these results are consistent with the NMR and CD spectroscopy results that have shown the occurrence of no regular geometry in Tat (48-60) peptide. Solid-state NMR shows that Tat (48-60) is highly dynamic and adopts a random coil conformation (56). The CD spectrum studies of Tat peptide (residues 34-56) have also reported a disordered conformation in buffer solution with a strong negative band at 198 nm and weak positive ellipticity between 212 and 222 nm (57). The <sup>1</sup>H/<sup>15</sup>N HSQC spectrum of Tat has also suggested that the protein is undergoing conformational exchange on the millisecond to microsecond time scale, indicating a transient structure formation (58). It is also worth mentioning here that almost 30% of the eukaryotic proteome is intrinsically distorted under physiological conditions *i.e.*, in the absence of binding parameters these proteins or protein segments do not fold into a stable conformation but exist in a more or less restricted ensemble of conformations determined by the amino acid sequence (57). Utility of this observation lies in the fact that the unfolded proteins have an advantage over folded proteins in providing a much larger surface area enabling multiple interactions with other molecules (59).

p10 peptide adopted the helical conformation in its most stable state (Table 5) and was found to be more stable by 5.8 kcal/mol than Conformation II.

**Table 5. MD results under NVT conditions for different conformations of Tat (48-60), Vim-TBS (58-81) and p10 peptide after 1 ns simulations with  $\Phi$ ,  $\Psi$ ,  $\omega$  values**

Vim			p10		Tat	
I	II	III	I	II	I	II
-, -143.8	-, 148.6	-, -131.6	-, 172	-, 135.6	-, 121.1	-, -133.5
-	-	-	-	-	-	-
118.1, 127.8	-66.4, -161.7	-75.8, -80.3	-54, 88.6	-54.4, 113.2	-53.5, -41.5	-52.1, -51.7
175.5	-178.1	-175	175.6	167.8	180	-166.8
-42.4, -56	-53.1, -50	-62.9, -49.2	-66, -27	-93, 84	-65.5, -44.1	-51, -49.1
-165.8	-179	178	-173.7	-170	-173	180
-90, -22.2	-63.5, -52.3	-98.4, 118	-52.8, -65.2	-76.9, 80	-74.1, 107.5	-65.2, -26.3
-174	-176	170	-177.4	163.4	-173	166.6
-57.2, -51.8	-50, -55	-110.5, 130.9	-44.6, -55.4	-94.2, 86.2	-65.6, 147.6	-63.7, -38.6
179	178	179	165.9	-176	162.2	167.2
-129.4, 132	-50.1, -32	-63.2, 133.2	-74, -33.4	-76.9, -58	-51.6, -73.7	-67.2, -50
-177	178.2	164.4	-172.1	174.6	166	177.7
59, 2.3	-80.2, -57	-124.2, 129	-62.7, -52.1	-97.8, 123.4	-93.5, -73.6	-57.6, -53.3
-178.6	167.6	175	170.3	-163.3	-166.5	-177.6
57.6, 120	-58.6, -54	-167.9, 148	-49.3, -34.4	-131, 144	-107.2, 180	-60.4, -37.7
172.9	-176	-172	164.8	172.3	-178.7	174.2
-155.7, 156	-56.1, -50.6	-92, 133	-61.7, -47.7	-67, -26.8	13.8, 100	-75.2, -27.6
178.3	-176.4	-176	169.2	176.3	-179.2	180
-105, 122	-45.3, -52.5	-91, 68.2	-58, -38.3	-84.4, -79.1	-119, 118.7	-52.6, -44
-171.6	172.4	-178	171.7	-172.5	-165.7	177.3
57.7, 145	-85, -29.2	-65, 121	-65.6, -51.4	-67.7, 119.1	-63.5, 150.4	-61.4, -54.9
173	-169	-172.4	178.3	167.7	164.3	168.6
-48.4, -42.6	-70.2, -54	-123.8, 83.1	-60.9, -40.7	-108, 158.8	-60.3, 143.6	-94.6, 59.1
-166.8	175.3	176	174	-178.3	171	165.4
-63, -37.8	-53, -52.2	-111.4, 103.8	-55.3, -38.6	-135.5, 104.1	-140.7, -	-121.8, -
180	172.6	163	172	180	-173.8	171
-104.8, 29.2	-45.8, -45	-148.3, 157.7	-70, -44	-83.6, 127		
178.1	172.6	168	173.3	163.5		
-112, 108	-52.4, -35.2	-9.3, -81.3	-65.4, -28.3	-95.6, -162		
170	170.4	178	180	180		
-56, 75	-116.5, -32.4	-124, 104.9	-76, -52.1	-78.3, 142		
-176	-173	-165.4	167	163.4		
-129, 120	-55.3, -53.6	36.4, 68.7	-112, 83.5	-66.8, 113.7		
-176	180	173.7	-172.6	160.4		
-63.4, 132.6	-50, -51.8	-75.1, 139.3	-87.4, -	-126, -		
-173.4	-178.1	177.5	-173.5	-174.8		
-123, -171	-55.4, -61	-97, -107.2				
2.3	179	-167.2				
50, 61	-62.1, -27.6	-97.4, -39.3				
177.2	-171	172.5				
-116.7, 141	-77, -49	-95.7, 148				
169	168	165				
-54.4, -46	-67.7, -38.5	-71.7, 104.6				
-177	178.5	180				
-110.8, 67.7	-69.3, -91.2	-90, 124.6				
172	176	-177				
-142.6, -	-105.9, -	-127.2, -				
177	-168.4	-176.8				
$\Delta E$ 6.2	0.0	11.5	0.0	5.8	0.0	5.0

Polar contacts with water which are present in both conformations, the extensive hydrogen network of carbonyl-oxygen of ith residue with the amide hydrogen of the ith+4 residue, ( $d_{\text{COi...HNi+40}} \sim 2.0, 1.8 \text{ \AA}$ ) along with the strong carbonyl-carbonyl interactions are the major factor in the stability of the helical state.

### 3.3. Simulation studies of the fusion peptides

To establish and analyze the conformational preference

of Vim-TBS (58-81) peptide in conjunction with cargo molecules, simulations of the fusion peptide Vim-TBS (58-81)-p10 and Tat (48-60)-p10 were carried out for 1 ns in water under NVT conditions.

#### 3.3.1. Tat (48-60)-p10 peptide

Two different starting conformations were selected for the structural study of the designed fusion peptide Tat (48-60)-p10, with  $\Phi$ ,  $\Psi$  values corresponding to those

**Table 6. Simulation results for Fusion peptides (Vim-TBS(58-81)-p10 peptide and Tat(48-60)-p10 peptide) after 1ns under NVT conditions**

Vim-TBS-p10		Tat-p10	
I	II	I	II
-,-122	-,114.2	-,170	-,161.2
-	-	-	-
80.2,121.4	-76,-166.9	-56.3,-74.1	-51.4,-40
-174	179.5	178.8	-178
-61.6,-26	-67.7,-61.7	-31.6,-51.2	-127.7,-61.4
180	-158.4	171.2	178.1
-75.6,-61.5	-49.8,-55.6	-62.6,-55.6	-38.4,109.1
170	-179	177.6	166.4
-40.2,-52.7	-51.8,-41.1	-44.4,-30.9	-67,165
178	169.8	164.7	-176.6
-78.5,-38	-66,-47.7	-67.5,-56	-63.3,-56.4
-174.3	174.5	165.5	179.4
-96.8,-78.7	-65.1,-46.2	-45.7,-47.8	-125.4,-58.4
178.5	-175.7	173.8	-166.7
-51.7,-52.6	-42.6,-55.8	-52.8,-50.5	-113.8,145.5
-172.3	177.3	174	170.9
-60.3,-56	-65.1,-28.9	-87.7,0.5	68.3,63.5
179.3	-177.3	176.4	173.9
-53.7,-44.8	-71.4,-41.4	-76.5,-40.2	-85.4,111.6
174.6	175.1	-170.6	-176.8
-52.6,-67	-46.5,-43.8	-61.7,-52.4	-73,115.2
175.6	163.5	161.8	175.6
-39.4,-63.3	-78.6,-55	-49,-41.5	-58.6,148.3
174.2	-176.7	175.3	178.6
-48.3,-51.1	-45,-53.7	-54.6,-40.9	-119.4,169.2
171.1	171.4	173.3	-164.4
-38.3,-40	-57.8,-44.3	-71.6,-48.3	-122.2,114.4
177.6	-179	175.3	177.3
-81.7,-30.8	-67.2,-32.5	-61.5,-32.7	70,94.1
166	178.6	-177.7	169.2
-90,-37	-67.5,-40	-71.8,-48.5	-55.4,-52.1
-166.6	175.7	168.6	-173.6
-52,-39.2	-60,-47	-55,-53.4	-43.7,-50
167.6	-171.7	167.4	174
-54.7,-64.3	-57.4,-40	-54.7,-3.2	-69.5,-29
174.1	167.8	-179.1	-175.2
-54.4,-42.8	-65.7,-56.4	-57.8,-54.7	-112,-95
-173.2	-177.7	-176.4	-175.5
-61,-54.3	-59.1,-35	-42.3,-42.4	-35,-66.5
177.5	176	173	176.9
-62.3,-51.5	-75,-28.7	-58,-65.4	-59.2,-51.7
-176.7	-173.9	177.1	180
-50,-44.1	-75,-40.3	-52.3,-41.7	-50.5,-41.9
170.2	175.8	173.8	172.5
-59,-65.3	-70.2,-43.9	-64.7,-39.4	-70,-37.2
171.7	172.8	173	176.4
-46.2,-48	-109.5,91.4	-54.5,-50.1	-48.9,-53.5
-172.4	175	175.3	162.1
-62.5,-44.7	-74.7,147.7	-57.2,-42.1	-57.1,-42.1
180	-164.3	177.4	165.4
-56.2,-38.1	56.6,129.1	-61.4,-53.5	-66.5,-61.8
173.1	-177.8	171.4	173.8
-76.6,-28.7	-77.3,-10	-58.4,-34.4	-53,-25.6
178.8	-174.4	-175.1	-178.5
-81.4,-29	-87,-45.8	-65.7,-45.5	-91,-48.2
166.2	168.8	176.2	178
-63,-48.5	-45.2,-55	-93.1,-21.5	-109.6,-67.4
167.8	171.7	-176.3	-171.5
-59.3,-35.3	-60.4,-40	-128.4,123.3	-116,101.5
173.8	172.5	-172.2	-175
-70.4,-38.1	-60,-45	-75,-	-130.7,-
174.7	-178	-172.5	180

**Table 6. Simulation results for Fusion peptides (Vim-TBS(58-81)-p10 peptide and Tat(48-60)-p10 peptide) after 1ns under NVT conditions (Continued)**

Vim-TBS-p10		Tat-p10	
I	II	I	II
-57.4,-56.6	-61.4,-50.4		
168.5	174.5		
-49.4,-53	-49.2,-55.6		
170.6	169.4		
-58,-56	-56.6,-42.7		
177.3	-179.8		
-54.8,-47.5	-54.1,-55.3		
176	1763.9		
-63.2,-44.6	-51.2,-52		
170.7	167.4		
-70.1,-25.4	-64,-26		
177.3	-176.1		
-70,-27.8	-81.1,-34.8		
162.8	173		
-75.3,-41.7	-60,-48.2		
168.1	171.6		
-65.8,-44.2	-74.6,-22.2		
173	173		
-134.6,136.5	62,67.5		
-176.4	-179		
-142.2,-	-133.5,-		
179	179.3		
ΔE	0.0	16.8	0.0
			11.3

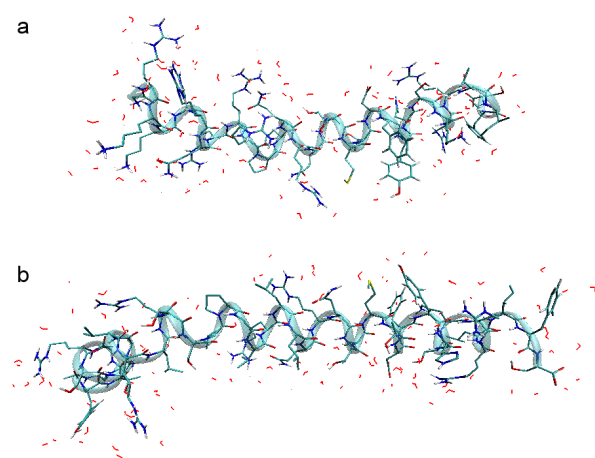


**Figure 3. Graphical views of the (a) Tat (48-60)-p10 fusion peptide, (b) Vim-TBS (58-81)-p10 fusion peptide; in the most stable  $\alpha$ -helical conformations (water molecules within 3 Å of the peptide surface are shown).**

obtained after MD simulations of individual peptides (Conformation I) and with  $\Phi$ ,  $\Psi$  values of  $-57^\circ$ ,  $-47^\circ$  (Conformation II). In the energetically most stable state it was found to adopt  $\Phi$ ,  $\Psi$  values that lie in the  $\alpha$ -helical region (Table 6, Figure 3a). Although, Tat peptide is unstructured in solution there are several reports suggesting the possibility of a conformational change to augment binding (60,61). These results are also supported by NMR spectroscopy and CD spectroscopy studies of a fusion protein consisting of the activation domain for the unreleased equine infectious anemia

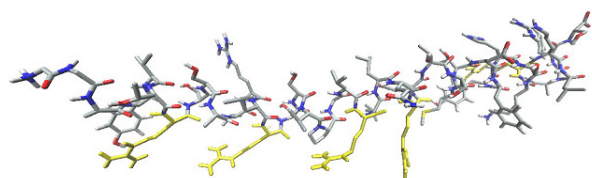


**Figure 4. Molecular view of the characteristic amphipathic structure formed in the fusion peptide Vim-TBS (58-81)-p10.** The hydrophilic face formed by arginine sidechains is displayed in yellow.

virus and Tat (48-57) that reported a highly helical conformation (62). Also 15N NMR relaxation measurements showed that Tat (47-58) became more ordered when binding heparin (63). Tat (48-60) has been reported to retain the penetrating properties of the full length HIV-Tat protein (64) and also is an effective vehicle for the delivery of biologically active peptide cargoes (65). Further, it retains a nuclear localization signal, has relatively low intrinsic toxicity and was thus considered to be an ideal candidate to deliver the p10 peptide to the nucleus. Arginine rich HIV-Tat peptide is able to translocate by destabilizing and inducing transient pores in phospholipid bilayers. The Arginine clusters can strongly interact with lipid head groups on the distal surface of the bilayer to drive translocation. The unstructured CPPs stabilize their backbone polar groups by forming transient intermolecular H-bonds with the lipid phosphates and water (66).

### 3.3.2. *Vim-TBS (58-81)-p10 peptide*

For the complete structural study of Vim-TBS (58-81)-p10 designed fusion peptide, different starting geometries were taken with  $\Phi$ ,  $\Psi$  values corresponding to those obtained after MD simulations of individual peptides (Conformation I) and with  $\Phi$ ,  $\Psi$  values of  $-57^\circ$ ,  $-47^\circ$  (Conformation II). Simulation results given in Table 6 reveal that the energetically most stable conformation (by 16.8 kcal/mol) corresponds to  $\alpha$ -helix type secondary structure with average  $\Phi$ ,  $\Psi$  values of  $-60^\circ$ ,  $-40^\circ$ . A molecular representation of this conformational state is shown in Figure 3b. It is evident that although both the fusion peptides form a helical structure in the most stable states but the structure obtained in the case of Vim-TBS-p10 fusion peptide is better characterized in terms of its amphipathic nature with defined hydrophilic and hydrophobic faces as revealed in the molecular view given in Figure 4. A similar structure was reported for Tat-p10 fusion peptide (67) and on this basis, it is suggested that the hydrophilic face formed by the positively charged arginine and lysine residues shall thus facilitate a better interaction of this fusion peptide with the membrane. Therefore, we predict Vim-TBS to display better cell penetrating properties and act as a potential drug delivery agent. This finding is well supported by the observations of Balzeau et al. that this fusion peptide

accumulates and distributes in glioblastoma cells (25). Furthermore, this fusion peptide crosses the plasma membrane and localizes to the nucleus where p10 maintains its pro-apoptogenic activity. In contrast, when the p10 peptide is ligated to the Tat (48-60) peptide, entry to the nucleus is strongly reduced and its pro-apoptogenic activity is also attenuated (25).

## 4. Discussion

The critical relation between peptide length and secondary structure was highlighted by the formation of stable  $\beta$ -strand like secondary structures in model oligopeptides of Vim-TBS (58-81) while the full length peptide was found to be stable when adopting an  $\alpha$ -helical structure. Such structures are particularly stabilized by minimization of steric constraints imposed by the lengthy and/or bulky aromatic and/or charged side chains. In the model oligopeptides of the Tat (48-60) peptide the population of variable conformations contrary to the prediction results further signified the importance of length and nature of the amino acid residues. Also, the type of positively charged residues (lys or arg) played a crucial role in the formation of stable helical secondary structures in short length cationic oligopeptides. Molecular mechanics energy minimization results of the full length peptides, Vim-TBS (58-81), Tat (48-60) and p10, revealed that the energetically most stable conformation formed a characteristic  $\alpha$ -helix like secondary structure. In water the three peptides adopted either a helical structure or a random conformation with an energy difference between the two states being  $\sim 5$ -6 kcal/mol which is not large enough to allow exclusive population of any state. The peptide Vim-TBS (58-81) had average  $\Phi$ ,  $\Psi$  values of  $\sim -63^\circ$ ,  $-54^\circ$  while in the Tat (48-60) peptide such a helical structure was marginally less stable. The stability of either of the two states is administered by the formation of polar contacts between the solvent water molecules and the various backbone and side chain functionalities (intermolecular interactions) of the peptide. Because these two conformations are labile on the energy scale it is argued that in water both helical and random coil like structures co-exist in a dynamic state. To establish and analyze the conformational preference of Vim-TBS (58-81) peptide in conjunction with cargo molecules, simulations of the fusion peptide Vim-TBS (58-81)-p10 and Tat (48-60)-p10 were carried out. Although, both fusion peptides formed helical structures the structure obtained for the fusion peptide; Vim-TBS-p10 is relatively better characterized in terms of its amphipathic nature with defined hydrophilic and hydrophobic faces. Consequently, the hydrophilic face formed by the positively charged residues should facilitate a better interaction of this fusion peptide with the membrane as compare to that of the Tat-p10 peptide. Such an acquired amphipathicity upon secondary structure induction

may guide the anchoring of the CPP in the hydrophobic region of the membrane. Thus, we predict Vim-TBS (48-60) peptide to display better cell penetrating properties and hence, act as a potential drug delivery agent.

## References

- Lindgren M, Hallbrink M, Prochiantz A, Langel U. Cell-penetrating peptides. Trends Pharmacol Sci. 2000; 21:99-103.
- Fatemeh M, Lindberg S, Langel U, Futaki S, Graslund A. Mechanisms of cellular uptake of cell-penetrating peptides. J Biophys. 2011; 2011:1-10.
- Trabulo S, Resina S, Simoes S, Lebleu B, Lima PMC. A non-covalent strategy combining cationic lipids and CPPs to enhance the delivery of splice correcting oligonucleotides. Mol Ther Nucleic Acids. 2010; 145:149-158.
- Brooks NA, Pouniotis DS, Tang CK, Apostolopoulos V, Pietersz GA. Cell-penetrating peptides: Application in vaccine delivery. Biochim Biophys Acta. 2010; 1805:25-34.
- Endoh T, Ohtsuki T. Cellular siRNA delivery using cell-penetrating peptides modified for endosomal escape. Adv Drug Deliv Rev. 2009; 61:704-709.
- Foged C, HM Nielsen. Cell-penetrating peptides for drug delivery across membrane barriers. Expert Opin Drug Deliv. 2008; 5:105-117.
- Grdisa M. The delivery of biologically active (therapeutic) peptides and proteins into cells. Curr Med Chem. 2011; 18:1373-1379.
- Jafari M, Chen P. Peptide mediated siRNA delivery. Curr Top Med Chem. 2009; 9:1088-1097.
- Johnson RM, Harrison SD, Maclean D. Therapeutic applications of cell-penetrating peptides. Methods Mol Biol. 2011; 683:535-551.
- Stewart KM, Horton KL, Kelley SO. Cell-penetrating peptides as delivery vehicles for biology and medicine. Org Biomol Chem. 2008; 6:2242-2255.
- Torchilin VP. Cell penetrating peptide-modified pharmaceutical nanocarriers for intracellular drug and gene delivery. Biopolymers 2008; 90:604-610.
- Snyder EL, Dowdy SF. Cell penetrating peptides in drug delivery. Pharmaceutical Research. 2004; 21:3.
- Niesner U, Halin C, Lozzi L, Gunthert M, Neri P, Wundern-Allenspach H, Zardi L, Neri D. Quantitation of the tumor-targeting properties of antibody fragments conjugated to cell-permeating HIV-1 TAT peptides. Bioconjug Chem. 2002; 13:729-736.
- Astriab-Fisher A, Sergueev D, Fisher M, Shaw BR, Juliano RL. Conjugates of antisense oligonucleosides with the Tat and antenapedia cell-penetrating peptides: Effects on cellular uptake, binding to target sequences, and biologic actions. Pharm Res. 2002; 19:744-754.
- Torchilin VP, Levchenko TS, Rammohan R, Volodina N, Papahadjopoulos-Stenberg B, D'Souza GC. Cell transfection *in vitro* and *in vivo* with nontoxic TAT peptide-liposome-DNA complexes. Proc Natl Acad Sci USA. 2003; 100:1972-1977.
- Herce, HD, Garcia AE. Molecular dynamics simulations suggest a mechanism for translocation of the HIV-1 TAT peptide across lipid membranes. Proc Natl Acad Sci USA. 2007; 104:20805-20810.
- Kersemans V, Kersemans K, Comelissen B. Cell penetrating peptides for *in vivo* molecular imaging applications. Curr Pharm Des. 2008; 14:2415-2447.
- Zorko M, Langel U. Cell-penetrating peptides: Mechanism and kinetics of cargo delivery. Adv Drug Del Reviews. 2005; 57:529-545.
- Eiriksdóttir E, Konate K, Langel U, Divita G, Deshayes S. Secondary structure of cell-penetrating peptides controls membrane interaction and insertion. Biochim Biophys Acta. 2010; 1798:1119-1128.
- Morris MC, Depollier J, Mery J, Heitz F, Divita G. A peptide carrier for the delivery of biologically active proteins into mammalian cells. Nat Biotechnol. 2001; 19:1173-1176.
- Meade BR, Dowdy SF. Exogenous siRNA delivery using peptide transduction domains/cell penetrating peptides. Adv Drug Deliv Rev. 2007; 59:134-140.
- Coulombe PA, Wong P. Cytoplasmic intermediate filaments revealed as dynamic and multipurpose scaffolds. Nature Cell Biol. 2004; 6:699-706.
- Raphael B, Julien B, Peterson AC, Eyer J. The vimentin-tubulin binding site peptide (Vim-TBS.58-81) crosses the plasma membrane and enters the nuclei of human glioma cells. Int J Pharma. 2011; 423:77-83.
- Richard JP, Melikov K, Vives E, Ramos C, Verbuere B, Gait MJ, Chernomordik LV, Lebleu B. Cell-penetrating peptides. A reevaluation of the mechanism of cellular uptake. J Biol Chem. 2003; 278:585-590.
- Balzeau J, Peterson A, Eyer J. The vimentin-tubulin binding site peptide (Vim-TBS.58-81) crosses the plasma membrane and enters the nuclei of human glioma cells. Int J Pharm. 2012; 4:77-83.
- Baker RD, Howl J, Nicholl ID. A synchological cell penetrating peptide mimic of p21 (WAF1/CIP1) is pro-apoptogenic. Peptides 2007; 28:731-740.
- Mutoh M, Lung FD, Long YQ, Roller PP, Sikorski RS, Connor PMO. A p21(Waf1/Cip1) carboxyl-terminal peptide exhibited cyclin-dependent kinase-inhibitory activity and cytotoxicity when introduced into human cells. Cancer Res. 1999; 59:3480-3488.
- Warbrick E, Lane DP, Glover DM, Cox LS. A small peptide inhibitor of DNA-replication defines the site of interaction between the cyclin-dependant kinase inhibitor p21(WAF1) and proliferating cell nuclear antigen. Curr Biol. 1995; 5:275-282.
- Jones AT. Protein secondary structure prediction based on position-specific scoring matrices. J Mol Biol. 1999; 292:195-202.
- Johansson MU, Zoete V, Michielin O, Guex N. Defining and searching for structural motifs using DeepView/Swiss-PdbViewer. BMC Bioinformatics. 2012; 13:173.
- Van der Spoel D, Lindahl E, Hess B, van Buuren AR, Apol E, Meulenhoff PJ, Tieleman DP, Sijbers ALTM, Feenstra KA, Van Drunen R, Berendsen HJC. Gromacs User Manual version 3.3, 2005.
- Berendsen HJC, Postma JPM, Van Gunsteren WF, Hermans J. Intermolecular Forces: Interaction models for water in relation to protein hydration. D. Reidel Publishing Company, Dordrecht, 1981; 331-342.
- Hockney RW, Eastwood JW. Computer simulation using particles. McGraw-Hill, New York, USA, 1981.
- Berendsen HJC, Postma JPM, DiNola A, Haak JR. Molecular dynamics with coupling to an external bath. J Chem Phys. 1984; 81:3684-3690.
- Hess B, Bekker H, Berendsen HJC, Fraaije JGEM. A linear constraint solver for molecular simulations. J

- Comp Chem. 1997; 18:1463-1472.
36. Essmann U, Perera L, Berkowitz ML, Darden T, Lee H, Pedersen LG. A smooth particle mesh Ewald method. *J Chem Phys.* 1995; 103:8577-8592.
  37. Humphrey W, Dalke A, Schulten K. VMD-Visual Molecular Dynamics. *J Molec Graphics.* 1996; 14:33-38.
  38. Nandel FS, Saini A. Peptoids with aliphatic sidechains as helical structures without hydrogen bonds and collagen/inverse-collagen type structures. *Journal of Biophysical Chemistry* 2011; 2:37-48.
  39. Nandel FS, Saini A. Construction and design of single stranded collagen-like structure. *Indian journal of biochemistry & biophysics.* 2007; 44:106-113.
  40. Nandel FS, Saini A. Conformational study of short peptoid models for future applications as potent antimicrobial compounds. *Macromolecular Theory and Simulations.* 2007; 16:295-303.
  41. Alias M, Ayuso-Tejedor S, Fernandez-Recio J, Cativiela C, Sancho J. Helix propensities of conformationally restricted amino acids. Non-natural substitutes for helix breaking proline and helix forming alanine. *Org Biomol Chem.* 2010; 8:788-792.
  42. Voet D, Voet JG, Pratt CW. *Fundamentals of Biochemistry.* John Wiley and Sons, New York, 2004.
  43. Gunasekaran K, Nagarajaram HA, Ramakrishnan C, Balam P. Stereochemical Punctuation Marks in Protein Structures: Glycine and Proline Containing Helix Stop Signals. *J Mol Biol.* 1998; 275:917-932.
  44. Nandel FS, Jaswal R. New Type of Helix and  $2_7$  Ribbon Structure Formation in Poly  $\Delta$ Leu Peptides: Construction of a Single-Handed Template. *Biomacromolecules.* 2007; 8:3093-3101.
  45. Niidome T, Takaji K, Urakawa M, Ohmori N, Wada A, Hirayama T, Aoyagi H. Chain length of cationic  $\alpha$ -helical peptide sufficient for gene delivery into cells. *Bioconjugate chemistry.* 1999; 10:773-780.
  46. Hilda C, Arellano A. Secondary structure prediction of protamines. *Int J Biol Macromol.* 1982; 1:3-8.
  47. Aduzbei AA, Sternberg JE. Left-handed polyproline II helices commonly occur in globular proteins. *J Mol Biol.* 1993; 229:472-493.
  48. Vives E, Brodin P, Lebleu B. A truncated HIV-1 Tat protein basic domain rapidly translocates through the plasma membrane and accumulates in the cell nucleus. *J Biol Chem.* 1997; 272:16010-16017.
  49. Mujeeb A, Bishop K, Peterlin BM, Turck C, Parslow TG, James TL. NMR structure of a biologically active peptide containing the RNA-binding domain of human immunodeficiency virus type 1 Tat. *Proc Natl Acad Sci U S A.* 1994; 91:8248-8252.
  50. Ambriz-Rivas M, Pastor N, Rio GD. Relating Protein Structure and Function Through a Bijection and Its Implications on Protein Structure Prediction. *Protein Interactions.* Dr. Jianfeng Cai (Ed.), 2012; ISBN: 978-953-51-0244-1.
  51. Mirsky AE, Pauling L. On the structure of native, denatured, and coagulated proteins. *Proc Natl Acad Sci U S A.* 1936; 22:439-447.
  52. Nemethy G, Peer WJ, Scheraga HA. Effect of Protein-Solvent Interactions on Protein Conformation Annual Review of Biophysics and Bioengineering 1981; 10: 459-497.
  53. Mitchell JBO, Price SL. The nature of the N-H O=C hydrogen bond-- An intermolecular perturbation-theory study of the formamide formaldehyde complex. *J Comp Chem.* 1990; 11: 1217-1233.
  54. BenTal N, Sitkoff D, Topol IA, Yang AS, Burt SK, Honig B. Free energy of amide hydrogen bond formation in vacuum, in water, and in liquid alkane solution. *J Phys Chem B* 1997; 101: 450-457.
  55. Miranda LP, Alewood PF. Chemistry-Accelerated chemical synthesis of peptides and small proteins. *Proc Natl Acad Sci USA* 1999; 96: 1181-1186.
  56. Yongchao S, Alan JW, Ruchala P, Hong M. Membrane-bound dynamic structure of an arginine-rich cell-penetrating peptide, the protein transduction domain of HIV Tat, from solid-state NMR. *Biochemistry* 2010; 49:6009-6020.
  57. McQueen P, Donald LJ, Vo TN, Nguyen DH, Griffiths H, Shojania S, Standing KG, O'Neil JD. Tat peptide-calmodulin binding studies and bioinformatics of HIV-1 protein-calmodulin interactions. *Proteins.* 2011; 79:2233-2246.
  58. Shojania S, O'Neil JD. HIV-1 Tat is a natively unfolded protein: the solution conformation and dynamics of reduced HIV-1 Tat-(1-72) by NMR spectroscopy. *J Biol Chem.* 2006; 281:8347-8356.
  59. Gunasekaran K, Tsai CJ, Kumar S, Zanuy D, Nussinov R. Extended disordered proteins: targeting function with less scaffold. *Trends Biochem Sci.* 2003; 28:81-85.
  60. Dennison SR, Baker RD, Nicholl ID, Phoenix DA. Interactions of cell penetrating peptide Tat with model membranes: A biophysical study. *Biochemical and Biophysical Research Communications.* 2007; 363:178-182.
  61. Tunnemann G, Martin RM, Haupt S, Patsch C, Edenhofer F, Cardoso MC. Cargo-dependent mode of uptake and bioavailability of TAT-containing proteins and peptides in living cells. *FASEB J.* 2006; 20:1775-1784.
  62. Puglisi JD, Tan R, Calnan BJ, Frankel AD, Williamson JR. Conformation of the TAR RNA-arginine complex by NMR spectroscopy. *Science.* 1992; 257:76-80.
  63. Hakansson S, Caffrey M. Structural and dynamic properties of the HIV-1 tat transduction domain in the free and heparin-bound states. *Biochemistry.* 2003; 42:8999-9006.
  64. Thoren PE, Persson D, Lincoln P, Norden B. Membrane destabilizing properties of cell-penetrating peptides. *Biophys Chem.* 2005; 114:169-179.
  65. Kaplan IM, Wadia JS, Dowdy SF. Cationic TAT peptide transduction domain enters cells by macropinocytosis. *J Control Release.* 2005; 102:247-253.
  66. Su Y, Waring AJ, Ruchala P, Hong M. Membrane-bound dynamic structure of an arginine-rich cell-penetrating peptide, the protein transduction domain of HIV-Tat from solid-state NMR. *Biochemistry.* 2010; 49:6009-6020.
  67. Ho A, Schwarze SR, Mermelstein SJ, Waksman G, Dowdy SF. Synthetic Protein Transduction Domains: Enhanced Transduction Potential *in vitro* and *in vivo*. *Cancer Res.* 2001; 61:474-477.

(Received August 21, 2013; Revised October 10, 2013; Accepted October 14, 2013)

## Characterization of anti-Tn-antigen MLS128 binding proteins involved in inhibiting the growth of human colorectal cancer cells

Normaiza Zamri<sup>1</sup>, Naoya Masuda<sup>1</sup>, Fumie Oura<sup>1</sup>, Kazuya Kabayama<sup>2</sup>, Yukiko Yajima<sup>1</sup>, Hiroshi Nakada<sup>3</sup>, Kazuo Yamamoto<sup>4</sup>, Yoko Fujita-Yamaguchi<sup>1,\*</sup>

<sup>1</sup>Department of Applied Biochemistry, Tokai University School of Engineering, Kanagawa, Japan;

<sup>2</sup>Institute of Glycoscience, Tokai University, Kanagawa, Japan;

<sup>3</sup>Department of Molecular Bioscience, Faculty of Life Sciences, Kyoto Sangyo University, Kyoto, Japan;

<sup>4</sup>Department of Integrated Biosciences, Graduate School of Frontier Sciences, University of Tokyo, Kashiwa, Chiba, Japan.

### Summary

MLS128 monoclonal antibody, which binds an epitope consisting of two or three consecutive Tn-antigens, inhibits colon cancer cell growth by binding to a 110 kDa glycoprotein (GP). Previous studies suggested a possible association of insulin-like growth factor-I receptor (IGF-IR) signaling in the inhibition of colon cancer cell growth by MLS128 (Morita *et al. Biosci Trends.* 3, 32-37, 2009; Zamri *et al. ibid.* 6, 303-312, 2012). The current study thus investigated the nature of 110 kDa GP and its possible association with IGF-IR. MLS128 treatment for 3 days caused down-regulation of IGF-IR and disappearance of 110 kDa GP in HT29 colon cancer cells. Immunoprecipitation/immunoblotting experiments did not reveal a direct association between the two molecules in HT29 cells. In LS180 and HT29 cells, however, 110 kDa GP and IGF-IR were found in microdomains. Treatment of these cells with MLS128 for 3 days caused a reduction in the IGF-IR and 110 kDa GP associated with microdomains. Two-dimensional gel electrophoresis/MLS128 immunoblotting of HT29 and LS180 cell lysates and immunoprecipitates revealed three spots, from which tryptic peptides were recovered for protein sequencing. Identification of 110 kDa GP was unsuccessful due to its heterogeneity and resistance to tryptic digestion. During this study, however, limited proteolysis of 110 kDa GP was observed in the microdomain-associated 110 kDa GP from HT29 and LS180 cells, suggesting that protease-susceptible sites or domains exist in the middle of 110 kDa GP. This information on limited proteolysis may provide a clue to identifying 110 kDa GP.

**Keywords:** Mucin-type O-glycans, microdomains, limited proteolysis, immunoprecipitation, immunoblotting, two-dimensional gel electrophoresis

### 1. Introduction

A common O-linked glycosylation with N-acetyl-galactosamine (GalNAc) occurs at serine or threonine residues of glycoproteins (GPs), including mucins. GalNAc $\alpha$ -Ser/Thr, which is known as Tn-antigen, is the precursor for all mucin-type O-glycans. Tn-antigens

are shielded by extended glycosylation in healthy and benign tissues but are uncovered in approximately 90% of carcinomas (1,2). The anti-Tn monoclonal antibodies (mAbs) MLS128 and 83D4 were produced two decades ago by immunizing mice with "cancerous antigens" respectively derived from LS180 colon cancer cells and breast carcinoma tissue (3-5).

MLS128 is IgG<sub>3</sub> that recognizes the structure of two or three consecutively arranged GalNAc of Tn-antigens (5). Osinaga *et al.* used surface plasmon resonance (SPR) to measure the kinetic parameters for anti-Tn-antigen 83D4 and MLS128, and they showed that MLS128 binds to a synthetic glycopeptide, Tn3, with approximately 10 times higher affinity than for

\*Address correspondence to:

Dr. Yoko Fujita-Yamaguchi, Department of Applied Biochemistry, Tokai University School of Engineering, 4-1-1 Kitakaname, Hiratsuka, Kanagawa 259-1292, Japan.

E-mail: yokoyamaguchi@tokai-u.jp

Tn2 whereas 83D4 binds to both glycopeptides with a similar level of affinity (6). Recent efforts by the current authors have focused on molecular cloning of the variable domains of MLS128 (7) and determining the thermodynamic properties of Tn3 affinity for MLS128 (8). The current authors previously reported that MLS128 significantly inhibits breast and colon cancer cell growth and suggested involvement of insulin-like growth factor-I receptor (IGF-IR) signaling in MLS128's inhibition of cancer cell growth (9). More recently, the current authors indicated that a 110 kDa GP is the receptor for MLS128 in colon cancer cells (10). That work yielded two significant findings.

First, treating three colon cancer cell lines, LS180, LS174T, and HT29, with MLS128 for 3 days resulted in inhibition of their cell growth and obvious disappearance of the 110 kDa band as indicated by immunoblotting with MLS128. The disappearance of the 110 kDa band was clearly evident in HT29 cells on Day 1, 2, and 3 after the mAb treatment but the disappearance of the 110 kDa band was seen only on Day 3 after the treatment of LS180 and LS174T cells. The disappearance of the 110 kDa band could be explained by either the loss of the Tn-antigen epitopes on the protein backbone or degradation of the protein backbone itself. Second, the growth of colon cancer cells depends in part on IGF-IR signaling, as suggested by anti-IGF-IR mAb treatment that inhibited cell growth *via* IGF-IR down-regulation. MLS128 treatment of LS180, LS174T, and HT29 cells did not significantly cause IGF-IR down-regulation as previously described except for HT29 cells on Day 3 (10). That study revealed that MLS128 bound specifically to 110 kDa GP in the three colon cancer cell lines examined and that IGF-IR signaling was not associated with MLS128's inhibition of the growth of LS180 and LS174T cells. Results, however, did not exclude a possible link between IGF-IR- and 110 kDa GP-mediated growth signaling pathways in HT29 cells.

Based on the above findings, the current study has further characterized the 110 kDa GP in order to understand MLS128's inhibitory action on cell growth in HT29 and LS180 colon cancer cells. Specifically, the original working hypothesis regarding the interaction between IGF-IR and the 110kDa GP has been intensively tested using HT29 colon cancer cells.

## 2. Materials and Methods

### 2.1. Materials

Production and characterization of MLS128 (anti-Tn antigen IgG<sub>3</sub>) and 1H7 (anti-IGF-IR IgG<sub>1</sub>) mAbs were previously described (1-4 and 11-14, respectively). LS180 and HT29 human colon adenocarcinoma cells were obtained from the American Tissue Type Culture Collection. Rabbit anti-IGF-IRβ (#3027) was purchased from Cell Signaling Technology (Beverly, MA, USA).

Mouse anti-actin clone C4 antibody was obtained from MP Biomedicals, LLC. (Santa Ana, CA, USA). Rabbit anti-Src family kinase (SFK) (SRC 2; sc-18) was purchased from Santa Cruz Biotechnology (Santa Cruz, CA, USA). Anti-rabbit or -mouse secondary antibody labeled with biotin was from Kirkegaard & Perry Lab. (Gaithersburg, MD, USA). Cell culture media (DMEM and McCoy's 5A) were purchased from Invitrogen (Carlsbad, CA, USA).

### 2.2. Cell culture

LS180 cells were cultured in DMEM containing 10% fetal bovine serum (FBS) supplemented with 4.5 mg/mL D-glucose and 110 µg/mL pyruvic acid. HT29 cells were cultured in McCoy's 5A containing 10% FBS. All culture media included a 1% penicillin-streptomycin solution (Sigma-Aldrich, St. Louis, MO, USA).

### 2.3. Effects of 1H7 or MLS128 on the growth of colon cancer cells

Cells ( $1 \times 10^4$ ) were plated in wells of a 96-well plate and cultured in 100 µL of respective media containing 10% FBS for 24 h. Attached cells were then washed twice with 10 mM phosphate buffer, pH 7.4, containing 0.14 M NaCl (PBS), and cultured in 100 µL of media containing 1% FBS in the presence or absence of MLS128 (25 µg/mL) or 1H7 (0.36 µg/mL) (*Note*: The mAb concentrations used were different due to the difference in their affinities for respective ligands or shed mucins which sequester MLS128 from binding to cell surface receptors). After culturing for 72 h, cell growth was determined using a CCK-8 cell counting kit (Dojindo, Kumamoto, Japan) in accordance with the manufacturer's instructions. Absorbance at 450 nm was measured with a plate reader (Bio-Rad, Hercules, CA, USA). Quadruple wells were prepared for each data point.

### 2.4. Western blotting

HT29 colon cancer cells were collected by scraping. They were then centrifuged at  $200 \times g$  for 5 min and solubilized in 50 mM Tris-HCl buffer, pH 7.4, containing 1% NP40, 2 mM EDTA, 100 mM NaCl, 10 mM sodium orthovanadate, 1 mM phenylmethylsulfonyl fluoride (PMSF), and protease inhibitors (Sigma-Aldrich P2714) (Lysis buffer A) on ice for 15 min. Supernatants were obtained from solubilized cells by centrifugation at  $17,000 \times g$  for 10 min. Protein concentrations were measured using the Bradford method. The solubilized proteins (2 µg) were separated by sodium dodecyl sulfate-polyacrylamide gel electrophoresis (SDS-PAGE) and transferred to polyvinylidene difluoride (PVDF) membranes. The membrane was blocked with 3% bovine serum albumin (BSA) in 50 mM Tris-HCl buffer, pH 7.4, containing 0.15 M NaCl and 1% Tween 20 for 1 h at

room temperature. Western blotting was carried out with anti-IGF-IR and MLS128 as primary antibodies. Bound primary antibodies were then detected with biotin-labeled secondary antibodies using the Vectastain ABC-Amp kit and an alkaline phosphatase kit (Vector Laboratories, Inc. Burlingame, CA, USA).

#### 2.5. Effects of 1H7 or MLS128 treatment on IGF-IR and 110kDa GP levels in HT29 colon cancer cells

HT29 colon cancer cells ( $8 \times 10^5$ ) were cultured in the media containing 10% FBS for 24 h in wells of 6-well plates. Cells were then cultured in the media containing 1% FBS in the presence or absence of MLS128 (25  $\mu\text{g}/\text{mL}$ ) or 1H7 (0.36  $\mu\text{g}/\text{mL}$ ). After culturing for 24, 48, and 72 h, cells were collected and solubilized in 50  $\mu\text{L}$  of the lysis buffer as described above. The solubilized proteins (2  $\mu\text{g}$  per lane) were separated by SDS-PAGE and transferred to PVDF membranes. Western blotting was performed thereafter as described above using primary antibodies against 110 kDa GP (1.6  $\mu\text{g}/\text{mL}$  MLS128), IGF-IR  $\beta$  subunit (1000-fold dilution), and  $\beta$ -actin (20,000-fold dilution). Bound primary antibodies were visualized and then analyzed using an NIH Image 1.63 Analysis system (Research Services Branch, the US National Institute of Mental Health).

#### 2.6. Immunoprecipitation (IP) and immunoblotting (IB) of IGF-IR or 110 kDa GP using 1H7, MLS128, and control antibodies from HT29 cell lysates

Whether IGF-IR and 110 kDa are associated or not was determined by IP with anti-IGF-IR, or MLS128, or control IgG<sub>3</sub> from cell lysates followed by IB. HT29 colon cancer cells cultured in the media containing 10% FBS in 150 mm dishes were collected by scraping and then centrifuged at  $200 \times g$  for 5 min. After they were washed with PBS, the cells were suspended in 1 mL of the lysis buffer on ice for 15 min. Supernatants obtained by centrifugation at  $17,000 \times g$  for 15 min were incubated with 20  $\mu\text{L}$  of protein G Sepharose at 4°C for 1 h by rotating. After centrifugation at  $17,000 \times g$  for 10 min, protein concentrations of the supernatants were determined. Lysis buffer A was added to yield a concentration of 500  $\mu\text{g}$  protein/200  $\mu\text{L}$ , to which 10  $\mu\text{g}$  of anti-IGF-IR, MLS128, or IgG<sub>3</sub> was mixed by rotation at 4°C overnight. To bring down associated protein complexes, 25  $\mu\text{L}$  of 50% protein G Sepharose was added to each tube and the tubes were rotated for 30 min. The gels were recovered by centrifugation at  $17,000 \times g$  for 10 min and then suspended in 1 mL of 10 mM Tris-HCl, pH 7.5, containing 150 mM NaCl and 0.05% Tween 20. After this washing process was repeated 5 times, the gels were suspended in 30  $\mu\text{L}$  of 1 $\times$  SDS-PAGE sample buffer and then subjected to heating at 100°C for 5 min. IP samples were analyzed by Western blotting using anti-IGF-IR, MLS128, or anti-IgG<sub>3</sub> as described above.

#### 2.7. Sucrose gradient fractionation of HT29 and LS180 cell lysates

All steps were carried out at 4°C as previously described (15,16). HT29 and LS180 cells grown in 3 ~ 5 150 mm-dishes were washed with chilled PBS and lysed in 2 mL lysis buffer B (50 mM Tris-HCl, pH 7.4, 100 mM NaCl, containing protease inhibitors and 1 mM PMSF, 10 mM sodium vanadate, and 0.1% NP40) on ice for 20 min. After centrifugation for 5 min at  $1300 \times g$ , supernatants (2 mL) were diluted with 2 mL of 85% (w/v) sucrose in 10 mM Tris-HCl, pH 7.5, containing 150 mM NaCl and 5 mM EDTA (TNE buffer). The diluted lysates were overlaid with 4 mL of 30% (w/v) sucrose and then with 4 mL of 5% (w/v) sucrose in TNE buffer in an ultracentrifuge tube. The samples were centrifuged at 39,000 rpm for 18 h in an SW41 rotor (Beckman Instruments, Palo Alto, CA, USA), and fractions were collected from the top for IB analysis. Fractions were immunoblotted with anti-Src family kinase (SFK) which served as an internal marker for microdomains (17).

#### 2.8. Two-dimensional gel electrophoresis

HT29 and LS180 cells ( $2 \times 10^7$ ) were lysed with 200  $\mu\text{L}$  of 7 M urea, 2 M thiourea, 2% 3[(3-cholamidopropyl) dimethylammonio]-1-propanesulfonate (CHAPS), 2% sulfobetaine 10, 1% protease inhibitor cocktail (Sigma-Aldrich), and 65 mM dithiothreitol (DTT); 40  $\mu\text{L}$  of the lysates were then subjected to two-dimensional gel electrophoresis. Two-dimensional gel electrophoresis was performed according to previous methods (18). Briefly, isoelectric focusing was carried out on Immobiline DryStrips (pH 4-7, 18 cm; GE Healthcare, Buckinghamshire, UK) using a CoolPhoreStar IPG-IEF type-P apparatus (Anatech, Tokyo, Japan) for 18 h. The strips were equilibrated in 50 mM Tris-HCl, pH 6.8, containing 6 M urea, 2% SDS, 30% glycerol, and 2% DTT and then electrophoresed on 10% polyacrylamide gels according to Laemmli's method. Proteins were visualized by Coomassie brilliant blue (CBB) and silver staining. For immunostaining, two-dimensional gels were transferred to an Immobilon-P Membrane (Millipore, Bedford, MA, USA) and the membrane was stained with 0.4  $\mu\text{g}/\text{mL}$  of MLS128 antibody followed by alkaline phosphatase-conjugated anti-mouse IgG (Zymed Laboratories, San Francisco, CA, USA). Binding of MLS128 was visualized *via* a chromogenic method using 5-bromo-4-chloro-3-indolylphosphate (BCIP)/nitro blue tetrazolium (NBT) color development substrate (Promega, Fitchburg, WI, USA) according to the manufacturer's instructions. Immunoprecipitates from HT29 and LS180 cell lysates by MLS128 were also separated on two-dimensional gels and immunoblotted under the same conditions described above.

2.9. Statistical analyses

Levels of cell growth and protein bands in Western blotting were expressed as means  $\pm$  S.E. from 3 or more experiments. An unpaired Student's *t*-test was used to compare the growth or intensity of the bands in two groups of experiments performed in the absence and presence of MLS128.

3. Results

3.1. HT29 cell growth is inhibited by 1H7 or MLS128 mAb treatment

The current authors previously found that 1H7 or MLS128 treatment of three colon cancer cell lines,

LS180, LS174T, and HT29, for three days significantly inhibited cell growth (10). Although the original hypothesis regarding a possible interaction between IGF-IR and 110 kDa GP-mediated signaling in LS180 cells (9) was not confirmed, a possible link between IGF-IR and 110 kDa GP signaling in HT29 cells has not been excluded (10). As a first step to test this hypothesis, the time-course effects of 1H7 or MLS128 mAb treatment on cell growth were measured on Day 1, 2, and 3 (Figure 1). 1H7 significantly inhibited cell growth from Day1 to Day 3. While HT29 cell growth was inhibited by MLS128 on Day 1, 2, and 3, this inhibition was only significant on Day 3. These results confirm that both mAb treatments inhibit cell growth for 3 days, as was previously reported (10), and they also demonstrate that 1H7 treatment has a more

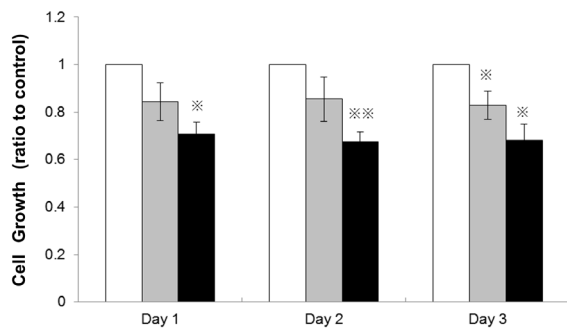


**Figure 1. Effects of anti-IGF-IR 1H7 or anti-Tn-antigen MLS128 mAb on the growth of HT29 colon cancer cells.** HT29 cells were cultured in the absence (control; white bars) or presence of 1H7 (black bars) or MLS128 (grey bars) as described in the Methods. Cell proliferation was measured on Day 1, 2, and 3 using a CCK-8 cell counting kit (Dojindo, Kumamoto, Japan). Cell growth in the presence of either mAb on Day 1 to 3 was compared to the control (without Ab treatment): average  $\pm$  S.D. (*n* = 5). \* *p* < 0.05; \*\* *p* < 0.01.

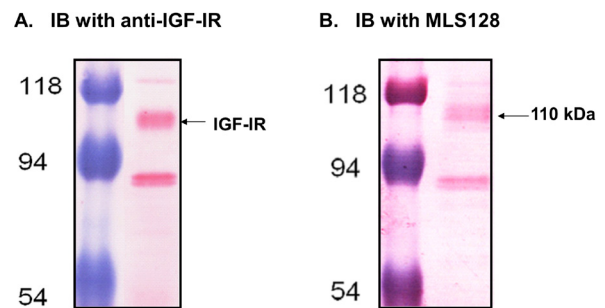


**Figure 2. Expression of IGF-IR and 110 kDa GP (the receptor for MLS128) in HT29 cells.** Solubilized proteins (2  $\mu$ g) prepared from HT29 cells were separated by SDS-PAGE and immunoblotted with anti-IGF-IR $\beta$  (A) or MLS128 (B) as described in the Methods. The 75 and 73 kDa proteins stained are endogenous biotin-containing enzymes (19).

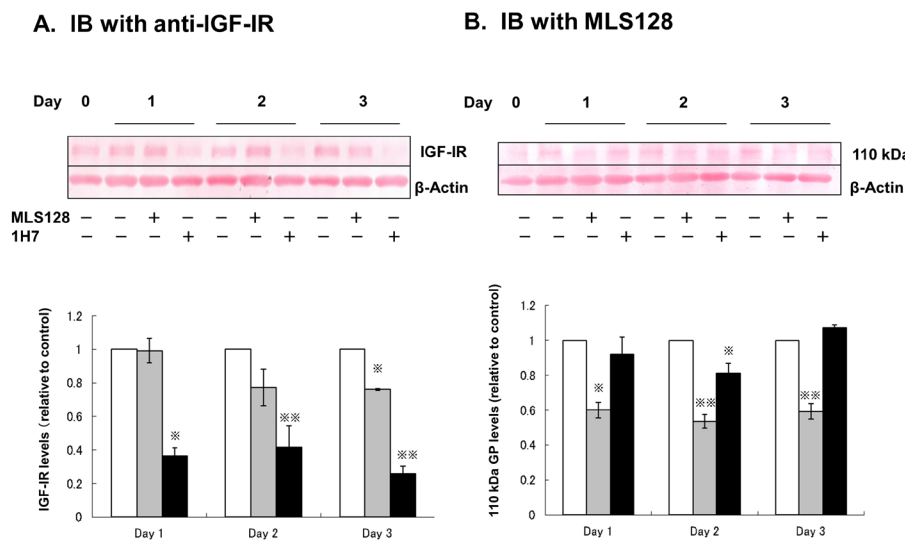


**Figure 3. Effects of 1H7 or MLS128 treatment on cellular levels of IGF-IR and 110 kDa GP in HT29 colon cancer cells.** HT29 cells were cultured in the absence of mAb (control; white bars) or presence of mAb (MLS128; grey bars, 1H7; black bars) for three days. Cells were harvested on Day 1, 2, and 3 and solubilized for Western blot analyses as described in the Methods. Shown are typical immunoblots from three experiments for IGF-IR (A) and 110 kDa GP (B). Average levels of IGF-IR (A) and 110 kDa GP (B) on Day 1, 2, and 3 were calculated as ratios to the respective control. \* *p* < 0.05; \*\* *p* < 0.01.

substantial effect than that of MLS128 treatment.

### 3.2. Effects of mAb treatment on IGF-IR or 110 kDa GP in HT29 cells

The receptors for 1H7 and MLS128 on HT29 cells were visualized by Western blotting with anti-IGF-IR $\beta$  (Figure 2A) and MLS128 (Figure 2B). The bands seen below the 94 kDa marker protein are 75 and 73 kDa endogenous biotin-containing enzymes (19), which served as an internal control. There were comparable levels of IGF-IR and 110 kDa GP expression in HT29 cells.

Treatment of HT29 cells with 1H7 resulted in the down-regulation of IGF-IR on Day 1-3 (Figure 3A, black bars). The levels of 110kDa GP decreased significantly in HT29 cells treated with MLS128 for 1-3 days (Figure 3B, grey bars). These results are consistent with those previously described for three colon cancer cell lines (10). MLS128 treatment caused down-regulation of IGF-IR on Day 2 and 3 (Figure 3A, grey bars). The effects were statistically significant on Day 3 but were not significant on Day 2. This result confirms the previous finding in LS180 cells (9) to some extent and provided the impetus to perform the following experiments.

### 3.3. Association of IGF-IR and 110 kDa GP examined using IP/IB

To test whether IGF-IR and 110 kDa GP are associated in HT29 cells, IP/IB experiments were carried out using combinations of anti-IGF-IR, MLS128, and control IgG<sub>3</sub>. Since one of two independent experiments originally performed indicated a possible co-immunoprecipitation of the two molecules, IP/IB was performed using 4 times the quantity of HT29 cell lysates used in previous experiments. In Figure 4A, IGF-IR (lane 1) was visible as expected. A band

was seen at the IGF-IR position in MLS128-IP (lane 2), but a band was also seen in the control-IP (lane 3), suggesting that it must be non-specific. In anti-IGF-IR IP (Figure 4B, lane 1), no band corresponding to 110 kDa GP (lane 2) was detected. These results thus suggested no direct association between IGF-IR and 110 kDa GP (Figure 4).

### 3.4. Characterization of IGF-IR and 110 kDa GP in microdomains examined using sucrose gradient centrifugation

Although there does not appear to be a direct association between IGF-IR and 110 kDa GP in HT29 cells, both molecules may exist in close proximity, such as in microdomains where receptors for various signaling have apparently been localized (15-17). Sucrose gradient fractionation of HT29 and LS180 cell lysates was performed to determine whether or not IGF-IR and 110 kDa GP exist in microdomains, and if so, to determine whether or not the treatment of cells with MLS128 for 3 days affects the distribution of 110 kDa GP and/or IGF-IR.

In HT29 cells, both IGF-IR and 110 kDa GP were localized in microdomains as shown in Figure 5A and B, respectively. The same results were obtained with LS180 cells (Figure 6B -MLS128). Anti-Src family kinase (SFK) blots indicated that the fractions 4-6 represent microdomains (Figure 5C, Figure 6 SFK).

Next, whether or not changes in the distribution of IGF-IR or 110 kDa GP occurred in HT29 and LS180 colon cancer cells after MLS128 treatment was examined. The results shown in Figure 6A (-MLS128) are, in fact, immunoblots derived from sucrose gradient centrifugation fractions of HT29 cells shown in Figures 5A, B, and C. The sucrose gradient fractionation experiments were actually performed in parallel, one for HT29 cells without MLS128 treatment (-MLS128) and the other for HT29 cells treated with MLS128 for 3 days (+MLS128), the results of which are summarized in Figure 6A. The same sets of data for LS180 cells are shown in Figure 6B. In both HT29 and LS180 cells, treatment with MLS128 for 3 days was followed by a reduction in band intensities of IGF-IR, 110 kDa GP, and control SFK in microdomains, suggested that the MLS128 treatment may have modulated microdomain organization.

During characterization of HT29 cells using sucrose gradient fractionation, an interesting phenomenon unexpectedly became apparent. Western blotting experiments were usually carried out immediately after sucrose gradient fractionation. The results shown in Figures 5A and D are, however, immunoblot experiments using the same fractions that had been kept frozen for 3 years. IB with anti-IGF-IR shown in Figure 5A was repeated 3 years after fractionation since the background of the original immunoblot was too high to

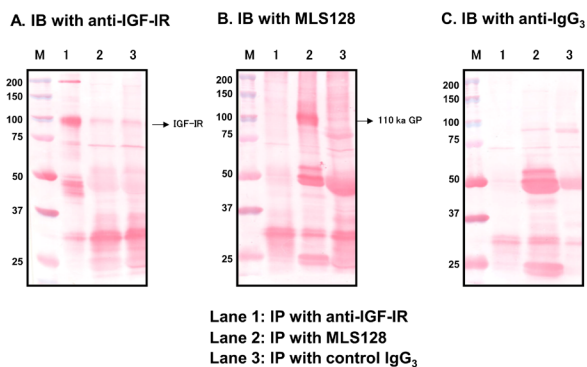


**Figure 4. Immunoprecipitation (IP) and immunoblotting (IB) of IGF-IR or 110 kDa GP using 1H7, MLS128, and control antibodies from HT29 cell lysates.** IP of HT29 cell lysates by anti-IGF-IR (1), MLS128 (2), or control IgG<sub>3</sub> (3) and IB with anti-IGF-IR (A), MLS128 (B), or anti-IgG<sub>3</sub> (C) were done as described in the Methods.

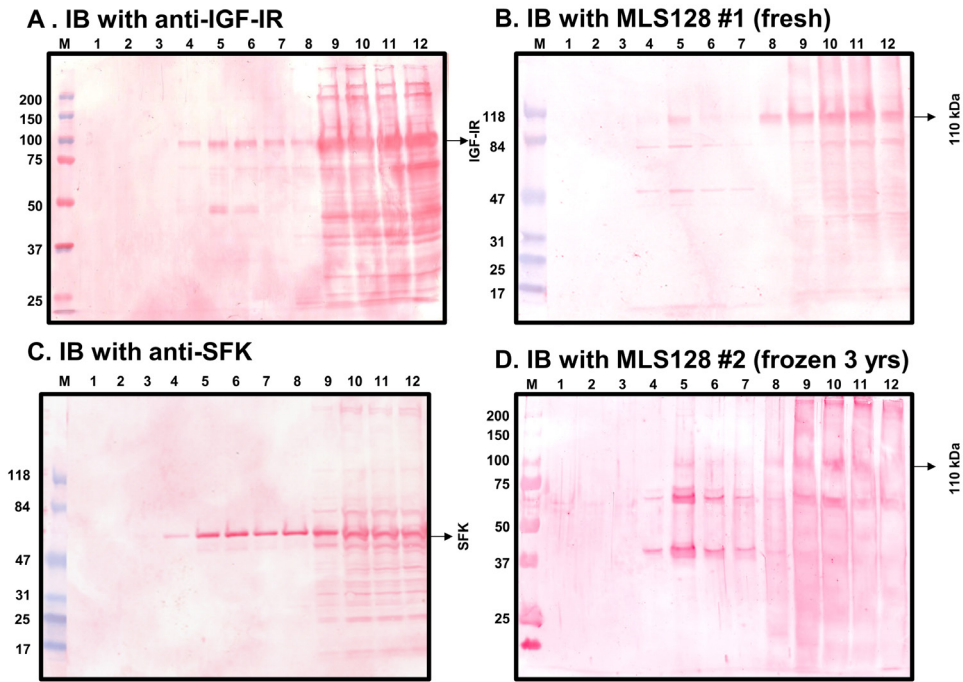


**Figure 5. Characterization of HT29 cells by sucrose gradient fractionation.** HT29 cell lysates were fractionated by sucrose gradient centrifugation, and then fractions were immunoblotted as described in the Methods. **(A)**, IB of fractions 1-12 stored at  $-80^{\circ}\text{C}$  for 3 years with anti-IGF-IR. **(B)**, IB of fresh fractions 1-12 with MLS128. **(C)**, IB of fresh fractions 1-12 with anti-SFK. **(D)**, IB of fractions 1-12 stored at  $-80^{\circ}\text{C}$  for 3 years with MLS128.

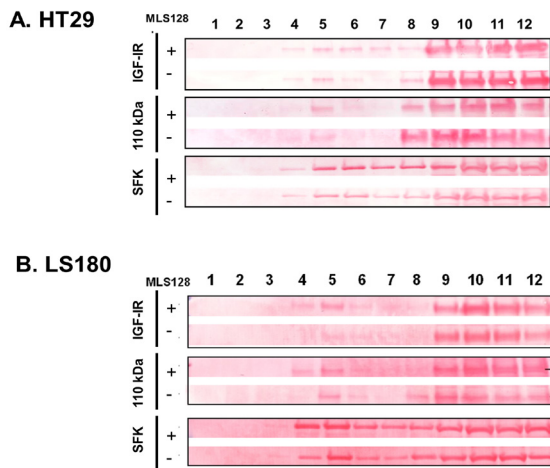


**Figure 6. Effects of MLS128 treatment on IGF-IR and 110 kDa GP in the microdomains of HT29 and LS180 cells.** Sucrose gradient fractionations of HT29 **(A)** and LS180 **(B)** cells that were treated with PBS (-MLS128) or MLS128 (+MLS128) were immunoblotted with anti-IGF-IR, MLS128, and anti-SFK antibodies as labeled.

clearly identify the IGF-IR band in microdomains. The IGF-IR blot redone with the frozen fractions revealed that IGF-IR is still intact after storage for 3 years (Figure 5A). In contrast, the MLS128 immunoblot of frozen samples shown in Figure 5D revealed degradation products with molecular masses of 66 and 41 kDa, which would add up to approximately 110 kDa, as seen in the immunoblot of fresh samples (Figure 5B). This observation suggested that a protease-susceptible region may exist in the middle of 110 kDa GP. Similar

degradation products of MLS128-stainable 46-48 kDa were observed in the microdomains of LS180 cell lysate fractions that had been frozen for 4 years (data not shown). The aforementioned phenomena suggested that the 110 kDa GP became susceptible to microdomain-associated proteases during storage, freezing, and thawing.

### 3.5. Identification of 110 kDa GP in HT29 and LS180 colon cancer cells

Extensive efforts have been made to identify the 110 kDa GP that was found to be the receptor for MLS128 in three colon cancer cell lines (10). It represents, after all, the first step in understanding the mechanisms by which MLS128 inhibits colon cancer cell growth. Figures 7A and B summarize two-dimensional gel electrophoresis of HT29 and LS180 cell lysates, respectively. Silver staining resulted in numerous proteins (Figure 7, A1 and B1) whereas CBB staining depicted around 100 abundant proteins (Figure 7, A2 and B2). Some of these were stained by MLS128 (Figure 7, A3 and B3), indicating that Tn-antigen epitopes are present in quite a few proteins. Spots depicting the candidate 110 kDa GP are indicated by arrows in Figure 7, A3 and B3. The position is identified by comparing the immunoblot of HT29 immunoprecipitates, which only revealed three MLS128-stainable spots in the area (Figure 7, C1). In two-dimensional electrophoresis, the same GPs with different numbers of sialic acid residues are most often separated on a scale with evenly

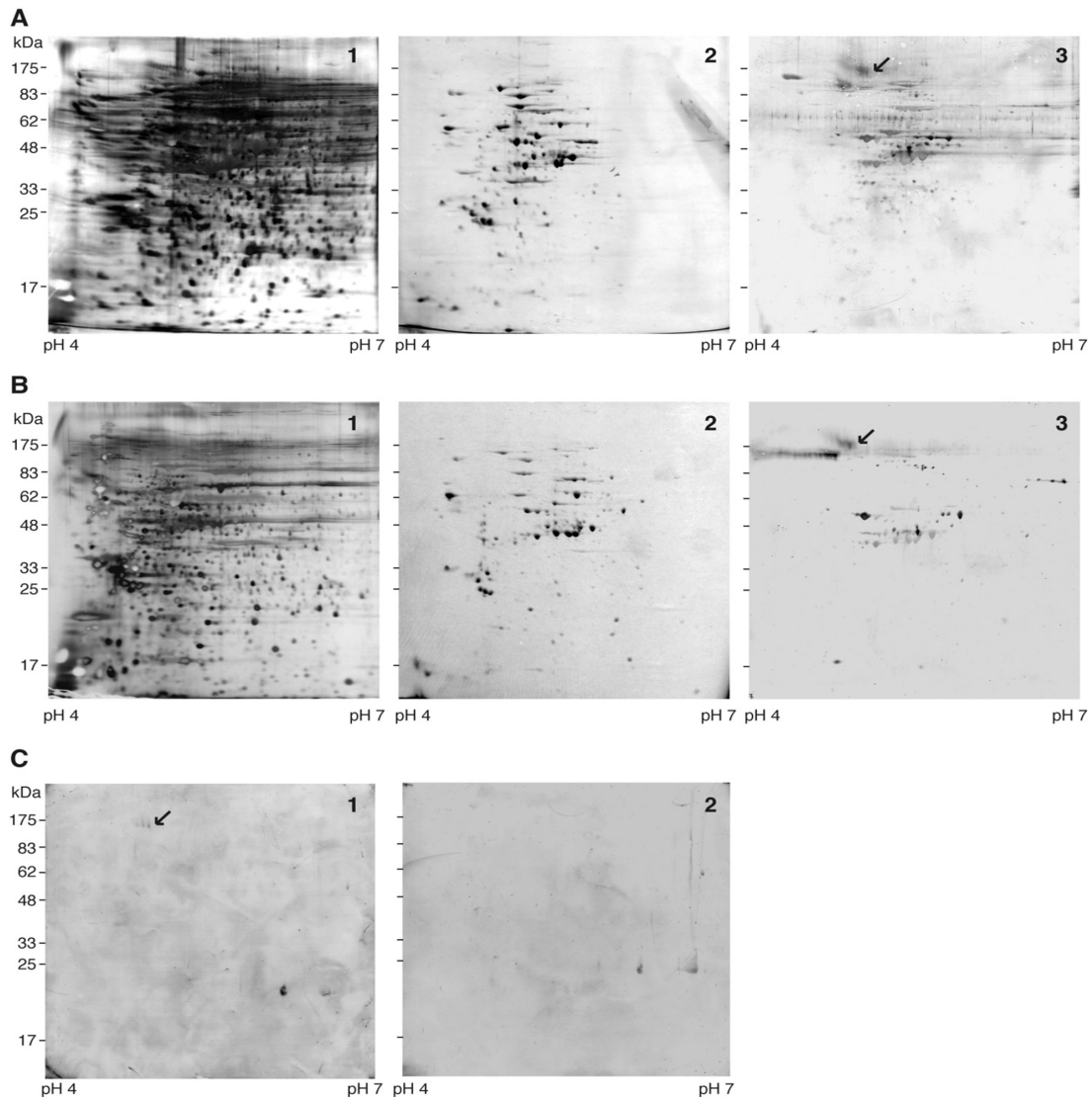


**Figure 7. Two-dimensional gel electrophoresis of HT29 and LS180 cell lysates, and immunoprecipitates of those lysates.** Cell lysates prepared from HT29 (A) and LS180 (B) were subjected to two-dimensional gel electrophoresis as described in the Methods. Silver staining (1), CBB staining (2), and IB with MLS128 (3) are shown. (C) shows results of two-dimensional gel electrophoresis of immunoprecipitates from HT29 lysates (1) and LS180 cell lysates (2) immunostained with MLS128. An arrow points to three spots in C1, identifying the location of 110 kDa GP in the immunoblots of HT29 and LS180 cell lysates (A3 and B3, respectively).

spaced intervals by isoelectric focusing. Since 110 kDa GP is expected to contain clustered *O*-glycans based on its reactivity with MLS128, these three spots may represent the same protein with microheterogeneity of their glycans. In contrast, these spots of 110 kDa GP were not observed in the immunoprecipitates from LS180 cell lysate (Figure 7, C2), although spots of 110 kDa were found in the lysate (indicated with an arrow in Figure 7, B3). The reason why the spots seen in the HT29 cell lysate IP were not detected in the two-dimensional electrophoresis of LS180 cell lysate IP may be because of the difference in the density of Tn-antigen clusters on 110 kDa GP. A triplet Tn glycoepitope on the 110 kDa GP from LS180 cells might be less abundant than that of 110 kDa GP from HT29 cells. In IB, target molecules are immobilized on a membrane, allowing multivalent binding with

antibodies, while they may have weaker interaction in solution in IP. This could cause a low recovery of 110 kDa GP in the immunoprecipitates from LS180 cell lysates.

To identify the 110 kDa proteins, these corresponding spots revealed by two-dimensional gel electrophoresis were subjected to in-gel digestion with trypsin. Tryptic peptides derived from these spots were then analyzed using matrix-assisted laser desorption ionization-time of flight (MALDI-TOF) mass spectrometry along with software to search databases. Despite repeated attempts, the 110 kDa protein could not be successfully identified. This failure may be due to the extremely low susceptibility to trypsin of 110 kDa GP as a result of interference by abundant *O*-glycosylation, the lack of a database for glycosylated peptides, and the limited availability of samples.

#### 4. Discussion

Previous studies (9,10) and the current study found that: (i) MLS128 inhibits LS180, LS174T, and HT29 colon cancer cell growth, (ii) MLS128 binds to 110 kDa GP on the surface of colon cancer cells, (iii) although IGF-IR signaling was not associated with MLS128's inhibition of LS180 cell growth as was originally proposed, a possible link between IGF-IR- and 110 kDa GP-mediated signaling pathways was still suggested in HT29 cells, (iv) the 110 kDa band diminished significantly in colon cancer cells treated with MLS128 for 3 days, (v) 110 kDa GP along with tyrosine protein kinases such as IGF-IR and SFK was found in microdomains, and (vi) the levels of 110 kDa GP and the tyrosine protein kinases in microdomains were modulated by MLS128 treatment of HT29 and LS180 cells. The 110 kDa GP in microdomains was susceptible to limited proteolytic degradation, resulting in two domains.

The major question asked in this study was whether or not IGF-IR and 110 kDa GP are associated in HT29 cells. Given the results of IP/IB experiments, this possibility was excluded. Co-localization of IGF-IR and the MLS128 receptor in microdomains was, however, indicated by sucrose gradient centrifugation and IB using HT29 and LS180 cell lysates. A reduction in 110 kDa GP along with tyrosine protein kinases such as IGF-IR and SFK in microdomains was noted after HT29 and LS180 cells were treated with MLS128 for 3 days, which suggested that MLS128 binding to colon cancer cells resulted in modulation of the signaling molecules associated with the microdomains. Whether or not the modulation of microdomain-associated signaling molecules plays a role in the ability of MLS128 to inhibit cancer cell growth remains to be answered.

Despite extensive efforts to identify the 110 kDa GP in HT29 and LS180 cell lysates and immunoprecipitates, this identification was unsuccessful. Although Western blotting as shown in Figure 2B revealed a broad but distinct band, two-dimensional electrophoresis and MLS128 IB revealed the heterogeneous nature of 110 kDa GP (Figure 7, A3 and B3). The three spots stained are characteristic of having a differing number of sialic acid residues on the same protein backbone. Identification of the 110 kDa protein was unsuccessful because of its microheterogeneity and extremely low susceptibility to trypsin due to its heavy glycosylation, both of which resulted in a low recovery of 110 kDa GP tryptic peptides. Methods of removing and purifying tryptic peptides from protein bands or spots on gels are sophisticated and well established. For mucin-type GPs, however, trypsin digestion as is commonly used may not have worked efficiently due to abundant *O*-glycosylation, which would clearly render 110 kDa GP resistant to trypsin digestion. Procedures must be

modified to optimize conditions for mucin-type GPs in order to identify 110 kDa GP.

A promising finding is that limited proteolysis of 110 kDa GP occurred in microdomains after freezing and storage. Two independent observations involving HT29 and LS180 cells suggested the existence of protease-susceptible sites in the 110 kDa GP. The first was the microdomain-associated 110 kDa GP degradation to two fragments with 66 and 41 kDa in HT29 cells. The second observation was that 46-48 kDa fragments were produced in the microdomains derived from LS180 cells stored at  $-80^{\circ}\text{C}$ . Since those bands were generated from 110 kDa GP in cells that had not been treated with MLS128, conformational relaxation during storage, freezing, and thawing must have exposed the cleavage site(s) to contaminating proteases, resulting in limited proteolysis as was observed. Although protease inhibitor cocktails were added to cell lysates and during sucrose gradient fractionation, degradation of 110 kDa still occurred, which suggests that unidentified proteases that are resistant to the added inhibitors are responsible for the limited proteolysis of 110 kDa GP. Degradation products in HT29 and LS180 cell microdomains had differing sizes of 66/41 kDa and 46-48 kDa, respectively. This finding may support the notion that there are differences in the abundance and/or heterogeneity of *O*-glycosylation of the 110 kDa GP produced by HT29 or LS180 cells.

In summary, the current study provided new insights into the nature of 110 kDa GP. Although 110 kDa GP is not directly associated with IGF-IR, it is found in microdomains together with IGF-IR. MLS128 treatment may modulate receptors in microdomains. The 110 kDa GP was apparently heterogeneous due to different degrees of its sialylation. Its heterogeneity and resistance to trypsin digestion were apparently major obstacles to its successful identification. During this study, however, 110 kDa GP was found to have sites or domains in the middle of the molecule that are susceptible to proteases. There was limited proteolysis of 110 kDa GP in the microdomains of cells that had been frozen for 3-4 years. Different sizes found in microdomain-associated 110 kDa GPs of HT29 and LS180 cells may provide clues to help identify 110 kDa GP.

#### Acknowledgements

The authors wish to thank Ms. Hitomi Miyasaka for her contribution to the first part of this project. This work was supported by grants (17570120 and 22570125) from Japan Society for the Promotion of Science.

#### References

1. Springer GF. Immunoreactive T and Tn epitopes in cancer diagnosis, prognosis, and immunotherapy. *J Mol Med.* 1997; 75:594-602.

2. Springer GF. T and Tn, general carcinoma autoantigens. *Science*. 1984; 224:1198-1206.
3. Takahashi HK, Metoki R, Hakomori S. Immunoglobulin G3 monoclonal antibody directed to Tn antigen (tumor-associated  $\alpha$ -N-acetylgalactosaminyl epitope) that does not cross-react with blood group A antigen. *Cancer Res*. 1988; 48:4361-4367.
4. Numata Y, Nakada H, Fukui S, Kitagawa H, Ozaki H, Inoue K, Kawasaki M, Funakoshi T, Yamashina I. A monoclonal antibody directed to Tn antigen. *Biochem Biophys Res Commun*. 1990; 170:981-985.
5. Nakada H, Numata Y, Inoue M, Tanaka N, Kitagawa H, Funakoshi I, Fukui S, Yamashina I. Elucidation of an essential structure recognized by an anti-GalNAc $\alpha$ -Ser(Thr) monoclonal antibody (MLS 128). *J Biol Chem*. 1991; 266:12402-12405.
6. Osinaga E, Bay S, Tello D, Babino A, Pritsch O, Assemat K, Cantacuzene D, Nakada H, Alzari P. Analysis of the fine specificity of Tn-binding proteins using synthetic glycopeptide epitopes and a biosensor based on surface plasmon resonance spectroscopy. *FEBS Lett*. 2000; 469:24-28.
7. Yuasa N, Ogawa H, Koizumi T, Tsukamoto K, Matsumoto-Takasaki A, Asanuma H, Nakada H, Fujita-Yamaguchi Y. Construction and expression of anti-Tn antigen-specific single-chain antibody genes from hybridoma producing MLS128 monoclonal antibody. *J Biochem*. 2012; 151:371-381.
8. Matsumoto-Takasaki A, Hanashima S, Aoki A, Yuasa N, Ogawa H, Sato R, Kawakami H, Mizuno M, Nakada H, Yamaguchi Y, Fujita-Yamaguchi Y. Surface plasmon resonance and NMR analyses of anti Tn-antigen MLS128 monoclonal antibody binding to two or three consecutive Tn-antigen clusters. *J Biochem*. 2012; 151:273-282.
9. Morita N, Yajima Y, Asanuma H, Nakada H, Fujita-Yamaguchi Y. Inhibition of cancer cell growth by anti-Tn monoclonal antibody MLS128. *Biosci Trends*. 2009; 3:32-37.
10. Zamri N, Masuda N, Oura F, Yajima Y, Nakada H, Fujita-Yamaguchi Y. Effects of two monoclonal antibodies, MLS128 against Tn-antigen and 1H7 against insulin-like growth factor-I receptor, on the growth of colon cancer cells. *Biosci Trends*. 2012; 6:303-312.
11. Li SL, Kato J, Paz IB, Kasuya J, Fujita-Yamaguchi Y. Two new monoclonal antibodies against the  $\alpha$  subunit of the human insulin-like growth factor-I receptor. *Biochem Biophys Res Commun*. 1993; 196:92-98.
12. Li SL, Liang SJ, Guo N, Wu AM, Fujita-Yamaguchi Y. Single-chain antibodies against human insulin-like growth factor I receptor: Expression, purification, and effect on tumor growth. *Cancer Immunol Immunother*. 2000; 49:243-252.
13. Sachdev D, Li SL, Hartell JS, Fujita-Yamaguchi Y, Miller JS, Yee D. A chimeric humanized single-chain antibody against the type I insulin-like growth factor (IGF) receptor renders breast cancer cells refractory to the mitogenic effects of IGF-I. *Cancer Res*. 2003; 63:627-635.
14. Ye JJ, Liang SJ, Guo N, Li SL, Wu AM, Giannini S, Sachdev D, Yee D, Br nner N, Ikle D, Fujita-Yamaguchi Y. Combined effects of tamoxifen and a chimeric humanized single chain antibody against the type I IGF receptor on breast tumor growth *in vivo*. *Horm Metab Res*. 2003; 35:836-842.
15. Kabayama K, Sato T, Kitamura F, Uemura S, Kang BW, Igarashi Y, Inokuchi J. TNF $\alpha$ -induced insulin resistance in adipocytes as a membrane microdomain disorder: Involvement of ganglioside GM3. *Glycobiology*. 2005; 15:21-29.
16. Oneyama C, Iino T, Saito K, Suzuki K, Ogawa A, Okada M. Transforming potential of Src family kinases is limited by the cholesterol-enriched membrane microdomain. *Mol Cell Biol*. 2009; 29:6462-6472.
17. Okamoto T, Schlegel A, Scherer PE, Lisanti MP. Caveolins, a family of scaffolding proteins for organizing "preassembled signaling complexes" at the plasma membrane. *J Biol Chem*. 1998; 273: 5419-5422.
18. Mikami K, Yamaguchi D, Tateno H, Hu D, Qin S, Kawasaki N, Yamada M, Matsumoto N, Hirabayashi J, Ito Y, Yamamoto K. The sugar-binding ability of human OS-9 and its involvement in ER-associated degradation. *Glycobiology*. 2010; 20:310-321.
19. Robinson BH, Oei J, Saunders M, Gravel R. [ $^3$ H]Biotin-labeled proteins in cultured human skin fibroblasts from patients with pyruvate carboxylase deficiency. *J Biol Chem*. 1983; 247:6660-6664.

(Received September 24, 2013; Revised October 2, 2013; Accepted October 4, 2013)

# A novel semi-synthetic andrographolide analogue A5 inhibits tumor angiogenesis *via* blocking the VEGFR2-p38/ERK1/2 signal pathway

Chenyuan Gong, Chong Xu, Lili Ji\*, Zhengtao Wang

The MOE Key Laboratory for Standardization of Chinese Medicines and The Shanghai Key Laboratory for Compound Chinese medicines, Institute of Chinese Materia Medica, Shanghai University of Traditional Chinese Medicine, Shanghai, China.

## Summary

The present study is designed to observe the inhibitory effect of compound A5, a semi-synthetic analogue of the natural compound andrographolide, on angiogenesis and its underlying mechanism. Compound A5 is semi-synthesized from natural compound neoandrographolide. Andrographolide, the aglycon of neoandrographolide, and A5 all inhibited vascular endothelial growth factor (VEGF)-induced human umbilical vein endothelial cells (HUVECs) proliferation, and that the inhibition shown by A5 is the best. A5 also inhibited VEGF-induced tube formation in HUVECs in a concentration-dependent manner. VEGF-induced neoangiogenesis *in vivo* was observed by Matrigel formation assay. The Matrigel picture and CD31 staining results showed that A5 inhibited VEGF-induced neoangiogenesis *in vivo*. Further, Western-blot results showed that A5 inhibited VEGF-induced phosphorylation of VEGF receptor 2 (VEGFR2), extracellular signal-regulated kinase 1 and 2 (ERK1/2), and p38 kinase. The antitumor effect of A5 was analyzed in a xenograft mouse tumor model inoculated with hepatoma Hep3B cells. The results showed that A5 decreased tumor weight and tumor size without affecting body weight in the xenograft mouse, and A5 also decreased CD31 staining in tumor tissue. Taken together, the present study demonstrates that compound A5 inhibits tumor growth via blocking neoangiogenesis, and the cellular VEGFR2-p38/ERK1/2 signal pathway.

**Keywords:** Andrographolide analogue, angiogenesis, VEGFR2, ERK1/2, p38

## 1. Introduction

Andrographolides is a type of natural diterpenoid lactone, which is distributed in traditional herbal medicine *Andrographis paniculata* Nees (Acanthaceae). Andrographolides like andrographolide and neoandrographolide are reported to have anti-inflammatory and anticancer activities in both *in vitro* and *in vivo* experimental models of inflammation and cancer (1). Specially, the antitumor effect of andrographolide has

attracted great interest, and there are various reports about the antitumor activity of andrographolide and its potential mechanisms (1-5). In previous studies, our lab has also found inhibition of andrographolide on hepatoma tumor growth *in vitro* and *in vivo*, and demonstrated that the cellular redox environment and c-Jun N-terminal kinase were important for its anticancer activity (6-8). Recently, there are various reports about research on andrographolide analogues, some of which demonstrate much greater therapeutic activity for cancer than andrographolide (9-12). Those studies suggest that based on the anticancer activity of andrographolide, we can design a series of analogues of andrographolide through structure modification, which will be the best way to find a stronger anticancer drug candidate than andrographolide.

Angiogenesis is the physiological process through which new blood vessels form from pre-existing vessels. Early in 1971, Judah Folkman first pointed out

\*Address correspondence to:

Dr. Lili Ji, The MOE Key Laboratory for Standardization of Chinese Medicines and The Shanghai Key Laboratory for Compound Chinese Medicines, Institute of Chinese Materia Medica, Shanghai University of Traditional Chinese Medicine, 1200 Cailun Road, Shanghai 201203, China.

E-mail: lichenyue1307@126.com

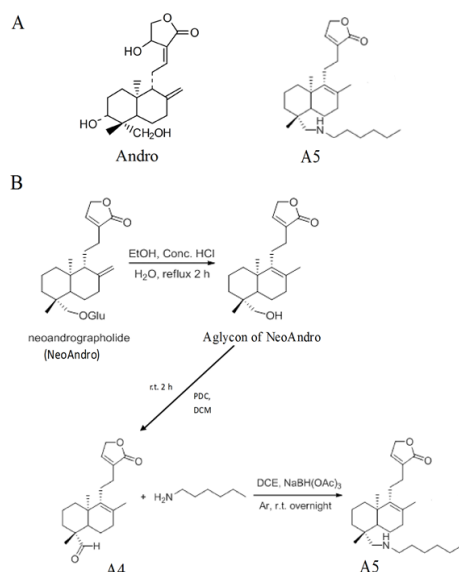


**Figure 1. (A) The chemical structure of andrographolide (Andro), A5. (B) The synthesis scheme of A5.**

the essential role of angiogenesis in tumor growth (13). Angiogenesis provides the required nutrients and oxygen for tumor expansion, and it is also helpful for tumor metastasis (14,15). Thus, blocking tumor angiogenesis is a promising strategy for cancer therapeutics. Recently, various reports have demonstrated the great potential of natural compounds for inhibiting angiogenesis, like various flavonoids, gambogic acid, ginsenoside Rg1, resveratrol, *etc.* (16-19). Meanwhile, there are reports that andrographolide also inhibits angiogenesis *via* regulating matrix metalloproteinase (MMP)-2/9 and hypoxia-inducible factor-1 $\alpha$ , which contributes to its antitumor activity (20,21).

19-*N*-hexylamino-8-methylandrograpanin (A5, Figure 1A) is an analogue of andrographolide synthesized in our lab. The whole synthetic route of A5 is shown in Figure 1B. First, we obtained the aglycon of neoandrographolide (NeoAndro) through acid hydrolysis, and then the product was oxidized with pyridinium dichromate (PDC) in the presence of dichloromethane (DCM) to compound A4, after which, A4 was reacted with hexylamine in the presence of sodium triacetoxyborohydride in 1, 2-dichloroethane under an argon atmosphere at room temperature to prepare compound A5. In our preliminary study, we found that A5 has the strongest inhibitory activity on VEGF-induced HUVEC cells proliferation, and it is even better than andrographolide. The present study is designed to observe the anti-angiogenic activity of A5 and its underlying mechanism.

## 2. Materials and Methods

### 2.1. Chemical compounds and reagents

19-*N*-hexylamino-8-methylandrograpanin (A5) and

the aglycon of neoandrographolide (NeoAndro) were prepared from neoandrographolide in our lab according to the synthetic route demonstrated in Figure 1B. Andrographolide (Andro) and neoandrographolide (NeoAndro) were isolated from leaves of *Andrographis paniculata* (The voucher specimen is deposited in the Herbarium of Shanghai University of Traditional Chinese Medicine, Shanghai, China). The chemical structures of those compounds were verified by MS and NMR analysis and are shown in Figure 1, and the purity of those compounds in our studies was over 98% as determined by HPLC.

Phosphospecific rabbit polyclonal antibodies against <sup>1175</sup>Tyr phosphorylated VEGFR2, <sup>202</sup>Thr and <sup>204</sup>Tyr dual-phosphorylated p44/42 MAPK (ERK1/2), <sup>180</sup>Thr and <sup>182</sup>Tyr dual-phosphorylated p38, VEGFR2, p44/42 MAPK (ERK1/2), p38 and  $\beta$ -actin were all purchased from Cell Signaling Technology (Danvers, MA, USA). Peroxidase-conjugated goat anti-Rabbit IgG (H + L) and peroxidase-conjugated goat anti-Mouse IgG (H + L) were purchased from Jackson ImmunoResearch (West Grove, PA, USA). Cell culture reagents, fetal bovine serum (FBS) and endothelial cell growth supplement (ECGS) were from Invitrogen (Carlsbad, CA, USA). Human recombinant VEGF (isoform 165) was purchased from PeproTech (Rocky Hill, NJ, USA). Matrigel was purchased from BD Biosciences (Bedford, MA, USA). Other reagents unless indicated were from Sigma Chemical Co. (St. Louis, MO, USA).

### 2.2. Cell culture

HUVECs were isolated from fresh umbilical cord veins by the previously described method (22). The isolated endothelial cells were cultured in M199 containing 20% FBS (which was heat-inactivated), 30  $\mu$ g/mL ECGS, 5 U/mL heparin and 100 U/mL penicillin and 100  $\mu$ g/mL streptomycin in a humidified atmosphere of 95% air and 5% CO<sub>2</sub> at 37°C. Experiments were performed on cell cultures of the third to sixth passages.

### 2.3. Cell viability assay

HUVECs were seeded into 96-well plates at a density of  $2 \times 10^4$  cells, treated with or without VEGF (10 ng/mL) for 48 h after pretreatment with different concentrations of A5, andrographolide, neoandrographolide and its aglycon for 15 min. After treatments, cells were incubated with 500  $\mu$ g/mL 3-(4, 5-dimethylthiazol-2-yl) 2, 5-diphenyltetrazolium bromide (MTT) for 4 h. The functional mitochondrial succinate dehydrogenases in surviving cells can convert MTT to formazan that generates a blue color. At last the formazan was dissolved in 10% SDS-5% iso-butanol-0.01 M HCl. The plates were read at 570 nm and 630 nm as a reference and cell viability was normalized as a percentage of control.

#### 2.4. Tube formation assay

96-well plates were coated with 30  $\mu$ L cold matrigel per well and incubated at 37°C for 30 min to promote solidification. HUVECs were incubated with M199 containing 0.1% BSA for 4 h and then treated with the indicated concentrations of A5 for 15 min at 37°C. Then, cells were seeded at a density of  $1 \times 10^4$  cells/well into previously prepared 96-well plates and incubated with or without 10 ng/mL VEGF at 37°C for 4 h. Images were taken using an inverted microscope (Olympus, IX81, Japan), and tubes forming intact networks were counted.

#### 2.5. Western-blot analysis

Cells were cultured in six-well microplates, and the growth medium was removed and replaced with M199 containing 1% FBS for 2 h. Cells were incubated with indicated concentrations of A5 and andrographolide for 6 h, and stimulated with or without VEGF (10 ng/mL) for 5 min. After treatments, cells were lysed with the SDS sample buffer containing 50 mM Tris (pH7.4), 2% SDS (wt/vol), 5% 2-mercaptoethanol and 10% glycerol. Samples were separated by SDS-PAGE and blots were probed with the appropriate combination of primary antibodies and HRP conjugated secondary antibodies. For repeated immunoblotting, membranes were stripped in 62.5 mM Tris (pH 6.7), 20% SDS and 0.1 M 2-mercaptoethanol for 30 min at 50°C.

#### 2.6. Matrigel plug assay

Matrigel (0.5 mL/plug) with no VEGF or A5, VEGF (10 ng/mL) but no A5, VEGF (10 ng/mL) and A5 (5 or 25  $\mu$ M) in liquid form at 4°C, respectively, were subcutaneously injected in the midventral abdominal region of C57BL/6 mice (5-6 weeks old,  $n = 6$  each group). After 7 d, the mice were sacrificed and the matrigel plugs were removed for taking pictures and immunohistochemistry.

#### 2.7. Immunohistochemistry

The matrigel plugs of each group were fixed with formalin and embedded into paraffin. 5  $\mu$ M sections were stained with a specific antibody against CD31. Images were taken using an inverted microscope (Nikon, Eclipse Ci, Japan).

#### 2.8. Xenograft tumor mouse model

Athymic nude mice (BALB/c nu/nu, 5 week old males) were purchased from Shanghai Laboratory Animal Center of Chinese Academy of Science, Shanghai, China. Mice were given a *s.c.* injection of Hep3B cells ( $1 \times 10^6$  cells per mouse) into the left front leg. After tumors were established ( $\sim 30$  mm<sup>3</sup>), the mice were given

a daily *i.p.* injection of A5 at different doses (0 mg/kg, 1 mg/kg, 10 mg/kg). The body weight and tumor sizes of all mice were recorded every three days. Tumor sizes were determined by Vernier caliper measurements and calculated as  $[(\text{length} \times \text{width}^2)/2]$ . After 7d, 4 mice from each group were sacrificed and tumors were removed for immunohistochemistry. The other 6 mice of each group were sacrificed 16 days after A5 administration and tumors were removed, weighed and photographed.

#### 2.9. Statistical analysis

For all experiments, data were expressed as means  $\pm$  S.E.M. Statistical comparisons were subjected to an analysis of variance (ANOVA) and LSD-test using SPSS version 18.0, and  $p < 0.05$  was considered as a statistically significant difference.

### 3. Results

#### 3.1. Effects of A5, andrographolide, neoandrographolide and its aglycon on VEGF-induced cell proliferation

VEGF-induced endothelial cell proliferation is the initial stage of neoangiogenesis. From Figure 2, we can see that andrographolide (Andro), the aglycon of neoandrographolide (aglycon of NeoAndro) and A5 all inhibit VEGF-induced cell proliferation in HUVECs, and that the inhibitory effect of A5 is the best.

#### 3.2. Effects of A5 on VEGF-induced tube formation

Figure 3A shows that VEGF induces obvious tube formation, while various concentrations of A5 all inhibit VEGF-induced tube formation. Figure 3A-g shows that

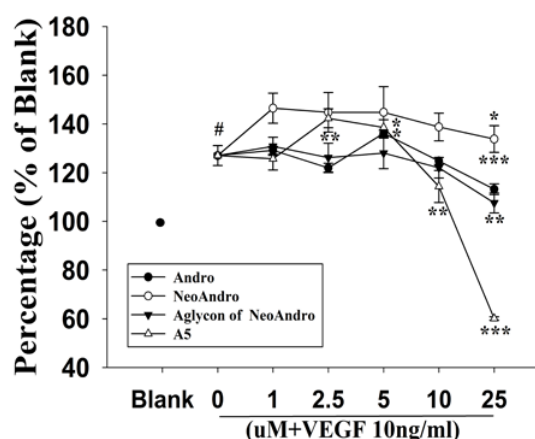


**Figure 2** Effect of A5, andrographolide, neoandrographolide and its aglycon on VEGF-induced cell proliferation. HUVECs were pretreated with different concentrations of A5, andrographolide (Andro), neoandrographolide (NeoAndro) and its aglycon for 15 minutes, followed by treatment with or without VEGF 10 ng/ml. Cell viability was detected by MTT assay. Data are expressed as means  $\pm$  S.E.M. # $p < 0.05$  compared with control; \* $p < 0.05$ , \*\* $p < 0.01$ , \*\*\* $p < 0.001$  compared with VEGF alone.

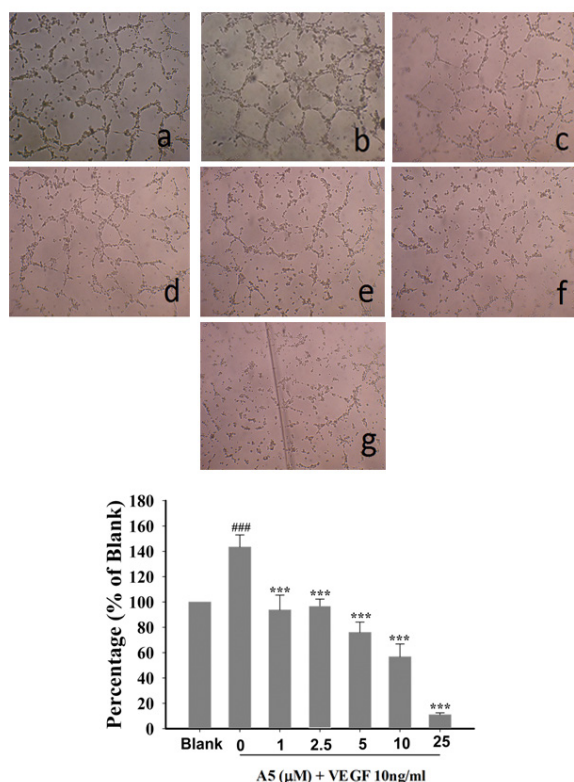


**Figure 3. Effect of A5 on VEGF-induced tube formation.** HUVEC cells were pretreated with the indicated concentrations of A5 for 15 min, and then incubated with or without 10 ng/ml VEGF for 4 h. Pictures were taken using an inverted microscope at 100× magnification. The tubular structures of HUVECs were quantified by manual counting. **a:** control (medium alone), **b:** VEGF (10 ng/mL), **c:** VEGF (10 ng/ml) plus A5 (1 μM), **d:** VEGF (10 ng/ml) plus A5 (2.5 μM), **e:** VEGF (10 ng/ml) plus A5 (5 μM), **f:** VEGF (10 ng/mL) plus A5 (10 μM), **g:** VEGF (10 ng/mL) plus A5 (25 μM). Data are means ± S.E.M. from four independent experiments. ### $p < 0.001$  versus control; \*\*\* $p < 0.001$  compared with VEGF alone.

there is almost no tube formation in 25 μM A5 treated cells. After counting the number of formed tubes, we can see from Figure 3B that A5 can inhibit VEGF-induced tube formation in HUVECs in a concentration-dependent manner ( $p < 0.001$ ). The inhibitory effect of 25 μM A5 is the best.

### 3.3. Effects of A5 on VEGF-induced matrigel formation *in vivo*

We further evaluated the inhibitory effect of A5 on VEGF-induced angiogenesis *in vivo* using the subcutaneously implanted matrigel plug assay. Compared with controls, the matrigel implants appear redder in the VEGF-treated group (Figure 4A), indicating formation of a functional vasculature inside the matrigel. After co-injection of A5 (5, 25 μM) with VEGF, the color of the matrigel implants gradually fades, and the matrigel implant in 25 μM A5 group has almost no color. CD31 is the biomarker of endothelial cells, as shown in Figure 4B we can see that in VEGF-treated matrigel there are more enlarged and denser blood vessels stained by CD31.

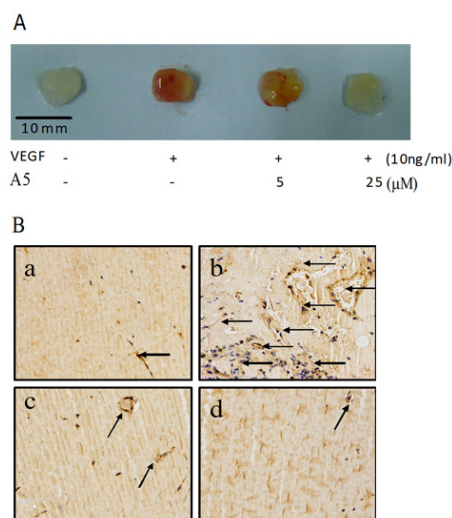


**Figure 4. A5 inhibited VEGF-induced neoangiogenesis *in vivo*.** (A) After 7 days, the mice were sacrificed and representative matrigel plugs were excised and photographed. (B) The 5 μm sections of matrigel were stained with specific antibody against CD-31 and photographed, and the arrows demonstrate the staining of CD31. **a:** control; **b:** VEGF; **c:** A5 (5μM) + VEGF; **d:** A5 (25μM) + VEGF.

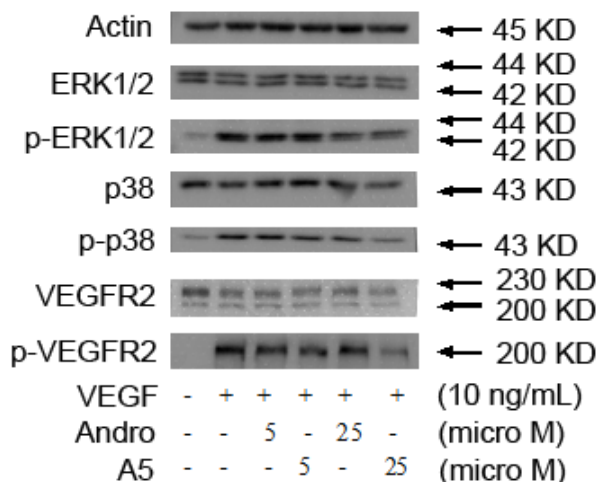


**Figure 5. A5 inhibited VEGF-induced the phosphorylation of VEGFR2, ERK1/2, and p38 kinase.** HUVECs were pretreated with indicated concentrations of A5 and andrographolide (Andro) for 6 h before exposure to VEGF (10 ng/mL) for 5 min. The expression of phosphorylated VEGFR2, ERK1/2, p38, the total VEGFR2, ERK1/2 and p38, and the loading control actin were detected by immunoblotting using specific antibodies. The Western blot figure represents one of at least three independent experiments with similar results.

After treatment with A5 (5, 25 μM), the CD31 staining becomes weak, indicating a decreased number of blood vessels.

### 3.4. Effects of A5 on VEGF-induced VEGFR2, ERK1/2, p38 phosphorylation

Figure 5 shows that VEGF (10 ng/mL) can obviously induce VEGFR2 phosphorylation, while A5 and andrographolide (Andro, 5 or 25 μM) all inhibit

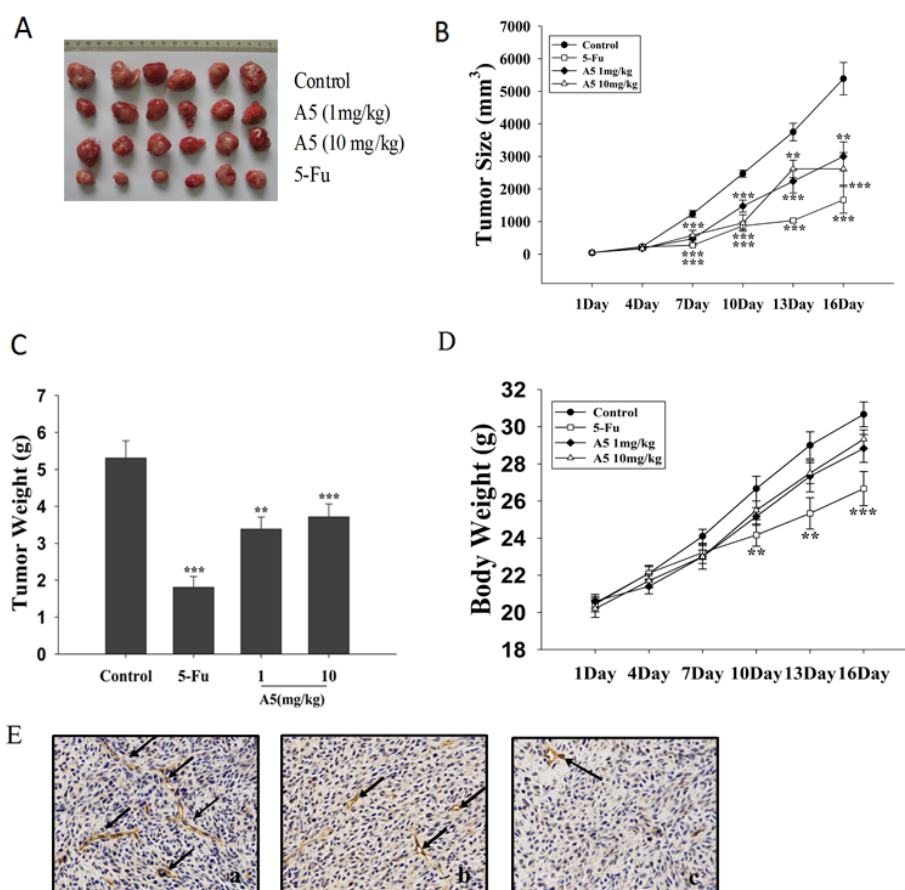


**Figure 6. A5 inhibited hepatoma tumor growth *in vivo*.** (A) Tumors were removed and photographed. (B) Tumor sizes were recorded every three days by Vernier caliper measurements and calculated as  $[(\text{length} \times \text{width}^2)/2]$ . (C) Tumors were weighed. (D) Body weights were recorded every three days. (E) The 5  $\mu\text{m}$  sections were stained with specific antibody against CD-31 and photographed, and the arrows demonstrate the staining of CD31. Data are expressed as means  $\pm$  S.E.M. ( $n = 6$ )  $**p < 0.01$ ;  $***p < 0.001$  versus control.

such phosphorylation, and that the inhibitory effect of A5 (25  $\mu\text{M}$ ) is the best. ERK1/2 and p38 are the important mitogen-activated protein kinases (MAPKs) downstream of VEGFR2. Figure 5 shows that A5 and andrographolide (Andro, 5 or 25  $\mu\text{M}$ ) also inhibit VEGF-induced ERK1/2 and p38 phosphorylation.

### 3.5. Effects of A5 on tumor growth *in vivo*

From Figures 6A-6C, we can see that A5 (1, 10 mg/kg) decreases tumor size and tumor weight ( $p < 0.01$ ,  $p < 0.001$ ). Further, Figure 6D shows that A5 has not much effect on the body weight of mice, while the chemotherapeutic agent 5-FU obviously decreases mouse body weight ( $p < 0.01$ ,  $p < 0.001$ ). Figure 6E of CD31 staining shows that there is decreased CD31 staining in tumors in A5 (1, 10 mg/kg) treated groups.

## 4. Discussion

Andrographolide is a prescribed drug used for clearing away heat and toxic material, and is generally used to prevent and treat the common cold, influenza, viral infections or allergies. In recent years, the

potential therapeutic effect of andrographolide on tumors has attracted the world-wide attention of scientific researchers. However, the poor water solubility enormously limits the bioavailability of andrographolide. Thus, there are various reports about the study of analogues of andrographolide, and their object is to find a compound with better solubility and activity than andrographolide (9-12, 23,24).

Previous studies in our lab have focused on the anti-tumor effect of andrographolide (6-8). Meanwhile, we designed a series of analogues of andrographolide, and in our preliminary study we found that compound A5, which is semi-synthesized from neoandrographolide through the route described in Figure 1B, demonstrated the best inhibitory effect on VEGF-induced HUVECs proliferation (Data not shown). The present study showed that the inhibitory effect of A5 on VEGF-induced cell proliferation was better than andrographolide (Andro), neoandrographolide (Neoandro) and its anglycon. Furthermore, A5 inhibited VEGF-induced tube formation in HUVECs in a concentration-dependent manner. The *in vivo* matrigel plug assay and the xenograft tumor mouse experiment further proved the anti-angiogenic and anti-cancer

effect of A5. All those results indicate the potential value of the development of A5 into an anti-angiogenic drug candidate in the clinic.

The contribution of angiogenesis in tumor expansion and metastasis is widely recognized, and the importance of anti-angiogenic drugs in cancer therapy has become more and more obvious in the past years (25,26). VEGF is one of the key angiogenic factors that stimulate angiogenesis, and VEGF exerts its function through binding to two high-affinity receptors, R1 (FLT-1/Flt-1) and R2 (KDR/Flk-1) (27,28). There is evidence that has proved the important roles of VEGFR2 in transducing the angiogenic effect of VEGF, and the tyrosine phosphorylation of VEGFR2 is detected upon VEGF stimulation (28,29). Our results found that A5 and andrographolide both inhibited VEGF-induced VEGFR2 phosphorylation, which will block the signal transduction cascade stimulated by VEGF. The results suggest that the potential target of A5-induced anti-angiogenesis is the VEGF signaling pathway.

MAPKs regulate diverse processes including cell proliferation, differentiation, apoptosis *etc.* (30). ERK1/2 and p38 are two important MAPKs, which are downstream signals of VEGFR2, and exert critical roles in regulating VEGF-induced cell proliferation and migration in the process of angiogenesis (31,32). Meanwhile, there are already reports about the blockage of the VEGF-VEGFR2-MAPKs signaling pathway by some compounds like isoflavone metabolite 6-methoxyequol, ellagic acid, norcantharidin, barbigerone *etc.* (32-35). Our results also showed that VEGF-induced phosphorylation of p38 and ERK1/2 were both inhibited by A5 and andrographolide.

Taken together, the present study shows that A5, which is a novel semi-synthetic analogue of andrographolide, inhibits VEGF-induced neoangiogenesis *in vitro* and *in vivo*, and blocks VEGF-induced activation of VEGFR2 and down-stream ERK1/2 and p38 kinase. Our research indicates the great potential of the development of A5 into an anti-angiogenic agent for a therapeutic anti-tumor treatment application.

### Acknowledgements

This work was financially supported by the Training Plan of Excellent Young Medical Talents in Shanghai (XYQ2011057), and National Natural Science Foundation of China (81173517).

### References

1. Lim JC, Chan TK, Ng DS, Sagineedu SR, Stanslas J, Wong SS. Andrographolide and its analogues: Versatile bioactive molecules for combating inflammation and cancer. *Clin Exp Pharmacol Physiol.* 2012; 39:300-310.
2. Chen W, Feng L, Nie H, Zheng XD. Andrographolide induces autophagic cell death in human liver cancer cells through cyclophilin D-mediated mitochondrial

- permeability transition pore. *Carcinogenesis.* 2012; 33:2190-2198.
3. Chun JY, Tummala R, Nadiminty N, Lou W, Liu C, Yang J, Evans CP, Zhou Q, Gao AC. Andrographolide, an herbal medicine, inhibits interleukin-6 expression and suppresses prostate cancer cell growth. *Genes Cancer.* 2010; 1:868-876.
4. Yang S, Evens AM, Prachand S, Singh AT, Bhalla S, David K, Gordon LI. Mitochondrial-mediated apoptosis in lymphoma cells by the diterpenoid lactone andrographolide, the active component of *Andrographis paniculata*. *Clin Cancer Res.* 2010; 16:4755-4766.
5. Tan Y, Chiow KH, Huang D, Wong SH. Andrographolide regulates epidermal growth factor receptor and transferrin receptor trafficking in epidermal carcinoma (A-431) cells. *Br J Pharmacol.* 2010; 159:1497-1510.
6. Ji LL, Shen KK, Jiang P, Morahan G, Wang ZT. Critical roles of cellular glutathione homeostasis and JNK activation in andrographolide-mediated apoptotic cell death in human hepatoma cells. *Mol Carcinog.* 2011; 50:580-591.
7. Ji LL, Shen KK, Liu J, Chen Y, Liu TY, Wang ZT. Intracellular glutathione regulates andrographolide-induced cytotoxicity on hepatoma Hep3B cells. *Redox Rep.* 2009; 14:176-184.
8. Ji LL, Liu TY, Liu J, Chen Y, Wang ZT. Andrographolide inhibits human hepatoma-derived Hep3B cell growth through the activation of c-Jun N-terminal kinase. *Planta Med.* 2007; 73:1397-1401.
9. Jada SR, Matthews C, Saad MS, Hamzah AS, Lajis NH, Stevens MF, Stanslas J. Benzylidene derivatives of andrographolide inhibit growth of breast and colon cancer cells *in vitro* by inducing G(1) arrest and apoptosis. *Br J Pharmacol.* 2008; 155:641-654.
10. Nanduri S, Nyavanandi VK, Thunuguntla SS, Kasu S, Pallerla MK, Ram PS, Rajagopal S, Kumar RA, Ramanujam R, Babu JM, Vyas K, Devi AS, Reddy GO, Akella V. Synthesis and structure-activity relationships of andrographolide analogues as novel cytotoxic agents. *Bioorg Med Chem Lett.* 2004; 14:4711-4717.
11. Sirion U, Kasemsook S, Suksen K, Piyachaturawat P, Suksamrarn A, Saeeng R. New substituted C-19-andrographolide analogues with potent cytotoxic activities. *Bioorg Med Chem Lett.* 2011; 22:49-52.
12. Nateewattana J, Saeeng R, Kasemsook S, Suksen K, Dutta S, Jariyawat S, Chairoungdua A, Suksamrarn A, Pawinee P. Inhibition of topoisomerase II  $\alpha$  activity and induction of apoptosis in mammalian cells by semi-synthetic andrographolide analogues. *Invest New Drugs.* 2013; 31:320-332.
13. Folkman J. Tumor angiogenesis: Therapeutic implications. *N Engl J Med.* 1971; 285:1181-1186.
14. Ambasta RK, Sharma A, Kumar P. Nanoparticle mediated targeting of VEGFR and cancer stem cells for cancer therapy. *Vasc Cell.* 2011; 3:26.
15. Fayette J, Soria JC, Armand JP. Use of angiogenesis inhibitors in tumor treatment. *Eur J Cancer.* 2005; 41:1109-1116.
16. Weng CJ, Yen GC. Flavonoids, a ubiquitous dietary phenolic subclass, exert extensive *in vitro* anti-invasive and *in vivo* anti-metastatic activities. *Cancer Metastasis Rev.* 2012; 31:323-351.
17. Yi TF, Yi ZF, Cho SG, Luo J, Pandey MK, Aggarwal BB, Liu MY. Gambogic acid inhibits angiogenesis and prostate tumor growth by suppressing VEGFR2

- signaling. *Cancer Res.* 2008; 68:1843-1850.
18. Yue PYK, Wong DYK, Ha WY, Fung MC, Mak NK, Yeung HW, Leung HW, Chan K, Liu L, Fan TPD, Wong RNS. Elucidation of the mechanisms underlying the angiogenic effects of ginsenoside Rg1 *in vivo* and *in vitro*. *Angiogenesis.* 2005; 8:205-216.
  19. Lin MT, Yen ML, Lin CY, Kuo ML. Inhibition of vascular endothelial growth factor-induced angiogenesis by resveratrol through interruption of Src-dependent vascular endothelial cadherin tyrosine phosphorylation. *Mol Pharmacol.* 2003; 64:1029-1036.
  20. Pratheeshkumar P, Kuttan G. Andrographolide inhibits human umbilical vein endothelial cell invasion and migration by regulating MMP-2 and MMP-9 during angiogenesis. *J Environ Pathol Toxicol Oncol.* 2011; 30:33-41.
  21. Lin HH, Tsai CW, Chou FP, Wang CJ, Hsuan SW, Wang CK, Chen JH. Andrographolide down-regulates hypoxia-inducible factor-1 $\alpha$  in human non-small cell lung cancer A549 cells. *Toxicol Appl Pharmacol.* 2011; 250:336-345.
  22. Marin V, Kaplanski G, Gres S, Farnarier C, Bongrand P. Endothelial cell culture: protocol to obtain and cultivate human umbilical endothelial cells. *J Immunol Methods.* 2001; 254:183-190.
  23. Yao H, Li S, Yu P, Tang X, Jiang J, Wang Y. Reaction characteristics of andrographolide and its analogue AL-1 with GSH, as a simple chemical stimulation of NF- $\kappa$ B inhibition. *Molecules.* 2012; 17:728-739.
  24. Guo W, Liu W, Chen G, Hong S, Qian C, Xie N, Yang X, Xu Q. Water-soluble andrographolide sulfonate exerts anti-sepsis in mice through down-regulating p38 MAPK, STAT3 and NF- $\kappa$ B pathways. *Int Immunopharmacol.* 2012; 14:613-619.
  25. Kerbel RS. Tumor angiogenesis: past, present, and the near future. *Carcinogenesis.* 2000; 21:505-515.
  26. Cao YH. Angiogenesis: What can it offer for future medicine? *Exp Cell Res.* 2010; 316:1304-1308.
  27. Ran S, Huang XM, Downes A, Thorpe PE. Evaluation of novel antimouse VEGFR2 antibodies as potential antiangiogenic or vascular targeting agents for tumor therapy. *Neoplasia.* 2003; 4:297-307.
  28. Shibuya M. Vascular endothelial growth factor (VEGF) and its receptor (VEGFR) signaling in angiogenesis: A crucial target for anti- and pro-angiogenic target for Anti- and Pro-Angiogenic therapies. *Genes Cancer.* 2011; 2:1097-1105.
  29. Waltenberger J, Claesson-Welsh L, Siegbahn A, Shibuya M, Heldin CH. Different signal transduction properties of KDR and Flt1, two receptors for vascular endothelial growth factor. *J Biol Chem.* 1994; 43:26988-26995.
  30. Qi MS, Elion EA. MAP kinase pathways. *J Cell Sci.* 2005; 118:3569-3572.
  31. Claesson-Welsh L, Welsh M. VEGFA and tumor angiogenesis. *J Intern Med.* 2013; 273:114-127.
  32. Bellou S, Karali E, Bagli E, Al-Maharik N, Morbidelli L, Ziche M, Adiercreutz H, Murphy C, Fotsis T. The isoflavone metabolite 6-methoxyequol inhibits angiogenesis and suppresses tumor growth. *Mol Cancer.* 2012; 11:35.
  33. Wang N, Wang ZY, Mo SL, Loo TY, Wang DM, Luo HB, Yang DP, Chen YL, Shen JG, Chen JP. Ellagic acid, a phenolic compound, exerts anti-angiogenesis effects *via* VEGFR-2 signaling pathway in breast cancer. *Breast Cancer Res Treat.* 2012; 134:943-955.
  34. Zhang L, Ji Q, Liu X, Chen XZ, Chen ZH, Qiu YY, Sun J, Cai JF, Zhu HR, Li Q. Norcantharidin inhibits tumor angiogenesis *via* blocking VEGFR2/MEK/ERK signaling pathways. *Cancer Sci.* 2013; 104: 604-610.
  35. Li XX, Wang XW, Ye HY, Peng AH, Chen LJ. Barbigerone, an isoflavone, inhibits tumor angiogenesis and human non-small-cell lung cancer xenografts growth through VEGFR2 signaling pathways. *Cancer Chemother Pharmacol.* 2012; 70:425-437.

(Received June 25, 2013; Revised September 18, 2013; Accepted October 14, 2013)

# SL1122-37, a novel derivative of sorafenib, has greater effects than sorafenib on the inhibition of human hepatocellular carcinoma (HCC) growth and prevention of angiogenesis

Yizhuo Qin<sup>1</sup>, Yuyin Lu<sup>1</sup>, Ruiqi Wang<sup>1</sup>, Wenbao Li<sup>2,\*</sup>, Xianjun Qu<sup>1,\*</sup>

<sup>1</sup> Department of Pharmacology, School of Pharmaceutical Sciences, Shandong University, Ji'nan, Shandong, China;

<sup>2</sup> Sanlugen PharmaTech, Ji'nan, Shandong, China.

## Summary

SL1122-37 is a novel derivative of sorafenib that was characterized by introducing trifluoromethyl on the 4-position of indazole. We aimed to evaluate the effects of SL1122-37 on human hepatocellular carcinoma (HCC) growth and on umbilical vein vascular endothelial cells (HUVECs) angiogenesis. Its efficacy and mechanisms were compared with sorafenib. SL1122-37 significantly prevented PLC/PRF/5 cell proliferation as estimated by colorimetric assay. Flow cytometry analysis showed the induction of apoptosis and arrest of cell cycle in G1 phase. Western blotting showed the decrease of cyclin D1 and regulation of apoptotic proteins. Further analysis suggested that these effects of SL1122-37 might arise from its roles in the inhibition of multi-kinases, including c-Kit and its downstream targets and the Wnt/ $\beta$ -catenin pathway in PLC/PRF/5 cells. SL1122-37 also possessed the activity of antiangiogenesis, showing the prevention of HUVEC migration and capillary tube formation. Western blotting indicated the inhibition of VEGF and phosphorylation of VEGFR-2 in HUVECs. Statistical analysis suggested that SL1122-37 might possess greater activities than sorafenib in the prevention of HCC proliferation and HUVEC angiogenesis. Conclusion, SL1122-37 could develop as a potent anticancer agent for the treatment of HCC.

**Keywords:** Sorafenib, SL1122-37, human hepatocellular carcinoma, multi-kinase inhibitor, antiangiogenesis

## 1. Introduction

Sorafenib is a multi-kinase inhibitor which is known to inhibit cancer cell proliferation by targeting Raf/MEK/ERK signaling, and to prevent angiogenesis by targeting vascular endothelial growth factor receptor tyrosine kinase. Sorafenib has shown clinical advantage in many cancers, such as hepatocellular carcinoma (HCC), breast cancer, thyroid cancer, renal cell carcinoma (RCC), and lung cancers (1). Sorafenib particularly exhibited benefit for the patients with advanced and unresectable HCC (2).

However, the drug was discontinued in many patients due to severe adverse effects. The most frequent adverse events include myelosuppression, neutropenia, lymphopenia, anemia, and thrombocytopenia, hypertension and cardiovascular events, liver dysfunction, kidney injury, and abdominal pain (3). Although most of these adverse effects are usually manageable, myelosuppression and renal injury would lead to discontinuation of treatment. Hypertension and cardiac toxicity would lead to fatal outcomes (4). Thus, new derivatives of sorafenib with higher activity and lower toxicity than sorafenib have remained to be investigated.

Sorafenib, N-(3-trifluoromethyl-4-chlorophenyl)-N'-(4-(2-methylcarbamoyl pyridin-4-yl)oxyphenyl)urea (Figure 1A), is structurally defined as bis-aryl ureas. Although the mechanism of sorafenib binding to its targets has remained unclear, the following analysis of its crystal structure might provide a helpful clue for designing new derivatives. Studies suggested that the carbamido in sorafenib is essential for its activity through binding with Raf protein by the formation of hydrogen bonds (5). After

\*Address correspondence to:

Dr. Xian-Jun Qu, Department of Pharmacology, School of Pharmaceutical Sciences, Shandong University, Ji'nan 250012, China.

E-mail: qxj@sdu.edu.cn

Dr. Wenbao Li, Sanlugen PharmaTech, Rm 506, No. 2766 Yingxiu Road, Ji'nan 250101, China.

E-mail: wbli92128@yahoo.com

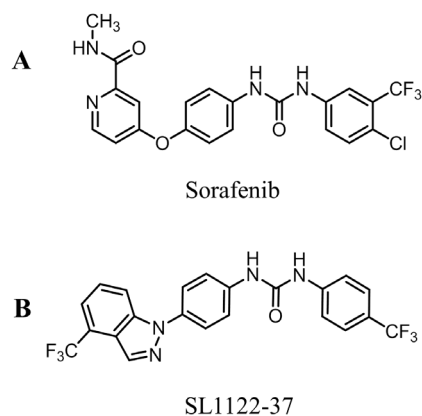


**Figure 1. Chemical structures of sorafenib and SL1122-37.**

binding, the distal pyridyl ring inserts into the ATP adenine binding pocket and then interacts with three aromatic residues in the hinge region, the catalytic loop, and the DFG motif. The trifluoromethyl phenyl ring at opposite end of sorafenib inserts into a hydrophobic pocket between the  $\alpha$ C and  $\alpha$ E helices and N-terminal regions of DFG motif and catalytic loop. These structures in sorafenib are considered to accommodate the active pockets in its targets and therefore improve the selectivity with these kinases (6). In our previous studies, we synthesized a series of compounds with bis-aryl ureas referenced the structure of sorafenib (6). In addition to the skeleton of sorafenib, these compounds contained the substituent structures of indazole or azaindazole. Our following screening assays in HCC and HUVECs indicated that some of these compounds exhibited higher activity than sorafenib. SL1122-37, 1-(4-(4-(trifluoromethyl)-1H-indazol-1-yl)phenyl)-3-(4-(trifluoromethyl)phenyl)urea (Figure 1B), was one of these compounds that exhibited strong activity against cancer cell proliferation and HUVEC angiogenesis. The characteristic of SL1122-37 structure is its trifluoromethyl on the 4-position of indazole. The role of trifluoromethyl in SL1122-37 might improve the electro-negativity for binding to the ATP adenine binding pocket in its target kinases. Meanwhile, the hydrogen bonds between the trifluoromethyl and the ATP adenine binding pocket could improve its activity against RAF kinase (7). We thus suggested that SL1122-37 might possess higher activity than sorafenib in the prevention of cancer proliferation and angiogenesis. SL1122-37 might be a promising agent that could develop as a potential agent for supplant the use of sorafenib. In this study, we evaluated the inhibitory effect of SL1122-37 on the growth of HCC cells and formation of angiogenesis in HUVECs. These effects of SL1122-37 were compared with those of sorafenib.

## 2. Materials and Methods

### 2.1. Chemicals

SL1122-37 as shown in Figure 1B was synthesized as

described in patent (6). The purity of SL1122-37 as determined by high performance liquid chromatography (HPLC) was 99.9%. Sorafenib was purchased from Biochempartner China (purity 99.5%). SL1122-37 and sorafenib were dissolved in dimethylsulfoxide at 50 mM as stock solution.

### 2.2. Cell lines and cell culture

The human hepatocellular carcinoma (HCC) cells PLC/PRF/5 and umbilical vein vascular endothelial cells (HUVECs) were purchased from the American Type Culture Collection (Manassas, VA, USA). PLC/PRF/5 cells were cultured in DMEM medium supplemented with 10% heat-inactivated fetal bovine serum. HUVECs were maintained in Medium 199 supplemented with endothelial cell growth factor at 37°C in a humid atmosphere (5% CO<sub>2</sub>-95% air). Cell proliferation was estimated by 3-[4,5-dimethylthiazol-2-yl]-2,5-diphenyltetrazolium bromide (MTT, Sigma-Aldrich, St. Louis, MO, USA) assay.

### 2.3. Cell cycle analysis

PLC/PRF/5 cells seeded in 6-well plates ( $1.5 \times 10^5$  per well) were synchronized by 24 h of growth in 0.5% serum medium, and then were exposed to 10% serum medium containing SL1122-37 or sorafenib for 24 h (8). Cells were harvested and fixed in cold 70% ethanol overnight. Cells were suspended in propidium iodide (PI) solution for 30 min. Cell cycle distribution was analyzed by using a FACScan flow cytometer (Becton Dickinson and Company, Franklin Lakes, NJ, USA).

### 2.4. Annexin V/FITC/PI staining assay

The apoptotic cells were estimated by determining the levels of phosphatidylserine on cell surface (9). PLC/PRF/5 cells seeded in 6-well plates ( $1.0 \times 10^5$  per well) were exposed to SL1122-37 or sorafenib. After exposure for 24 h, the levels of phosphatidylserine were determined by using Annexin-V/FITC and PI kit (Labtek, Dalian, Liaoning, China). The experiment was performed on a FACScan flow cytometry. The population of apoptotic cells was estimated by comparing to the vehicle control.

### 2.5. Scratch assay

The effects of SL1122-37 or sorafenib on HUVEC migration was evaluated by using a wound scratch assay. HUVECs were seeded into 6-well dish at  $2.0 \times 10^5$  cells/well. Cells were allowed to attach and reach 80% confluence and a scratch (1 mm) was made through dish with a micropipette tip to generate one homogeneous wound. After wounding, the peeled off cells were removed with PBS washes. Cells were further incubated with SL1122-37 or sorafenib for 24 h and then the wound widths were measured under microscope using an ocular

grid. Cell migration = 0 time wound width (1 mm) - 24 h wound width.

### 2.6. Capillary tube formation assay

The capillary tube formation assay was performed to evaluate the activity of SL1122-37 or sorafenib against capillary tube formation of HUVECs on 3-D Matrigel. Matrigel (50  $\mu$ L/per well, Becton Dickinson and Company) at 4°C was used to coat each well of a 96-well plate and then allowed to polymerize for 1 h at 37°C. Cell suspension was added to each well ( $2.0 \times 10^4$ ), together with or without SL1122-37 or sorafenib, and incubated at 37°C in a humidified chamber with 5% CO<sub>2</sub>. The morphogenesis of capillary tube was visualized after 24 h. Images from a total of five microscopic fields per well were analyzed by Motic Image Plus 2.0 software (Motic Instruments Inc., Richmond, Canada). The tube formation was defined by counting the branch points of the formed tubes and average numbers of branch points were calculated.

### 2.7. Western blotting analysis

Cells ( $3.0 \times 10^5$  per well) seeded in 6-well plates were exposed to SL1122-37 or sorafenib for 24 h. Cells were harvested and cell lysates (30  $\mu$ g of protein per lane) were fractionated by 10% SDS-PAGE. The proteins were electro-transferred onto nitrocellulose membranes and the protein levels were detected using the primary antibodies with appropriate dilution (10). The primary antibodies included those to caspase-9 (9502), caspase-3 (9662), cleaved PARP (9541), Bax (2772), cyclin D1 (2922), phospho-c-Kit (3391), c-Kit (3308), PI3K (4249), phospho-p44/42 MARK (9101), p44/42 MARK (4370), Wnt-2 (3169-1),  $\beta$ -catenin (9562), survivin (2808), PCNA (2586), phospho-VEGFR-2 (2478, Cell Signaling), Mcl-1 (YT2679, Immuno Way), phospho-Akt (sc-13565), Akt (sc-8312), phospho-NF- $\kappa$ B (sc-33020), NF- $\kappa$ B (sc-8008), VEGF (sc-152, Santa Cruz), c-Myc (ab32072), and  $\beta$ -actin (ab6276, Abcam). The bound antibodies were visualized using an enhanced chemiluminescence reagent and quantified by densitometry using ChemiDoc XRS+ image analyzer (Bio-Rad, Hercules, CA, USA). Densitometric analyses of bands were adjusted with  $\beta$ -actin as loading control. The percentages of increase or decrease of protein were estimated by comparison to the vehicle control (100%).

### 2.8. Statistical analysis

Data was expressed as mean  $\pm$  S.D. for three different determinations. Statistical significance was analyzed by one-way analysis of variance (ANOVA) followed by Dunnett's multiple range tests.  $p < 0.05$  was considered as statistically significant. Statistical analysis was performed using the SPSS/Win 13.0 software (SPSS, Inc, Chicago, IL, USA).

## 3. Results

### 3.1. Inhibition of HCC proliferation

PLC/PRF/5 cells were exposed to SL1122-37 or sorafenib for 72 h and then subjected to the MTT assay. As shown in Figure 2A, SL1122-37 had the similar profiles of inhibition to sorafenib, whereas a greater inhibitory effect was observed in SL1122-37 than sorafenib (0.04-1  $\mu$ M,  $p < 0.05$ ; 5 and 25  $\mu$ M,  $p < 0.01$  vs. the vehicle control). Statistical analysis indicated the difference between SL1122-37 and sorafenib (0.04-1  $\mu$ M,  $p < 0.05$ ; 5 and 25  $\mu$ M,  $p < 0.01$ ). The IC<sub>50</sub> values based on the rates of inhibition at 72 h exposure in SL1122-37 and sorafenib were 4.34 and 11.39  $\mu$ M, respectively.

### 3.2. Arrest of cell cycle in G1 phase

The inhibition of SL1122-37 on HCC proliferation was also determined by its activity of cell cycle arrest in G1 phase. SL1122-37 at 1.25, 2.5 and 5  $\mu$ M for 24 h exposure significantly increased the population of cells with G1 phase by 25.3%, 27.6%, and 29.7%, respectively (Figure 2B c-e,  $p < 0.01$  vs. the vehicle control). Sorafenib at 5  $\mu$ M increased G1 phase cells by 10.5% (Figure 2B-b, 5  $\mu$ M,  $p < 0.05$  vs. the vehicle control). A significant difference existed between SL1122-37 and sorafenib ( $p < 0.01$ ).

Western blotting indicated the inhibition of cyclin D1 expression in the SL1122-37- or sorafenib-treated cells. SL1122-37 at 1.25, 2.5 and 5  $\mu$ M, the levels of cyclin D1 were significantly decreased by 4.1%, 51.2% and 55.5%, respectively (Figure 2C, 1.25  $\mu$ M,  $p > 0.05$ ; 2.5 and 5  $\mu$ M,  $p < 0.01$  vs. the vehicle control). Sorafenib at 5  $\mu$ M reduced cyclin D1 expression by 46.1% ( $p < 0.01$  vs. the vehicle control).

### 3.3. Induction of cancer cell apoptosis

HCC cells were analyzed by flow cytometry following staining with Annexin-V/FITC and PI. Similar profiles of cell apoptosis were observed after treatment with SL1122-37 or sorafenib. SL1122-37 at 1.25 to 5  $\mu$ M for 24 h, the percentages of apoptotic cells were significantly increased to 16.1%, 24.7%, and 29.3%, respectively (Figure 3A c-e, 1.25  $\mu$ M,  $p < 0.05$ ; 2.5 and 5  $\mu$ M,  $p < 0.01$  vs. the vehicle control). Sorafenib at 5  $\mu$ M induced apoptotic cells to 25.2% (Figure 3A-b, 5  $\mu$ M,  $p < 0.01$  vs. the vehicle control).

Western blotting suggested that this effect of SL1122-37 might arise from its roles in regulation of apoptotic proteins. As shown in Figure 3B, SL1122-37 at 1.25, 2.5 and 5  $\mu$ M for 24 h exposure, the levels of the cleaved caspase-9 were significantly increased by 28.7%, 14.5% and 53.3%, respectively ( $p < 0.01$  vs. the vehicle control); cleaved caspase-3 by 6.8%, 87.5% and 57.2%, respectively (1.25  $\mu$ M,  $p > 0.05$ ; 2.5 and 5  $\mu$ M,  $p < 0.01$  vs. the vehicle control); cleaved PARP by 20.2%, 287.5% and 350.5%,

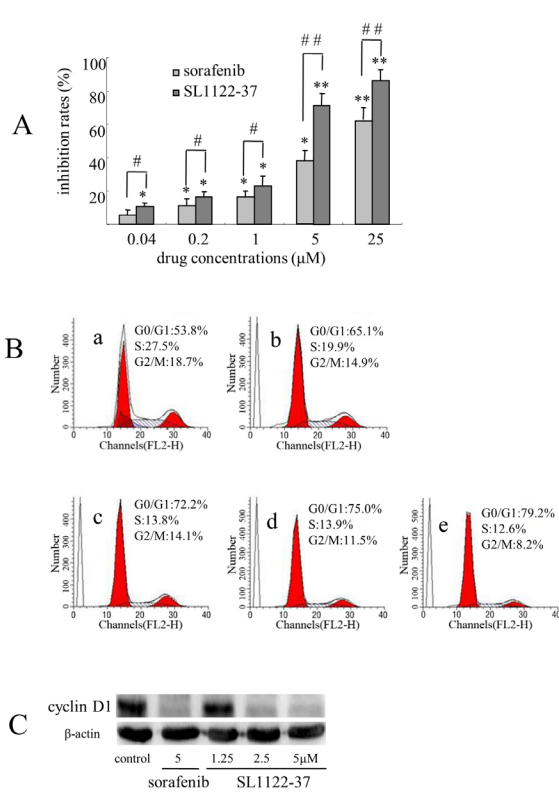


**Figure 2. The effects of SL1122-37 on PLC/PRF/5 proliferation.** (A) The inhibition of PLC/PRF/5 proliferation was estimated by the MTT assay. \* $p < 0.05$ , \*\* $p < 0.01$  vs. the vehicle control. # $p < 0.05$ , ## $p < 0.01$  between SL1122-37 and sorafenib. (B) SL1122-37 arrested cell cycle in G1 phase as determined by a FACS-can flow cytometer. a: the vehicle control; b: sorafenib 5  $\mu\text{M}$ ; c-e: SL1122-37 1.25, 2.5 and 5  $\mu\text{M}$ , respectively. (C) Western blotting showed the inhibition of cyclin D1 expression by SL1122-37 or sorafenib. Western blotting assay was performed as described in the Materials and methods. Densitometric analyses of bands were adjusted with  $\beta$ -actin as loading control. The percentages of decrease of protein were estimated by comparison to the vehicle control (100%). The bars indicated mean  $\pm$  S.D. ( $n = 3$ ).

respectively (1.25  $\mu\text{M}$ ,  $p < 0.05$ ; 2.5 and 5  $\mu\text{M}$ ,  $p < 0.01$  vs. the vehicle control). While the levels of pro-caspase-9, pro-caspase-3 were consequently decreased, respectively. Further analysis indicated the increase of Bax and decrease of Mcl-1 in the SL1122-37-treated cells. The ratio of Bax/Mcl-1 was significantly increased as compared with the vehicle control (Figure 3B, 1.25  $\mu\text{M}$ ,  $p < 0.05$ ; 2.5 and 5  $\mu\text{M}$ ,  $p < 0.01$  vs. the vehicle control). Sorafenib at 5  $\mu\text{M}$  increased the level of the cleaved caspase-9 by 36.8% ( $p < 0.05$  vs. the vehicle control); cleaved caspase-3 by 10.5% ( $p > 0.05$  vs. the vehicle control); and cleaved PARP by 278.2% ( $p < 0.01$  vs. the vehicle control), respectively. A significant difference existed between SL1122-37 and sorafenib (5  $\mu\text{M}$ ,  $p < 0.05$ ).

### 3.4. Inhibition of a multiple tyrosine kinase activity in HCC cells

Western blotting analysis determined the levels of the multi-kinases in PLC/PRF/5 cells. Both sorafenib and SL1122-37 had the activity of modulating the expression of these tyrosine kinases, whereas SL1122-37 possessed more potential than sorafenib. SL1122-37 at 1.25, 2.5 and 5  $\mu\text{M}$  for 24 h exposure prevented phosphor-c-Kit expression by 6.4%, 46.1%, and 88.2%, respectively (Figure 4A,  $p < 0.01$  vs. the vehicle control); PI3K by 5.8%, 29.1%, 57.3%, respectively (2.5  $\mu\text{M}$ ,  $p < 0.05$ ; 5  $\mu\text{M}$ ,  $p < 0.01$  vs. the vehicle control); phospho-Akt by 3.4%, 28.6%, 82.9%, respectively (2.5  $\mu\text{M}$ ,  $p < 0.05$ ; 5  $\mu\text{M}$ ,  $p < 0.01$  vs. the vehicle control); phospho-ERK1/2 by 26.2%, 65.6%, 84.5%, respectively (1.25  $\mu\text{M}$ ,  $p < 0.05$ ; 2.5 and 5  $\mu\text{M}$ ,  $p < 0.01$  vs. the vehicle control) (Figure 4B); NF- $\kappa\text{B}$  by 13.2%, 30.3%, 89.9%, respectively (2.5  $\mu\text{M}$ ,  $p < 0.05$ ; 5  $\mu\text{M}$ ,  $p < 0.01$  vs. the vehicle control); phospho-NF- $\kappa\text{B}$  by 16.4%, 26.7%, 72.7%, respectively

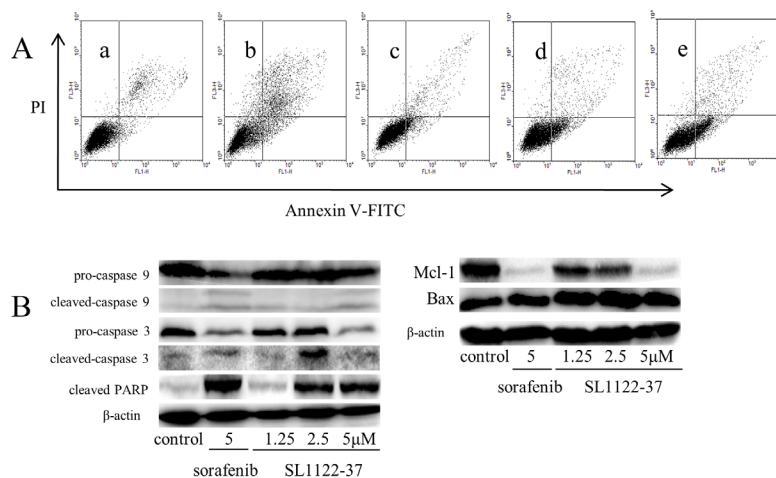


**Figure 3. SL1122-37 or sorafenib induced PLC/PRF/5 cells to apoptosis.** (A) Flow cytometry analyzed the apoptotic cells exposed to 5  $\mu\text{M}$  of sorafenib (b) or different concentrations of SL1122-37 for 24 h (a, the vehicle control; c-e, 1.25, 2.5 and 5  $\mu\text{M}$ , respectively). (B) Western blotting analyzed the changes of apoptotic proteins in PLC/PRF/5 cells. The procedure was described as Figure 2. The ratio of Bax/Mcl-1 was calculated by dividing the density value of Bax by that of Mcl-1 at same point. Triplicate experiments were performed with triplicate samples.

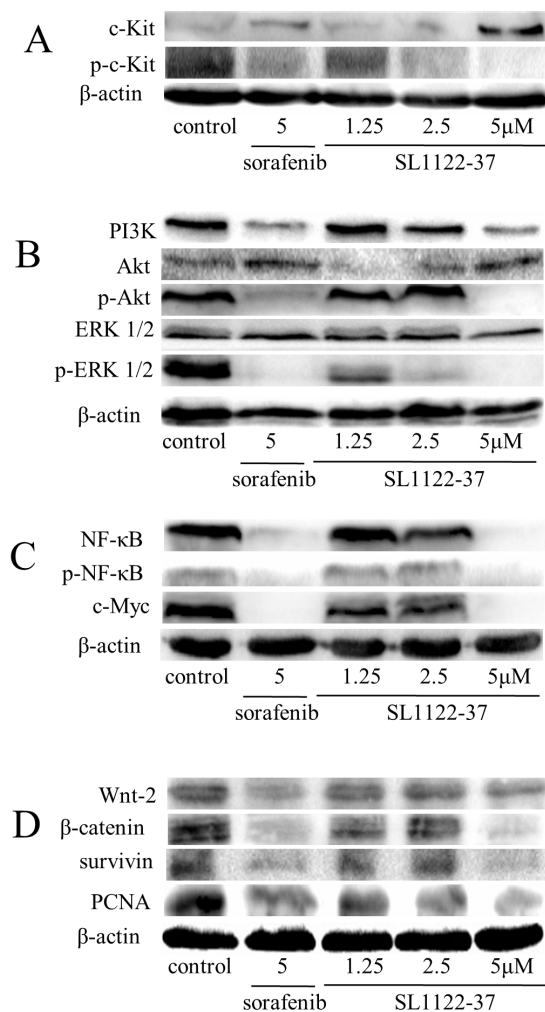


**Figure 4. Western blotting analysis demonstrated the inhibition of multi-kinases and modulation of the Wnt/ $\beta$ -catenin pathway in PLC/PRF/5 cells exposed to SL1122-37 or sorafenib.** Western blotting assay was performed as described in Figure 2. Densitometric analyses of bands were adjusted with  $\beta$ -actin as loading control. The percentages of decrease or increase of protein were estimated by comparison to the vehicle control (100%). Triplicate experiments were performed separately.

(2.5  $\mu$ M,  $p < 0.05$ ; 5  $\mu$ M,  $p < 0.01$  vs. the vehicle control); c-Myc by 10.6%, 25.9%, 89.7%, respectively (1.25 and 2.5  $\mu$ M,  $p < 0.05$ ; 5  $\mu$ M,  $p < 0.01$  vs. the vehicle control) (Figure 4C). Sorafenib at 5  $\mu$ M reduced the level of phosphor-c-Kit by 35.5%, PI3K by 40.8%, phospho-Akt by 18.4%, phospho-ERK1/2 by 67.2%, NF- $\kappa$ B by 69.4%, phospho-NF- $\kappa$ B by 72.6%, c-Myc by 79.9% ( $p < 0.01$  vs. the vehicle control). The comparative analysis of these data indicated that SL1122-37 had greater activity than sorafenib in the modulation of these kinases ( $p < 0.05$  between SL1122-37 and sorafenib).

### 3.5. Modulation of the Wnt/ $\beta$ -catenin signaling pathway

We evaluated the activity of SL1122-37 in the modulation of the Wnt/ $\beta$ -catenin pathway. As shown in

Figure 4D, SL1122-37 at 1.25, 2.5 and 5  $\mu$ M significantly reduced the level of Wnt-2 expression by 11.6%, 30.4% and 49.8%, respectively (1.25 and 2.5  $\mu$ M,  $p < 0.05$ ; 5  $\mu$ M,  $p < 0.01$  vs. the vehicle control);  $\beta$ -catenin by 31.6%, 39.0% and 81.9%, respectively (1.25 and 2.5  $\mu$ M,  $p < 0.05$ ; 5  $\mu$ M,  $p < 0.01$  vs. the vehicle control); PCNA by 36.6%, 55.0%, and 75.9%, respectively (1.25  $\mu$ M,  $p < 0.05$ ; 2.5 and 5  $\mu$ M,  $p < 0.01$  vs. the vehicle control); survivin by 25.0%, 44.3%, and 59.8%, respectively (1.25 and 2.5  $\mu$ M,  $p < 0.05$ ; 5  $\mu$ M,  $p < 0.01$  vs. the vehicle control). Sorafenib at 5  $\mu$ M inhibited the level of Wnt-2 expression by 36.9% ( $p < 0.05$  vs. the vehicle control);  $\beta$ -catenin by 65.4% ( $p < 0.01$  vs. the vehicle control); PCNA by 37.0% ( $p < 0.05$  vs. the vehicle control); survivin by 47.9% ( $p < 0.05$  vs. the vehicle control), respectively. Statistic analysis showed the significant difference between SL1122-37 and sorafenib (survivin,  $p < 0.05$ ; Wnt-2,  $\beta$ -catenin and PCNA,  $p < 0.01$ ).

### 3.6. Prevention of angiogenesis in HUVECs

Figure 5A showed the similar profiles of SL1122-37 and sorafenib in the inhibition of HUVECs growth. SL1122-37 at 0.04 and 0.2  $\mu$ M did not obviously inhibit HUVECs proliferation ( $p > 0.05$  vs. the vehicle control), whereas SL1122-37 at the concentrations range from 1 to 25  $\mu$ M, the inhibition of HUVECs was significantly increased by 17.6%, 36.8%, and 79.3%, respectively (1  $\mu$ M,  $p < 0.05$ ; 5 and 25  $\mu$ M,  $p < 0.01$  vs. the vehicle control). Sorafenib at the same concentrations inhibited HUVEC proliferation by 12.0%, 21.8%, and 59.9%, respectively (1 and 5  $\mu$ M,  $p < 0.05$ ; 25  $\mu$ M,  $p < 0.01$  vs. the vehicle control). A significant difference was seen between SL1122-37 and sorafenib at the range from 1  $\mu$ M to 25  $\mu$ M ( $p < 0.05$ ).

The prevention of HUVEC migration by SL1122-37 or sorafenib was then determined (Figure 5B). HUVECs in the control group exhibited highly spontaneous migration. The average spontaneous distance at 24 h incubation was 620  $\mu$ m. The ability of migration was markedly reduced in the presence of SL1122-37 or sorafenib. The migration distances of HUVEC exposure to 1.25, 2.5 and 5  $\mu$ M of SL1122-37 were 228, 146 and 87  $\mu$ m, respectively ( $p < 0.01$  vs. the vehicle control). The migration distances of HUVEC exposure to the same concentrations of sorafenib were 388, 263 and 157  $\mu$ m, respectively ( $p < 0.05$  vs. the vehicle control). Statistical analysis of these data showed the difference between SL1122-37 and sorafenib ( $p < 0.05$ ).

SL1122-37 possessed the activity against capillary tube formation and this activity was greater than sorafenib. As shown in Figure 5C, the branch points of capillary tube in the vehicle control cells were 27 ( $26.6 \pm 3.8$ ). SL1122-37 at 1.25, 2.5 and 5  $\mu$ M for 24 h exposure, the number of branch points were significantly reduced to 16 (by 40%), 15 (by 42.5%) and 9 (by 67.5%), respectively (1.25  $\mu$ M,  $p < 0.05$ ; 2.5 and 5  $\mu$ M,  $p < 0.01$  vs. the vehicle control). Sorafenib by 5  $\mu$ M reduced the branch points of capillary tube to 14 (47.3%) (Figure 5C-b,  $p < 0.05$  vs. the vehicle control).

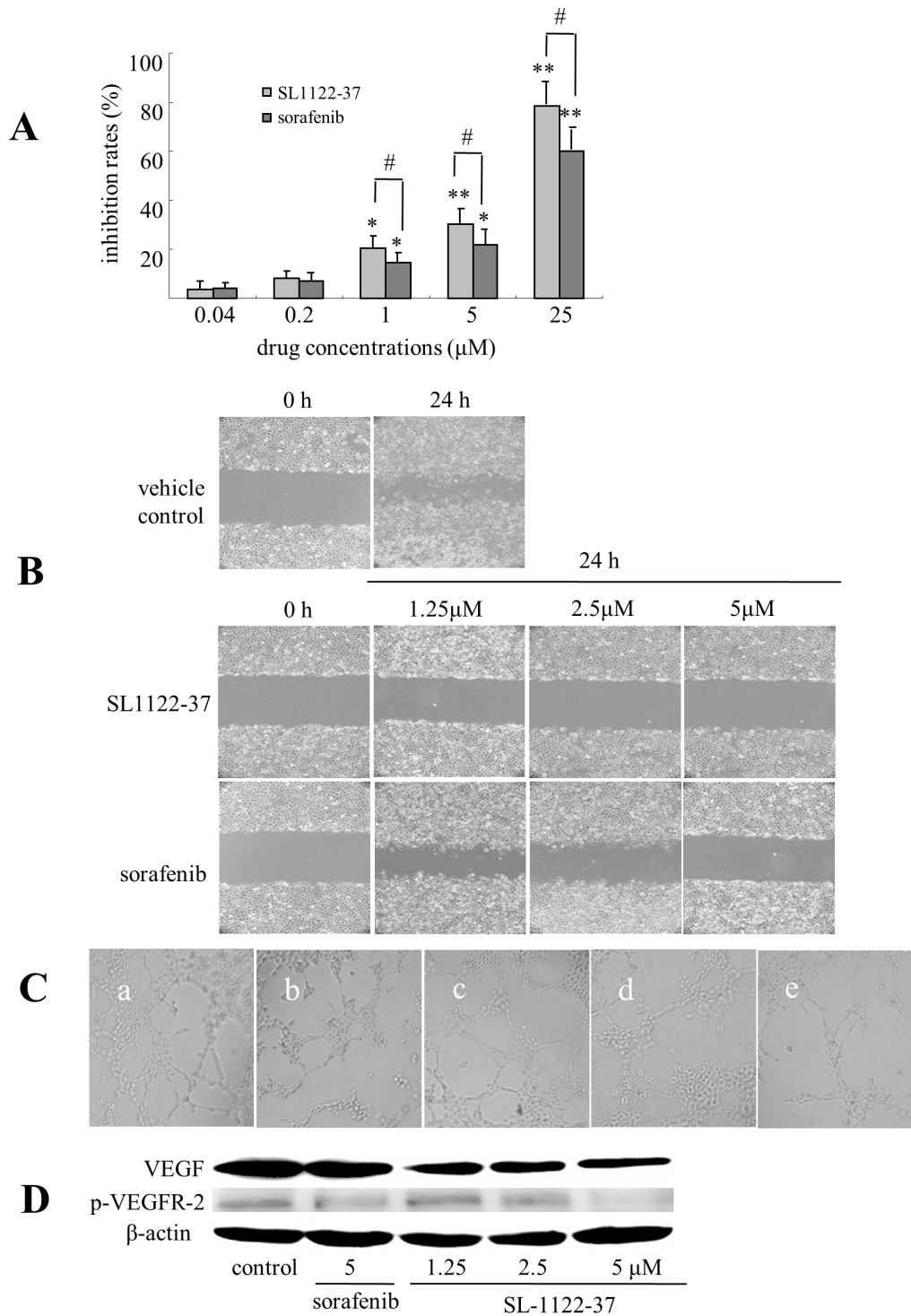


**Figure 5. The effects of SL1122-37 on HUVECs. (A)** The inhibition of cell growth was estimated by the MTT assay. The bars indicated mean  $\pm$  S.D. ( $n = 3$ ). \* $p < 0.05$ , \*\* $p < 0.01$  vs. the vehicle control. # $p < 0.05$  between SL1122-37 and sorafenib. **(B)** The inhibition of HUVECs migration by SL1122-37 or sorafenib as determined by the scratch assay. Cell migration = 0 time wound width (1 mm) - 24 h wound width. **(C)** The prevention of HUVEC tube formation on 3-D Matrigel, **a**: vehicle control; **b**: sorafenib 5  $\mu$ M; **c-e**: SL1122-37 1.25, 2.5 and 5  $\mu$ M, respectively. **(D)** Western blotting showed the inhibition of VEGF and phosphor-VEGFR-2 in HUVECs exposed to SL1122-37 or sorafenib. Triplicate experiments were performed separately.

There was a significant difference between SL1122-37 and sorafenib ( $p < 0.05$ ).

Western blotting determined the levels of VEGF and phospho-VEGF receptor 2 in HUVECs (Figure 5D). SL1122-37 at 1.25, 2.5 and 5  $\mu$ M reduced the levels of VEGF by 38.8%, 57.7%, and 79.9%, respectively (1.25

$\mu$ M,  $p < 0.05$ ; 2.5 and 5  $\mu$ M,  $p < 0.01$  vs. the vehicle control); phospho-VEGF receptor 2 by 22.3%, 53.0%, and 81.8%, respectively (1.25 and 2.5  $\mu$ M,  $p < 0.05$ ; 5  $\mu$ M,  $p < 0.01$  vs. the vehicle control). Sorafenib at 5  $\mu$ M reduced the level of VEGF expression by 21.5% ( $p < 0.05$  vs. the vehicle control); phospho-VEGF receptor 2 by 30.9% ( $p$

< 0.05 vs. the vehicle control), respectively. Significant differences existed between SL1122-37 and sorafenib ( $p < 0.05$ ).

#### 4. Discussion

In this study, we determined the inhibitory effects of SL1122-37, a novel derivative of sorafenib, on the proliferation of HCC PLC/PRF/5 cells and the formation of angiogenesis of HUVECs. Its efficacy and mechanisms were compared with those of sorafenib. SL1122-37 possessed the activity against cancer cell proliferation. We suggested that these high effects of SL1122-37 might arise from its roles in the apoptotic induction and regulation of cell cycle. The mechanisms of SL1122-37 action might associate with its activity in the inhibition of multi-kinases. The following assays were performed to determine its activity of antiangiogenesis. SL1122-37 strongly prevented HUVECs migration and capillary tube formation. The activity of SL1122-37 against angiogenesis was greater than sorafenib. The effect of antiangiogenesis might be due to the prevention of VEGF and phospho-VEGFR in HUVECs. These results support our strategy of designing new derivatives based on sorafenib.

Studies showed that the inhibition of sorafenib on cancer growth was mainly due to its activity of apoptotic induction (11). Sorafenib might induce cancer cells to apoptosis through activating the intrinsic mitochondria-mediated pathway (12). Further studies suggested that the crucial event for initiating this pathway might due to its role in the inhibition of myeloid cell leukemia-1 (Mcl-1) (13). As a member of the antiapoptotic Bcl-2 family, Mcl-1 is overexpressed in HCC. Overexpression of Mcl-1 could protect cancer cells from apoptosis. Down-regulation of Mcl-1 is related to the release of cytochrome c from mitochondria into cytosol, caspase activation, and apoptotic cell death. The Bax/Mcl-1 ratio has thus been considered to be a marker of apoptosis activation (14). In this study, SL1122-37 was found to have the similar profiles in the inhibition of HCC and induction of apoptosis, whereas its activities were more potential than sorafenib. We thus suggested that SL1122-37 might induce cancer cells to apoptosis through initiating the intrinsic mitochondria-mediated pathway.

RAF/mitogen-activated protein/extracellular signal-regulated kinase (ERK) kinase (MEK)/ERK cascade signaling pathway has been considered to play crucial roles in the development of HCC (15). In this pathway, the activation of c-Kit might be an important initial event. Activated c-Kit could regulate the transcription of its multiple downstream targets, such as the Ras-Raf-MEK-ERK cascade and PI3K/Akt pathway. The cytoplasmic target of ERK and Akt is IKK (16). Activation of IKK leads to the degradation of I $\kappa$ B, resulting in the translocation of NF- $\kappa$ B into nucleus and transcription of targeted genes. High level of NF- $\kappa$ B has been implicated in the regulation of apoptosis, proliferation and c-Myc expression (17). We

evaluated the activity of SL1122-37 against these kinases and compared them with those of sorafenib. SL1122-37 possessed the similar profiles against these kinases, whereas its effect was greater than sorafenib. We thus suggested that SL1122-37 might be a promising multi-kinase inhibitor.

The high efficacy of SL1122-37 might also be contributed by its roles in the modulation of the Wnt/ $\beta$ -catenin pathway. Over-expression of the Wnt/ $\beta$ -catenin pathway is frequently observed in HCC. Activation of Wnt-2 and  $\beta$ -catenin has been considered to be the initial events for HCC proliferation (18). Its downstream targets, such as cyclin D1, survivin, PCNA and c-Myc, are consequently amplified following the initial event (19). Among these targets, PCNA is a marker of cell proliferation and is highly expressed during G1 and S phases. Cyclin D1 is a cell cycle protein frequently overexpressed in HCC. High level of c-Myc could stimulate cancer growth and prevent them from apoptosis. Survivin is an anti-apoptotic molecule widely expressed in HCC. Overexpression of survivin leads to antiapoptosis (20). In this study, SL1122-37 was observed to have a greater activity than sorafenib in modulation of this pathway, suggesting its roles in the inhibition of HCC.

HCC is a hypervascular tumor and the progression of invasion is highly correlated to the formation of angiogenesis (21). Angiogenesis actually starts with vascular endothelial cells and cancerous tumor cells releasing molecules. These signals activate the proliferation and migration of vascular endothelial cells leading to endothelial cell sprouts in stromal space. The crucial signal of angiogenesis is the release of vascular endothelial growth factor (VEGF). Circulating VEGF binds to its receptors (VEGFR1-3, mainly 2) on endothelial cells and induces the dimerization and autophosphorylation of the receptor, which activates the downstream signal eventually leading to angiogenesis (16). Using HUVECs, SL1122-37 was found to have a greater inhibitory effect than sorafenib on the angiogenesis. This effect might arise from its roles in the inhibition of VEGF and its autophosphorylation of the receptors. These results support our strategy of designing SL1122-37 to be an angiogenesis inhibitor. However, more evidence of antiangiogenesis and mechanisms of action are needed.

In summary, SL1122-37 possessed greater activity than sorafenib in the inhibition HCC growth and HUVECs angiogenesis. These inhibitory effects of SL1122-37 might arise from its roles in the induction of apoptosis and inhibition of multiple kinases. We suggested that SL1122-37 might be a promising compound that could be developed as a potential agent for the treatment of HCC.

#### Acknowledgements

This project was supported by the Ministry of Science and Technology of China (2010ZX09401-302-2-07 and 2011ZX09102-001-03).

## References

1. Wilhelm S, Carter C, Lynch M, Lowinger T, Dumas J, Smith RA, Schwartz B, Simantov R, Kelley S. Discovery and development of sorafenib: A multikinase inhibitor for treating cancer. *Nat Rev Drug Discov.* 2006; 5:835-844.
2. Waghray A, Balci B, El-Gazzaz G, Kim R, Pelley R, Narayanan Menon K, Estfan B, Romero-Marrero C, Aucejo F. Safety and efficacy of sorafenib for the treatment of recurrent hepatocellular carcinoma after liver transplantation. *Clin Transplant.* 2013; 27:555-561.
3. Wu S, Chen JJ, Kudelka A, Lu J, Zhu X. Incidence and risk of hypertension with sorafenib in patients with cancer: a systematic review and meta-analysis, Incidence and risk of hypertension with sorafenib in patients with cancer: A systematic review and meta-analysis. *Lancet Oncol.* 2008; 9:117-123.
4. Veronese ML, Mosenkis A, Flaherty KT, Gallagher M, Stevenson JP, Townsend RR, O'Dwyer PJ. Mechanisms of hypertension associated with BAY 43-9006. *J Clin Oncol.* 2006; 24:1363-1369.
5. Wan PT, Garnett MJ, Roe SM, Lee S, Niculescu-Duvaz D, Good VM, Jones CM, Marshall CJ, Springer CJ, Barford D, Marais R. Mechanism of activation of the RAF-ERK signaling pathway by oncogenic mutations of B-RAF. *Cell.* 2004; 116:855-867.
6. Li WB. The design and synthesze of anti-cancer agent belong to indazole or azaindazole based diarylureas or diarylsulfoureas, China patent (2012), CN 102153551B.
7. Zhu T, Jiao Y, Chen YD, Wang X, Li HF, Zhang LY, Lu T. Pharmacophore identification of Raf-1 kinase inhibitors. *Bioorg Med Chem Lett.* 2008; 18:2346-2350.
8. Cui CZ, Wen XS, Cui M, Gao J, Sun B, Lou HX. Synthesis of solasodine glycoside derivatives and evaluation of their cytotoxic effects on human cancer cells. *Drug Discov Ther.* 2012; 6:9-17.
9. Bommareddy A, Zhang XY, Kaushik RS, Dwivedi C. Effects of components present in flaxseed on human colon adenocarcinoma Caco-2 cells: Possible mechanisms of flaxseed on colon cancer development in animals. *Drug Discov Ther.* 2010; 4:184-189.
10. Zamri N, Masuda N, Oura F, Yajima Y, Nakada H, Fujita-Yamaguchi Y. Effects of two monoclonal antibodies, MLS128 against Tn-antigen and 1H7 against insulin-like growth factor-I receptor, on the growth of colon cancer cells. *Biosci Trends.* 2012; 6:303-312.
11. Sun NK, Huang SL, Chang TC, Chao CC. Sorafenib induces endometrial carcinoma apoptosis by inhibiting Elk-1-dependent Mcl-1 transcription and inducing Akt/GSK3 $\beta$ -dependent protein degradation. *J Cell Biochem.* 2013; 114:1819-1831.
12. Kurosu T, Ohki M, Wu N, Kagechika H, Miura O. Sorafenib induces apoptosis specifically in cells expressing BCR/ABL by inhibiting its kinase activity to activate the intrinsic mitochondrial pathway. *Cancer Res.* 2009; 69:3927-3936.
13. Gauthier A, Ho M. Role of sorafenib in the treatment of advanced hepatocellular carcinoma: An update. *Hepatol Res.* 2013; 43:147-154.
14. Li G, Zhang S, Fang H, Yan B, Zhao Y, Feng L, Ma X, Ye X. Aspirin overcomes Navitoclax-resistance in hepatocellular carcinoma cells through suppression of Mcl-1. *Biochem Biophys Res Commun.* 2013; 434:809-814.
15. Wei W, Chua MS, Grepper S, So S. Small molecule antagonists of Tcf4/beta-catenin complex inhibit the growth of HCC cells *in vitro* and *in vivo*. *Int J Cancer.* 2010; 126:2426-2436.
16. Perkins ND. Integrating cell-signalling pathways with NF- $\kappa$ B and IKK function. *Nat Rev Mol Cell Biol.* 2007; 8:49-62.
17. Baldwin AS Jr. Series introduction: the transcription factor NF-kappaB and human disease. *J Clin Invest.* 2001; 107:3-6.
18. Wei Z, Doria C, Liu Y. Targeted therapies in the treatment of advanced hepatocellular carcinoma. *Clin Med Insights Oncol.* 2013; 7:87-102.
19. Zhang YS, Xie JZ, Zhong JL, Li YY, Wang RQ, Qin YZ, Lou HX, Gao ZH, Qu XJ. Acetyl-11-keto- $\beta$ -boswellic acid (AKBA) inhibits human gastric carcinoma growth through modulation of the Wnt/ $\beta$ -catenin signaling pathway. *Biochim Biophys Acta.* 2013; 1830:3604-3615.
20. Wei Y, Shen N, Wang Z, Yang G, Yi B, Yang N, Qiu Y, Lu J. Sorafenib sensitizes hepatocellular carcinoma cell to cisplatin *via* suppression of Wnt/ $\beta$ -catenin signaling. *Mol Cell Biochem.* 2013; 381:139-144.
21. Inagaki Y, Tang W, Zhang L, Du GH, Xu WF, Kokudo N. Novel aminopeptidase N (APN/CD13) inhibitor 24F can suppress invasion of hepatocellular carcinoma cells as well as angiogenesis. *Biosci Trends.* 2010; 4:56-60.

(Received October 3, 2013; Revised October 12, 2013; Accepted October 15, 2013)

## Japan's advanced medicine

Ri Sho<sup>1,\*</sup>, Hiroto Narimatsu<sup>1</sup>, Masayasu Murakami<sup>2</sup>

<sup>1</sup>Department of Public Health, Yamagata University Graduate School of Medical Science, Yamagata, Japan;

<sup>2</sup>Department of Health Care Policy, Yamagata University Graduate School of Medical Science, Yamagata, Japan.

### Summary

Like health care systems in other developed countries, Japan's health care system faces significant challenges due to aging of the population and economic stagnation. Advanced medicine (*Senshin Iryou*) is a unique system of medical care in Japan offering highly technology-driven medical care that is not covered by public health insurance. Advanced medicine has recently developed and expanded as part of health care reform. Will it work? To answer this question, we briefly trace the historical development of advanced medicine and describe the characteristics and current state of advanced medical care in Japan. We then offer our opinions on the future of advanced medicine with careful consideration of its pros and cons. We believe that developing advanced medicine is an attempt to bring health care reform in line rather than the goal of health care reform.

**Keywords:** Advanced medicine, universal health insurance, health care

### 1. Introduction

After taking power last December as Prime Minister of Japan, Shinzo Abe implemented a bold new approach known as "Abenomics" - a portmanteau of Abe and economics - to reinvigorate Japan's economy. Indeed, Abenomics is a "quiver" of policies featuring "three arrows": monetary relaxation, fiscal stimulus, and economic growth strategies (1). The first two arrows were fired during Abe's early days in office and have already hit their marks. The overvalued yen has fallen sharply and the stock market has surged, both spurring corporate profits. Although the two strategies did not result in real changes in the economy, these signs of economic recovery did lead to hope and skepticism around the country. Seeking to boost Japan's long-term economic performance, the keenly awaited third arrow of Abenomics was just recently released (2). It focused on structural reform and creating special rooms within the public sector, including the energy industry, medical care, and infrastructure, to revitalize the private sector. As a result, innovations in medical technology and

health care reforms represent a stepping stone towards achieving further economic growth, primarily in the health care field.

Advanced medicine (*Senshin Iryou*) is the frontier of innovations in medical technology and health care reform. Advanced medicine is a unique medical care system in Japan offering highly technology-driven medical care that is not covered by health insurance along with conventional medical care that is covered by health insurance (3,4). Advanced medicine has received a great deal of public attention. National debates among professional health workers, local governments, and policymakers concerning the practice, implications, and theory of advanced medicine have also been refueled by Abenomics' growth strategies (5,6). Here, the basic concept of advanced medicine in Japan will first be explained. Next, its origin and history will be described. The current state of advanced medicine around the country will then be documented. Last, the future of advanced medicine will be predicted.

### 2. Basic concept of advanced medicine

Advanced medicine literally means to practice medicine by integrating the best of alternative medicine and conventional medicine to diagnose and treat patients. This term often appears in the medical literature and the media (4,6). In Japan, however, the term "advanced medicine" commonly refers to the

\*Address correspondence to:

Dr. Ri Sho, Department of Public Health, Yamagata University Graduate School of Medical Science, Yamagata 990-2331, Japan.

E-mail: shori@med.id.yamagata-u.ac.jp

use of newly developed medical devices, drugs, or technologies that have been authorized by the Ministry of Health, Labor, and Welfare (MHLW) but have not yet been covered by health insurance (3). Actually, this term is used more frequently in health care than in medicine. Here, advanced medicine is considered to be a Japanese version of off-label use of technology-driven medications and medical devices. In order to better understand this concept, one first needs a brief introduction to the history of advanced medicine and the health insurance system in Japan.

The current public health insurance system in Japan was established in 1961 and subsequently revised several times (Figure 1)(7,8). This system is universal health coverage called *Kaihoken*. Based on *Kaihoken*, everyone in Japan is able to choose his/her desired medical facility at which to receive the same medical care for sickness or injury at the same cost by making a co-payment of 10-30% of the cost depending on his/her age and/or income. If that monthly co-payment exceeds the maximum co-payment limit, the patient can apply for the High-Cost Medical Care Benefits (*Kougaku-Ryouyohi*) (9). This national system of additional benefits ensures that the patient pays only medical costs capped at the maximum co-payment. To ensure equity and equality in health care, the health care system has combined varied health care delivery systems with a nationally uniform payment system known as the Medical Fee Schedule (*Shinryou-Housyuu-Seido*) (10).

The Central Medical Council on Social Insurance, appointed by MHLW, revises this fee schedule every two years to individually set appropriate fees for all drugs, medical devices, and procedures. The medical fee schedule is uniformly applied to all medical facilities being reimbursed by public health insurance. To control health care costs, the public health insurance system excludes some health care services, such as those for routine childbirth and cosmetic surgery, and special forms of medical care, including cutting-edge medicine. In principle, conventional medical care

would qualify for coverage by public health insurance, but public health insurance will not cover any medical care, in whole or in part, that involves the usage of any cutting-edge drug or device that is not listed in the medical fee schedule. In other words, patients receiving a new medicine that is not covered by health insurance along with other care that would normally be covered by insurance must pay for both forms of medical care out-of-pocket. This provision is known as the ban on combining medical care covered by health insurance and medical care not covered by health insurance (*Kougou-Shinryou No Kinshi*) (Figure 2) (11).

Japan's universal health care system has led to excellent health of the population as a whole at a low cost over the past half century (7, 12), but this system also faces challenges in terms of improving the quality of medical care while controlling cost (7,9). The ban on combining medical care covered by health insurance and medical care not covered by health insurance has resulted in delayed development or use of cutting-edge treatments (13,14). To meet the growing demand for good care and newly developed drugs and treatments, the Government revised the health insurance system

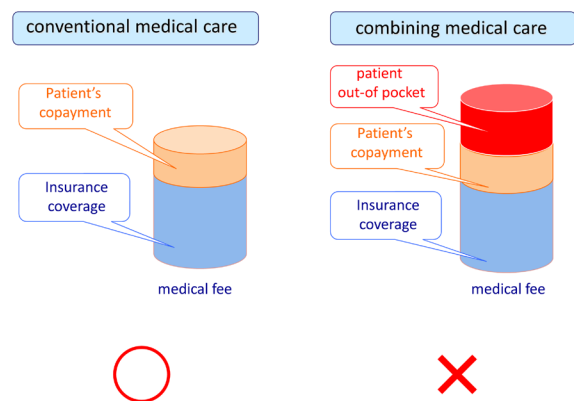


**Figure 2. Ban on combining medical care covered by health insurance and medical care not covered by health insurance.**

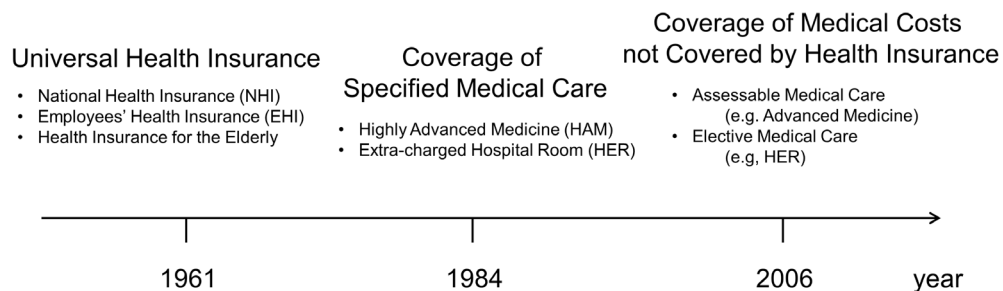


**Figure 1. Timeline of the history of advanced medicine.** Universal Health Insurance is also called public health insurance in Japan and consists of three parts: Health Insurance (for employers and their dependents), National Health Insurance (mainly for agricultural workers, the self-employed, and retirees), and Health Insurance for the Elderly (for those over the age of 75). Coverage of Specified Medical Care is an older system that reimburses specified medical expenses. Coverage of Medical Costs not Covered by Health Insurance is a new system that reimburses medical expenses not covered by health insurance. Assessable Medical Care refers to medical care that has to be assessed as appropriate to be covered by health insurance while Elective Medical Care refers to medical care that the patient has chosen to receive.

in 1984 (Figure 1). The Government introduced a new system called the Coverage of Specified Medical Care (*Tokutei Ryouyouhi*) that makes some exceptions to the ban on combined medical care covered by health insurance and not covered by health insurance. The new system potentially allows health insurance to cover highly advanced medical care while still disallowing patient preferences, such as a private hospital room (9). If, under the new system, a patient receives a MHLW-approved cutting-edge treatment at a specially authorized medical facility, then the portion of medical care that would have been covered by health insurance is in fact covered, and the patient pays only for the portion of care that is not covered by health insurance (4,9). To keep pace with the emergence of new medical technologies and drugs in some fields, like cancer therapies, and to meet the diverse needs of patients, the Government accelerated reforms and partially relaxed the ban on combining medical care covered by health insurance and medical care not covered by health insurance. The Government amended the Health Insurance Act in 2006 and replaced the system for coverage of specified medical care with another system known as the Coverage of Medical Costs not Covered by Health Insurance (*Hokengai-Heiyou-Ryouyouhi*) (Figure 1). Under this new system, the definition of advanced medicine was revised. Advanced medicine consists of two parts, one of which is highly advanced medicine (as mentioned earlier) and the other of which is advanced medical care (*Kouido Iryou*) (3). Advanced medical care includes certain new drugs or state-of-the-art medical technologies that have not been approved by the Pharmaceutical Affairs Act (PAA). This revision has led to more technology-driven medications and medical devices than ever being covered, regardless of the status of their approval by the PAA, when medical care combines care covered by health insurance and care not covered by health insurance as long as those medications or medical devices are proven safe and effective and are authorized by the MHLW.

### 3. Current state of advanced medicine

Since its emergence, advanced medicine, together with relaxing the ban on combining medical care covered by health insurance and medical care not covered by health insurance, has become a controversial issue in the area of health care reform (4,15). The Japan Medical Association (JMA) opposed the proposed reform, primarily from the perspective of equity, whereas the Government intended to promote advanced care planning in response to the rapid rise in health expenditures and increased demand for innovative drugs and medical devices. Abenomics seeks to encourage companies developing advanced medical technology as part of its growth strategy. To encourage exports of advanced medical technology and hasten approval of

new drugs and devices, the MHLW recently announced its reclassification of advanced medicine into Parts A and B, and revised the approval process (3). Advanced medicine A represents highly advanced medicine (as mentioned earlier) while Advanced medicine B includes most of the advanced medical care just mentioned. According to the latest data from the MHLW (16), Advanced medicine A includes 65 types of diagnostic tests and treatments while Advanced medicine B includes 45 types. In total, 791 diagnostic tests and treatment approaches falling under Advanced Medicine A and 505 diagnostic tests and treatment approaches falling under Advanced Medicine B were performed in clinics, hospitals, or medical centers across the country. The current state of advanced medicine in Japan is as follows (3):

- 1) The total number of medical facilities providing advanced medical services and total expenditures on advanced medicine have both been steadily increasing. The number of types of advanced medicine, however, has not changed significantly, partly because of the strict approval process in which each previously approved advanced medical technology or drug has to be periodically evaluated to decide whether to continue or revoke its status based on its efficacy and safety. One example of advanced medicine from 2011, da Vinci Surgery – surgery with a multi-armed robot and a magnified 3D high-definition vision system – was recently removed from the list because it was approved by the Central Medical Council on Social Insurance for coverage by health insurance in 2012.
- 2) Most currently available advanced medical solutions are newly developed medical devices, technologies, and drugs used in regenerative medicine and cancer treatment such as homografts and heavy ion radiotherapy. However, some advanced medical solutions relate to diagnosis, such as genetic testing for resistance to chemotherapy and genetic testing for sensitivity to antiviral therapy.
- 3) Advanced medicine has been provided to outpatients as well as inpatients.
- 4) The cost of advanced medical care varies widely, ranging from 10,000 yen for genetic testing for drug intolerance (e.g., CYP2C19 genotyping for tailored treatment of *H. pylori* infection) to several million yen for one round of cancer immunotherapy or radiotherapy (e.g., heavy ion radiotherapy).
- 5) Although medical facilities providing advanced medical care are found in every prefecture, their numbers vary quite widely among the different prefectures (Figure 3).
- 6) In concert with the government's decision to hasten approval of new drugs and devices, major university hospitals are rushing to establish a center or facility to provide various forms of advanced medical care.

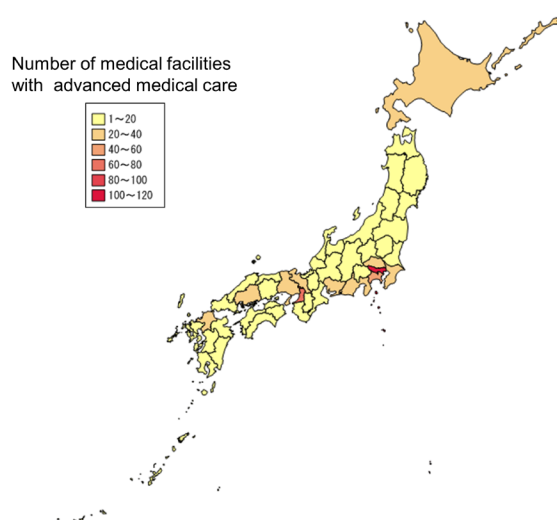


**Figure 3. Nationwide distribution of medical facilities offering advanced medical care.** Source: Ministry of Health, Labor, and Welfare. List of medical facilities offering advanced medical care (in Japanese). <http://www.mhlw.go.jp/topics/bukyoku/isei/sensiniryu/kikan02.html>. This map was drawn by HAKUCHIZU II software (ver. 2).

#### 4. Prospects for the future

Given Japan's rapidly aging population and continuous budget deficits, there is no doubt that the current health care system faces significant challenges (17,18). Without substantial reform, the system's sustainability will be called into question. Advanced medical care has developed and expanded since it emerged as part of proposed health care reform. This has been especially true since Abe announced his economic growth strategies (1,2). Nonetheless, one must not forget that advanced medicine itself cannot solve fundamental problems that the health care system faces, such as aging of the population. Reaching the ultimate goal of health care reform – controlling costs, improving quality and ensuring equity – will also be extremely difficult.

On the positive side, the expansion of advanced medical care will increase the availability of innovative drugs and cutting-edge medical devices, and thereby keep up with growing demand and also improve the quality of care. It will also encourage advances and innovation in basic and translation research, which in turn will promote exports of advanced medical technology and accelerate economic growth. Moreover, most advanced medicine is not covered by public health insurance, so expanding advanced medical care will indirectly reduce healthcare expenditures (4,11). That said, expanding advanced medical care will probably widen the healthcare gap between the rich and poor, particularly, if the ban on combining medical care covered by health insurance and medical care not covered by health insurance is totally lifted (15). This may reduce equity in medical care, thereby

contravening the fundamental principle of universal health coverage. In addition, there are also concerns about how to ensure the safety and efficacy of new drugs and highly technology-driven medical care (17).

The problems facing Japan's health care system are multi-dimensional (7,17). Expanding advanced medicine is an attempt to address these problems but is not a magic bullet. Despite growing awareness of advanced medicine, there is still little consensus about what to do or how to make things better. Advanced medicine cannot be implemented politically, nor must it be implemented all at once. Indeed, it should be debated in more detail and be implemented in accordance with evidence-based practices.

*Note: The opinions expressed here are solely those of the authors and do not necessarily reflect the views of Yamagata University Graduate School of Medical Science.*

#### References

1. Ministry of Finance Japan. What is Abenomics? current and future steps of Japanese economic revival. [http://www.mof.go.jp/english/public\\_relations/statement/others/20130419.pdf](http://www.mof.go.jp/english/public_relations/statement/others/20130419.pdf) (accessed June 19, 2013).
2. Prime Minister of Japan and His Cabinet. Japan Revitalization Strategy – JAPAN is BACK. [http://www.kantei.go.jp/jp/singi/keizaisaisei/pdf/en\\_saikou\\_jpn.pdf](http://www.kantei.go.jp/jp/singi/keizaisaisei/pdf/en_saikou_jpn.pdf) (accessed June 14, 2013).
3. Ministry of Health, Labor and Welfare. Advanced Medicine (in Japanese). [http://www.mhlw.go.jp/stf/seisakunitsuite/bunya/kenkou\\_iryuu/iryuu/hoken/sensiniryu/index.html](http://www.mhlw.go.jp/stf/seisakunitsuite/bunya/kenkou_iryuu/iryuu/hoken/sensiniryu/index.html) (accessed September 18, 2013).
4. Sakurai H. Advanced medical technology and health insurance in Japan. *JMAJ*. 2006; 49:41-43.
5. The Economist. Misfire. <http://www.economist.com/news/asia/21579514-shinzo-abe-disappoints-timid-attempt-structural-reform-misfire> (accessed June 15, 2013).
6. Fortune. Japan: Where medical miracles are waiting to get out of the lab. <http://tech.fortune.cnn.com/2013/04/08/where-medical-miracles-are-just-waiting-to-get-out-of-the-lab/> (accessed April 8, 2013).
7. Ikegami N, Yoo BK, Hashimoto H, Matsumoto M, Ogata H, Babazono A, Watanabe R, Shibuya K, Yang BM, Reich MR, Kobayashi Y. Japanese universal health coverage: Evolution, achievements, and challenges. *Lancet*. 2011; 378:1106-1115.
8. Fukawa T. Public health insurance in Japan. In: Promoting knowledge and learning for a better world (World Bank Institute, eds). Washington, DC, USA, 2002; pp. 1-14.
9. Jones RS. Health-care reform in Japan: Controlling costs, improving quality and ensuring equity. OECD Economics Department Working Papers, No. 739 (OECD publishing, eds). 2009; pp. 1-39.
10. Hashimoto H, Ikegami N, Shibuya K, Izumida N, Noguchi H, Yasunaga H, Miyata H, Acuin JM, Reich MR. Cost containment and quality of care in Japan: Is there a trade-off? *Lancet*. 2011; 378:1174-1182.
11. Kawaguchi H. Unique mixtures of public and private funding in Japan – The ban on billing for mixed medical

- care service –. Public Policy Rev. 2012; 8:145-170
12. Ikeda N, Saito E, Kondo N, *et al.* What has made the population of Japan healthy? Lancet. 2011; 378:1094-1105.
  13. Hatanaka N, Matsumoto S, Tanaka Y, Kami M. Why do Japan's advanced medical treatments never get ahead? Keio J Med. 2010; 59:46-51.
  14. Hamada H, Lapalme-Remis S. International perspective on mixed health care: Japan. McGill J Med. 2008; 11:79-80.
  15. Saito H. Theoretical and empirical analysis of mixed medical care services in Japan – what is equity? –. GRIPS Policy Information Center. 2008; 8:1-26.
  16. Ministry of Health, Labor and Welfare. List of the medical facilities offering advanced medical care (in Japanese). <http://www.mhlw.go.jp/topics/bukyoku/isei/sensiniryu/kikan02.html> (accessed September 18, 2013).
  17. Shibuya K, Hashimoto H, Ikegami N, Nishi A, Tanimoto T, Miyata H, Takemi K, Reich MR. Future of Japan's system of good health at low cost with equity: Beyond universal coverage. Lancet. 2011; 378:1265-1273.
  18. Uetsuka Y. Characteristics of Japan's healthcare systems and the problems. JMAJ. 2012; 55:330-333.
- (Received October 15, 2013; Revised October 29, 2013; Accepted October 29, 2013)*

## Standardizing management of hepatocellular carcinoma in China: Devising evidence-based clinical practice guidelines

Peipei Song\*

Hepato-Biliary-Pancreatic Surgery Division, Department of Surgery, Graduate School of Medicine, The University of Tokyo, Tokyo, Japan.

### Summary

Evidence-based clinical practice guidelines (CPGs) have been used in many countries around the world to promote standardized management of hepatocellular carcinoma (HCC). Guidelines implemented in Japan provide a good example of "translating the best current research evidence into clinical practice and obtaining new evidence in the course of influencing practitioners' attitudes and clinical decision-making". The Japanese guidelines have achieved remarkable results in terms of HCC management in Japan. The first Japanese evidence-based CPGs for HCC (J-HCC Guidelines) were published in 2005 and then revised in 2009. A second updated version that incorporates new evidence was just published on October 15, 2013. China accounts for 55% of HCC cases worldwide. Although the Government devised a series of directives on the management of HCC and Chinese Guidelines on HCC were published in 2009, neither were based on systematic review and evaluation of the literature and neither included recommendations supported by data. The novel concept of "precision surgery" was recently proposed in China. This concept is based on surgeons' clinical experience and should encourage the standardized management of HCC in China. However, recommendations supported by data are still urgently needed to guide clinical decision-making in order to facilitate standardized management of HCC in China.

**Keywords:** Liver cancer, clinical guideline, evidence-based medicine (EBM), precision surgery, evaluation

In recent years, the concept of "standardized management of care" has garnered substantial attention worldwide. Drafting of disease management guidelines that specify appropriate diagnosis and treatment based on scientific evidence and collaborations between medical professionals involved in the treatment of a given condition is the key to standardized management of care (1,2). The purpose of evidence-based clinical practice guidelines (CPGs) is to "translate the best current research evidence into clinical practice and obtain new evidence in the course of influencing practitioners' attitude and clinical decision-making".

CPGs have been used for the standardized management of hepatocellular carcinoma (HCC) in many countries worldwide, as exemplified by guidelines implemented in Japan and South Korea. China accounts for 55% of HCC cases worldwide (3). However, such evidence-based CPGs have not yet to be drafted, hampering the standardized management of HCC in China.

In Japan, HCC management has achieved remarkable results that are attributed to a combination of quantitative and qualitative evaluations incorporated in the Japanese guidelines (4). Since the first Japanese evidence-based CPGs for HCC (J-HCC Guidelines) were published in 2005, the CPGs have been included a process of systematic evaluation in accordance with evidence-based medicine (EBM) (5,6). Updated J-HCC Guidelines incorporating new evidence were published in 2009 (7), and the third version of J-HCC Guidelines (2013 version) were just published on October 15, 2013 (8). The systematic J-HCC Guidelines should further

\*Address correspondence to:

Dr. Peipei Song, Hepato-Biliary-Pancreatic Surgery Division, Department of Surgery, Graduate School of Medicine, The University of Tokyo, 7-3-1 Hongo, Bunkyo-ku, Tokyo 113-8655, Japan.  
E-mail: ppsong-tky@umin.ac.jp

promote the standardized management of HCC in Japan.

To draft the 2013 version of J-HCC Guidelines, literature consisting of 6,750 papers was systematically reviewed to obtain the best current evidence. After a second round of review, 596 articles were ultimately selected to form 57 pairs of clinical questions and recommendations with different levels of evidence to guide clinical decision-making. A multi-disciplinary expert panel consisting of surgeons, internists, radiologists, statisticians, and health care economists supervised their individual specialties. The guidelines cover aspects including prevention, diagnosis and surveillance, surgery, local treatment, transcatheter arterial chemoembolization (TACE), chemotherapy, radiotherapy, follow-up, prevention and treatment of recurrence. The guidelines also take the Japanese health insurance system into account to make surveillance, diagnosis, and treatment of HCC feasible. In order to adequately reflect disparate views, an internal evaluation and an external evaluation were conducted prior to publication and then the draft guidelines were modified. Moreover, plans are to revise the current guideline yet again. An updated vision of the J-HCC Guidelines will be published in the coming 3-4 years and incorporate new evidence (8).

In China, HCC is the second most common cancer in urban areas and the most common in rural areas; it ranks as the second leading cause of cancer-related deaths in males, with a total mortality rate of 26.26/100,000 (9,10). Over the past decades, the Government has devised a series of directives on the management of HCC in order to reduce incidence and mortality and to improve healthcare quality overall for patients. For instance, "Treatment Standards for Common Malignant Tumors in China (Vol. 2, Hepatocellular Carcinoma)" was published in 1989, "Guiding Principles for Clinical Research on Treatment of Hepatocellular Carcinoma Involving New Drugs/Traditional Chinese Medicines" was published in 1990, and "Choices for Hepatocellular Carcinoma Treatment Therapies" was published in 2000. However, none of these directives was based on a systematic review and evaluation of the literature. Cognizant of the concept of "standardized management of care", the Chinese Guidelines on HCC — Expert Consensus on the Treatment Standards for Hepatic Carcinoma — was published in 2009 (11). However, the guidelines were based on expert consensus, so they provided recommendations regarding the management of HCC based on the experience of those experts instead of recommendations supported by data provided by a systematic review and evaluation of the literature (12).

Fortunately, a high level of liver surgery is currently practiced at leading medical facilities in China (13). A team in Beijing led by Dr. Jiahong Dong put forth the novel concept of "precision surgery". This concept

represents a new surgical paradigm that includes preoperative evaluation, clinical decision-making, surgical planning, surgical technique, and perioperative management, and this concept should encourage the standardized management of HCC in China (14). "Precision surgery" involves certainty-based practices to ensure the best result for each patient with multi-objective optimization of therapeutic effectiveness, surgical safety, and minimal invasiveness. However, this paradigm is based on the clinical experience of surgeons who perform over 700 hepatic resections each year. Recommendations supported by data are still urgently needed to guide clinical decision-making.

In conclusion, the practice of systematic evidence-based CPGs in Japan provides a good example of standardized management of HCC. Such guidelines need to be promptly drafted in China through systematic review and evaluation of the literature by a multi-disciplinary expert panel in order to provide recommendations supported by data to guide clinical decision-making.

## References

1. Gao JJ, Song PP, Tamura S, Hasegawa K, Sugawara Y, Kokudo N, Uchida K, Orii R, Qi FH, Dong JH, Tang W. Standardization of perioperative management on hepatobiliary-pancreatic surgery. *Drug Discov Ther.* 2012; 6:108-111.
2. Song PP, Gao JJ, Kokudo N, Tang W. New opportunity for orphan drug development in Japan: Early exploratory clinical trial bases promote drug translation from basic studies to clinical application. *Intractable Rare Dis Res.* 2012; 1:95-97.
3. International Agency for Research on Cancer. Cancer incidence and mortality worldwide in 2008 (GLOBOCAN 2008). <http://globocan.iarc.fr/factsheets/cancers/liver.asp> (accessed October 16, 2013)
4. Song PP, Tang W, Tamura S, Hasegawa K, Sugawara Y, Dong J, Kokudo N. The management of hepatocellular carcinoma in Asia: A guideline combining quantitative and qualitative evaluation. *Biosci Trends.* 2010; 4:283-287.
5. Makuuchi M, Kokudo N, Arii S, Futagawa S, Kaneko S, Kawasaki S, Matsuyama Y, Okazaki M, Okita K, Omata M, Saida Y, Takayama T, Yamaoka Y. Development of evidence-based clinical guidelines for the diagnosis and treatment of hepatocellular carcinoma in Japan. *Hepatol Res.* 2008; 38:37-51.
6. Song PP, Tobe RG, Inagaki Y, Kokudo N, Hasegawa K, Sugawara Y, Tang W. The management of hepatocellular carcinoma around the world: A comparison of guidelines from 2001 to 2011. *Liver Int.* 2012; 32:1053-1063.
7. Makuuchi M, Kokudo N. Clinical practice guidelines for hepatocellular carcinoma – The Japan Society of Hepatology 2009 update. *Hepatol Res.* 2010; 40(Suppl. 1):2-144.
8. Japan Society of Hepatology. Clinical practice guidelines for hepatocellular carcinoma (2013 version). Kanehara, Tokyo, Japan, 2013. (in Japanese)
9. Song P, Feng X, Zhang K, Song T, Ma K, Kokudo

- N, Dong J, Tang W. Perspectives on using des- $\gamma$ -carboxyprothrombin (DCP) as a serum biomarker: Facilitating early detection of hepatocellular carcinoma in China. *Hepatobiliary Surg Nutr.* 2013; 2: 227-231.
10. Song P, Feng X, Zhang K, Song T, Ma K, Kokudo N, Dong J, Yao L, Tang W. Screening for and surveillance of high-risk patients with HBV-related chronic liver disease: Promoting the early detection of hepatocellular carcinoma in China. *BioScience Trends.* 2013; 7:1-6.
  11. Chinese HCC Chinese Anti-Cancer Association Society of Liver Cancer, Chinese Society of Clinical Oncology, Chinese Society of Hepatology Liver Cancer Study Group. The expert consensus on the treatment standards for hepatocellular carcinoma. *Digestive Disease and Endoscopy.* 2009; 3:40-51. (in Chinese)
  12. Song PP, Gao JJ, Kokudo N, Dong JH, Tang W. "Knowledge into action" Exploration of an appropriate approach for constructing evidence-based clinical practice guidelines for hepatocellular carcinoma. *Biosci Trends.* 2012; 6:147-152.
  13. Emond JC, Kluger MD. International perspectives on advanced liver surgery. *Semin Liver Dis.* 2013; 33:187-188.
  14. Dong J, Yang S, Zeng J, *et al.* Precision in liver surgery. *Semin Liver Dis.* 2013; 33:189-203.

(Received October 19, 2013; Accepted October 26, 2013)

## Complementary and alternative medicine is expected to make greater contribution in controlling the prevalence of influenza

Zhengang Tao<sup>1</sup>, Yuxiu Yang<sup>2</sup>, Wenna Shi<sup>3</sup>, Mingming Xue<sup>1</sup>, Weiqiang Yang<sup>5</sup>, Zhenju Song<sup>1</sup>, Chenling Yao<sup>1</sup>, Jun Yin<sup>1</sup>, Dongwei Shi<sup>1</sup>, Yaping Zhang<sup>1</sup>, Yingyun Cai<sup>4</sup>, Chaoyang Tong<sup>1</sup>, Ying Yuan<sup>4,\*</sup>

<sup>1</sup> Emergency Department of Zhongshan Hospital, Fudan University, Shanghai, China;

<sup>2</sup> The Special Care Division, Liaocheng People's Hospital, Liaocheng, Shandong, China;

<sup>3</sup> Department of Pharmacy, Shandong Tumor Hospital, Ji'nan, Shandong, China;

<sup>4</sup> Geriatrics Department of Zhongshan Hospital, Fudan University, Shanghai, China;

<sup>5</sup> Emergency Department of Renji Hospital, Shanghai Jiaotong University, Shanghai, China.

### Summary

Influenza pandemics are a serious threat to public health in today's world. In the past 10 years, the outbreak of three forms of severe influenza – H5N1, H1N1, and H7N9 – has caused tremendous loss of life and property. In order to better cope with pandemics, antivirals such as oseltamivir are being stockpiled in great quantities, placing a substantial burden on government budgets and potentially resulting in massive waste because of the uncertainty as to when an influenza pandemic will strike and whether emerging virus strains will be resistant to the stockpiled drugs. Complementary and alternative medicine (CAM) is generally available, affordable, and commonly used in China and many other countries and CAM has a long track record of fighting influenza. The Chinese Government appropriated funds to intensively investigate herbal medicines in accordance with the principles of evidence-based medicine in order to identify effective, inexpensive, and easily stockpiled medicines. Thus far, several drugs including Shufeng Jiedu capsules, Lianhua Qingwen capsules, Maxing Shigan decoction, Yinqiao powder, and Jinhua Qinggan granules have demonstrated effectiveness in fighting influenza. In the future, CAM is expected to make greater contribution in controlling the prevalence of influenza pandemics.

**Keywords:** Complementary and alternative medicine (CAM), influenza, H5N1, H1N1, H7N9

Influenza virus infection is a serious public health problem because of its significant mortality in humans. As an example, pandemic human influenza A (H1N1) caused 18,449 laboratory-confirmed deaths worldwide in one and a half years from early April 2009, when the first case of infection appeared, to August 2010, when the end of the pandemic was announced (1,2). Due to the great adaptability and ready variation of the influenza virus, frequent outbreaks of highly pathogenic avian influenza H5N1 and H7N9 during the past 10 years sounded the alarm regarding the pressing need to control human influenza pandemics in the near future.

\*Address correspondence to:

Dr. Ying Yuan, Geriatrics Department of Zhongshan Hospital, Fudan University, Shanghai, China.

E-mail: yuan.ying@zs-hospital.sh.cn

Currently, neuraminidase inhibitors including zanamivir, oseltamivir, laninamivir, and peramivir are widely used clinically to treat influenza. In order to efficiently deal with possible influenza pandemics, the World Health Organization (WHO) implemented regulations on antiviral stockpiles (1). As a result of this policy, the drug oseltamivir was promptly delivered to affected countries and regions, where it played an important role in controlling the prevalence of H1N1. However, large antiviral stockpiles require substantial expenditures because of the expense of antiviral drugs, potentially imposing a massive economic burden on less developed countries. In addition, when an influenza outbreak occurs is uncertain, so stockpiled drugs may lose their effectiveness, thus causing massive waste. Most importantly, evidence shows that clinical isolates of viruses are rapidly becoming more resistant to

neuraminidase inhibitors currently in use (3,4). These factors necessitate the development of effective, easily accessible, and inexpensive anti-influenza regimens.

Complementary and alternative medicine (CAM) is characterized by unique concepts that differ from those of Western medicine. Around the world, traditional medicines are generally available, affordable, and commonly used in large parts of Asia, Africa, and Latin America (5). Traditional Chinese medicine (TCM) is a typical CAM that has been widely used in China for thousands of years and TCM has a long record of treating influenza (6). After the H1N1 outbreak in China in 2009, the Beijing Municipal Government allocated a special fund of 10 million RMB to launch one preclinical study and one clinical trial, *i.e.* a "Study to Screen and Evaluate Effective Traditional Chinese Medicines to Prevent and Treat H1N1 Influenza" and a "Prospective Multicenter Randomized Controlled Trial of TCM to Prevent and Treat H1N1 Influenza" (7). Based on the characteristics and advantages of TCM and the principles of evidence-based medicine, the study and trial seek to discover safe, effective, inexpensive, and easily stockpiled traditional Chinese medicines and develop corresponding therapeutic regimens (7). Researchers screened approximately 40 traditional Chinese medicines that were previously used to treat the common cold, flu, severe acute respiratory syndrome (SARS), and avian influenza to identify potential drugs to fight H1N1 virus infection. Thus far, several drugs including Shufeng Jiedu capsules (SFJDC), Lianhua Qingwen capsules (LHQWC), Maxing Shigan decoction (MXSGD), Yinqiao powder (YQP), and Jinhua Qinggan granules (JHQGG) have been found to possess potent action against influenza (Table 1).

SFJDC is usually used to treat patients with an acute upper respiratory infection and symptoms of fever, sore throat, headaches, runny nose, and coughing. SFJDC's efficacy against the H1N1 virus has been investigated in both normal and immunocompromised mice (8). Models of pneumonia were created by giving those mice nasal drops containing H1N1 virus strain FM1 or PR8. In normal mice with pneumonia, treatment with SFJDC for 4 days markedly reduced the viral load and increased the level of interferon  $\gamma$  in the lung tissue. In immunocompromised mice with pneumonia, treatment with SFJDC significantly decreased the mortality of mice infected with the FM1 strain and increased the survival time for mice infected with the PR8 strain. In addition, the viral load and lung index both dramatically decreased in mice treated with SFJDC. These findings suggest that SFJDC may have the potential to clinically treat H1N1 virus infection. In a subsequent clinical study of 130 patients with an acute viral upper respiratory tract infection (43 patients with H1N1 infection) at Jiangsu Provincial Hospital of TCM (Nanjing, Jiangsu Province), Nanjing Hospital of TCM (Nanjing, Jiangsu Province), Hebei Provincial Hospital of TCM (Shijiazhuang, Hebei Province), The Second Hospital of Nanjing (Nanjing, Jiangsu Province), and the People's Hospital of Maizhokunggar County (Lhasa, Tibet Autonomous Region), administration of SFJDC caused fever to abate within 4 h in 39 patients (30.0%) and within 72 h in 118 patients (90.8%) (9). This medicine caused fever to abate in an average time of 20.5 h. A point of note is that body temperature started to drop in 30% of patients 4 h after the medicine was administered, suggesting that SFJDC usually has rapid and effective antipyretic action (9). Currently,

**Table 1. Traditional Chinese medicines to treat influenza**

Drug	Indication	Formulation
Shufeng Jiedu capsule	Acute upper respiratory infection (wind-heat cold)	Rhizoma Et Radix Polygoni Cuspidati; Fructus Forsythiae; Radix Isatidis; Radix Bupleuri; Herba Berberae; Rhizoma Phragmitis; Radix Et Rhizoma Glycyrrhizae
Lianhua Qingwen capsule	Influenza with symptoms including fever, aversion to cold, muscular soreness, nasal congestion, runny nose, cough, headache, <i>etc.</i>	Fructus Forsythiae; Flos Lonicerae Japonicae; Herba Ephedrae; Semen Armeniacae Amarum; Gypsum Fibrosum; Radix Isatidis; Rhizoma Dryopteridis Crassirhizomatis; Herba Houptuyniae; Herba Pogostemonis; Radix Et Rhizoma Rhei; Radix Et Rhizoma Rhodiolae Crenulatae; Mentholum; Radix Et Rhizoma Glycyrrhizae
Maxing Shigan decoction	Pneumonia, chronic bronchitis, bronchial asthma	Herba Ephedrae; Semen Armeniacae Amarum; Gypsum Fibrosum; Radix Et Rhizoma Glycyrrhizae
Yinqiao powder	Anemopyretic cold with symptoms including fever, headache, cough, sore throat, scanty dark urine	Flos Lonicerae Japonicae; Fructus Forsythiae; Radix Platycodonis; Radix Et Rhizoma Glycyrrhizae; Spica Schizonepetae; Semen Sojae Praeparatum; Fructus Arctii; Rhizoma Phragmitis
Jinhua Qinggan granule	Influenza with symptoms including pharyngalgia, nasal congestion, runny nose, cough, <i>etc.</i>	Flos Lonicerae Japonicae; Gypsum Fibrosum; Herba Ephedrae; Semen Armeniacae Amarum; Radix Scutellariae; Fructus Forsythiae; Bulbus Fritillariae Thunbergii; Rhizoma Anemarrhenae; Fructus Arctii; Herba Artemisiae Annuae; Mentholum; Radix Et Rhizoma Glycyrrhizae

Information is from corresponding drug labels.

the Guidelines for Diagnosis and Treatment of H1N1 Infection issued by the Chinese Ministry of Health (MOH) recommend SFJDC as a treatment for H1N1 virus infection.

LHQWC is used to treat influenza in individuals with symptoms of a fever, muscle soreness, nasal congestion, runny nose, coughing, headaches, *etc.* The effects of this medicine in treating H1N1 infection were reported at the International Scientific Symposium on Influenza A (H1N1) Pandemic Response and Preparedness held by the Chinese MOH, the WHO, and the journal *Lancet* on August 21, 2009 (10,11). Studies by the Academy of Military Medical Sciences and Beijing Ditan Hospital found that LHQWC markedly suppresses the H1N1 virus (11). The results of those studies indicated that LHQWC is comparable to oseltamivir in clearing the H1N1 virus from the blood of patients. However, fever abated significantly sooner in patients treated with LHQWC compared to those treated with oseltamivir. Moreover, treatment with LHQWC cost just one-eighth of treatment with oseltamivir. These advantages of LHQWC indicate that this medicine may have great promise in controlling the prevalence of influenza pandemics.

MXSGD and YQP are traditionally used to treat febrile infectious diseases in China. Studies directed by Beijing Chao-Yang Hospital investigated the efficacy of these two traditional Chinese medicines in the treatment of H1N1 influenza infection (12). The study of 410 adult patients with mild symptoms sought to examine the fever-reducing action of MXSGD and YQP. Results indicated that the control group had a fever for 26 h, patients treated with oseltamivir had a fever for 20 h, patients treated with TCM had a fever for 16 h, and patients treated with oseltamivir plus TCM had a fever for 15 h. Thus, MXSGD and YQP were able to effectively shorten the duration of fever in patients with H1N1 influenza infection. These two medicines had efficacy that was comparable or slightly superior to that of oseltamivir. In order to develop more effective drugs to fight H1N1 virus infection, experts in TCM developed JHQGG based on the formulations for MXSGD and YQP (13). In one preclinical study, JHQGG was found to possess potent action at decreasing mortality, increasing surviving time, and reducing the severity of pulmonary lesions in mice infected with the H1N1 virus (13). In another study, JHQGG was able to reduce fever in a rabbit model of fever (13). A clinical study showed that JHQGG markedly reduced the duration of fever and alleviated symptoms in patients with H1N1 influenza infection (13). Thus far, JHQGG has been approved and used to treat influenza in hospitals. The cost for a course of treatment (5-7 days) is approximately 80-110 RMB, which is one-fourth of the cost of oseltamivir, thus significantly reducing the economic burden for patients (13).

The results cited thus far indicate that TCM could be an option in situations where neuraminidase inhibitors such as oseltamivir are in insufficient quantity or strains of influenza are resistant to those drugs. Of 845 patients infected with H1N1 influenza who admitted to hospitals in Beijing by September 1, 2009, 326 were cured by TCM alone (14). Given the potential efficacy of TCM, the Beijing Government allocated 70 million RMB to stockpile 2 million doses of TCM to prevent a possible influenza pandemic (14). This revision of the policy on drug stockpiling means that more types of drugs are available and a greater number of people benefit.

The outbreak of H7N9 avian influenza in China in 2013 caused public alarm about a new influenza pandemic. By August 31, 2013, a total of 134 confirmed cases had been reported in mainland China; 45 of the patients died while 86 recovered (15). Laboratory testing showed that the virus is sensitive to the neuraminidase inhibitors oseltamivir and zanamivir. In addition, the MOH's Guidelines for Diagnosis and Treatment of H7N9 Infection recommend SFJDC and LHQWC to cope with symptoms like a high fever, coughing, and chest tightness induced by H7N9 infection. Although no evidence to date has indicated that the virus has increased transmissibility or is spreading from person to person, cross-over of genes between the avian and human influenza viruses may result in a more dangerous form of the flu in the future.

Clearly, potent antivirals should be developed, but the potential of CAM to deal with the challenge of influenza pandemics should also be closely investigated. Compared to antivirals, these medicines offer various advantages such as their low cost, accessibility, and the ease with which they can be stockpiled. In instances where influenza has developed resistance to drugs or those drugs cause serious adverse reactions, CAM could help to treat patients. In this sense, CAM is expected to make greater contribution in controlling the prevalence of influenza in the future.

## References

1. Mei L, Song P, Tang Q, Shan K, Tobe RG, Selotlegeng L, Ali AH, Cheng Y, Xu L. Changes in and shortcomings of control strategies, drug stockpiles, and vaccine development during outbreaks of avian influenza A H5N1, H1N1, and H7N9 among humans. *Biosci Trends*. 2013; 7:64-76.
2. Mei L, Tang Q, Cui YM, Tobe RG, Selotlegeng L, Ali AH, Xu LZ. Changes in and shortcomings of drug stockpiling, vaccine development and related policies during outbreaks of avian influenza A H5N1, H1N1, and H7N9 among humans. *Drug Discov Ther*. 2013; 7:95-100.
3. Hayden FG. Antiviral resistance in influenza viruses – implications for management and pandemic response. *N Engl J Med*. 2006; 354:785-788.
4. Watanabe K, Takatsuki H, Sonoda M, Tamura S, Murakami N, Kobayashi N. Anti-influenza viral effects of novel nuclear export inhibitors from *Valeriana Radix* and *Alpinia galanga*. *Drug Discov Ther*. 2011; 5:26-31.

5. World Health Organization (WHO). <http://www.who.int/dg/speeches/2008/20081107/en/index.html> (accessed August 21, 2013).
6. Lu CH, Li YY, Li LJ, Liang LY, Shen YM. Anti-inflammatory activities of fractions from Geranium nepalense and related polyphenols. *Drug Discov Ther.* 2012; 6:194-197.
7. News. [http://www.dss.gov.cn/Article\\_Print.asp?ArticleID=304368](http://www.dss.gov.cn/Article_Print.asp?ArticleID=304368) (accessed September 1, 2013).
8. Liu Y, Shi H, Jin YH, Gao YJ, Shi YJ, Liu FZ, Guo SS, Cui XL. Experimental pharmacodynamic research in vivo of Shufengjiedu capsule on treatment and prevention of influenza. *World Journal of Integrated Traditional and Western Medicine.* 2010; 5:107-110.
9. Xi ZQ, Zhou JZ, Mei JQ, Tan SZ, Ge AQ, Zheng Y, Chen FQ, Zhao QF, Geng LY, Shao M, Zhang L. Effect of Shufengjiedu capsule on the fever caused by viral upper respiratory tract infection: A report of 130 cases. *J Tradit Chin Med.* 2010; 51:426-427.
10. News. <http://politics.people.com.cn/GB/1024/9908770.html> (accessed October 10, 2013).
11. News. <http://www.chinanews.com/jk/jk-hyxw/news/2009/08-21/1829479.shtml> (accessed September 21, 2013).
12. Wang C, Cao B, Liu QQ, *et al.* Oseltamivir compared with the Chinese traditional therapy maxingshigan-yinqiaosan in the treatment of H1N1 influenza: A randomized trial. *Ann Intern Med.* 2011; 155:217-225.
13. Yan D. Treatment of influenza A (H1N1) by traditional Chinese medicine Jinhuaqinggan formulation. *Jia Ting Zhong Yi Yao.* 2010; 1:26-28.
14. News. <http://medicine.people.com.cn/GB/10068962.html> (accessed October 10, 2013).
15. News. [http://www.chinacdc.cn/tjsj/fdcrbbg/201309/t20130911\\_88023.htm](http://www.chinacdc.cn/tjsj/fdcrbbg/201309/t20130911_88023.htm) (accessed October 12, 2013).

(Received September 21, 2013; Revised October 22, 2013; Accepted October 25, 2013)

## Combat with emerging infectious diseases: Clinicians should do better

Hongzhou Lu<sup>1,2,3,\*</sup>

<sup>1</sup> Department of Infectious Disease, Shanghai Public Health Clinical Center affiliated to Fudan University, Shanghai, China;

<sup>2</sup> Department of Infectious Disease, Huashan Hospital affiliated to Fudan University, Shanghai, China;

<sup>3</sup> Department of Internal Medicine, Shanghai Medical College, Fudan University, Shanghai, China.

**Keywords:** Infectious diseases, avian influenza, genomics, pathogen

**Summary:** In the spring of 2013, an emerging infectious disease emerged in China, 132 cases of human were infected with the H7N9 avian influenza virus, 39 cases were resulted in death within 3 month, which sparked a global concern about public health. Many reports have been published about this disease, including clinical characteristics and genomic information. However, more emerging infectious disease may infect human in the future. Confronted with the escalating scale of compounding probabilities, physicians or clinicians as the first line that meet patients who suffering from emerging infectious disease, we should do better by using our intellect and strong will to carry out public health measures, biomedical research, and technological advances.

Globally, infectious diseases are the second leading cause of death (following cardiovascular disease), but the leading cause of mortality among young people (under the age of 50) overwhelmingly (1). According to the World Health Organization, infectious diseases accounted for about 26% of the 57 million deaths worldwide (2).

Emerging infectious diseases (EIDs) are infectious disease whose incidence has increased in the past 35 years and may increase in the near future which account for about 12% of all human pathogens (3). EIDs are caused by newly identified species or strains that may have evolved from a known infection (e.g. influenza) or spread to a new population or areas undergoing ecologic transformation, or reemerging. Of growing concern are adverse synergistic interactions between

emerging diseases and other communicable and non-communicable conditions leading to the development of novel epidemics. A criterion was given by the U.S. Centers for Disease Control and Prevention (CDC) that identifies the following factors contributing to disease emergence: microbial adaption, changes in human susceptibility, etc.

From March 31 to May 31, 2013, 132 cases of human were infected with the H7N9 avian influenza virus in China, 39 cases were resulted in death, which sparked global concerns about public health (4,5), and many reports have been published. As a clinician in front line to combat with H7N9 infection in Shanghai, our research group has also published some papers about this emerging infectious disease, especially about its clinical characteristic (6). Now I would like to illustrate some of the lessons we have learned as we combat the emerging infectious disease – the avian influenza H7N9 – with the purpose of providing references for other clinicians and researchers to face crisis that will continue to haunt mankind in the future.

On February 26, 2013, I was invited to go to the Fifth People's Hospital, Min-hang District, Shanghai, affiliated to Fudan University and took part in a clinical consultation. Three members of a family, the father and his two sons were suffering from severe pneumonia and had been hospitalized, one of which was on the verge of death. The onset of unknown disease in this family was located between February 11 and February 20, 2013. High fever and severe pneumonia developed 1 week after the onset of illness, of which interstitial lung disease was considered initially. Multiple organ failure appeared 7-9 days later, with low white blood cells and dramatically decreased in platelets. He had no known history of exposure to live birds during the 2 weeks before the onset of symptoms. Sputum and sera from patients were sent to district CDC, Shanghai for identification of common subtypes of influenza virus,

\*Address correspondence to:

Dr. Hongzhou Lu, Department of Infectious Disease, Shanghai Public Health Clinical Center affiliated to Fudan University, Shanghai 201508, China.  
E-mail: luhongzhou@fudan.edu.cn

chlamydia, mycoplasma and bacteria which had been confirmed negative later on. Based upon these typical manifestations, infectious viral pneumonia was taken into my consideration. So I decided to use anti-viral drug, Oseltamivir, immediately, the dosage would be as twice as normal. Meanwhile, as I asked, all specimens had been sent to our lab, Shanghai Public Health Clinical Center affiliated to Fudan University in which P3 laboratory was available. After real-time RT-PCR test, viral isolation, and full genome sequencing, two of the three patients were infected with a novel avian-origin influenza A (H7N9) virus (7), and the results have been confirmed by China CDC.

As we all know, multiple factors, including economic development, climate changes and land use, human demographics and behavior, and international travel and commercial activities, contribute to the emergence and reemergence of infectious diseases (8,9). As basic or laboratory scientists know, genomics has played a critical role in basic research in infectious diseases. Nowadays, an unknown pathogen can often be identified and sequenced within days. The ability to sequence microbes has taken its place at the forefront of how we handle with emerging infections. Fundamental research underlies almost everything we do in studying and responding to infectious diseases. From understanding pathogenesis, virulence factors, patterns of transmission, and host susceptibility, to developing new technologies and countermeasures such as vaccines, therapeutic measures, and diagnostics.

However, physicians or clinicians are the first line that can meet patients who suffering from unidentified disease. We will never forget the epidemic of severe acute respiratory syndrome (SARS), for which it costed a very heavy and painful price 10 years ago (10), including reported clinician's victims (11,12). Over the past few years, more influenza strains have emerged with the capability of infecting humans (13,14) and more emerging infectious disease will infected in the future. The H5N1 strain likely evolved from a few flocks of chickens in Hong Kong to the situation today where it has infected numerous flocks, as well as wild birds throughout Southeast Asia (15). Now we are confronted with what I call an escalating scale of compounding probabilities. If a few birds are infected, there is a problem, but not a big one. When more birds get infected, the problem will get bigger. When the virus is transmitted to humans, the problem is getting even worse. If it jumps to significant numbers of humans, the threat becomes a lethal one.

In our battle with emerging infectious diseases, we have a number of weapons in our armamentarium. Most important, we have an intellect and a strong will. We use these to carry out public health measures,

biomedical research, and technological advances. I was proud to do it instead of being asked to do this, because a clinician can do better.

## References

1. Fauci AS. Emerging and reemerging infectious diseases: The perpetual challenge. *Acad Med.* 2005; 80:1079-1085.
2. Many countries hit by health threats from both infectious and chronic diseases new data site makes WHO data and analyses widely available. *Cent Eur J Public Health.* 2011; 19:72.
3. Del Rey Calero J. Emerging and reemerging infectious diseases. *An Med Interna.* 2002; 19:443-445.
4. Song PP, Xia JF, Gao JJ, Xu LZ, Huang Y, Yao LN, Tang W. Measures to combat H7N9 virus infection in China: Live poultry purchasing habits, poultry handling, and living conditions increase the risk of exposure to contaminated environments. *Biosci Trends.* 2013; 7:168-171.
5. Mei L, Song P, Tang Q, Shan K, Tobe RG, Selotlegeng L, Ali AH, Cheng Y, Xu L. Changes in and shortcomings of control strategies, drug stockpiles, and vaccine development during outbreaks of avian influenza A H5N1, H1N1, and H7N9 among humans. *Biosci Trends.* 2013; 7:64-76.
6. Lu S, Xi X, Zheng Y, Cao Y, Liu X, Lu H. Analysis of the clinical characteristics and treatment of two patients with avian influenza virus (H7N9). *Biosci Trends.* 2013; 7:109-112.
7. Gao R, Cao B, Hu Y, *et al.* Human infection with a novel avian-origin influenza A (H7N9) virus. *N Engl J Med.* 2013; 368:1888-1897.
8. Weiss RA, McMichael AJ. Social and environmental risk factors in the emergence of infectious diseases. *Nat Med.* 2004; 10:S70-S76.
9. Church DL. Major factors affecting the emergence and re-emergence of infectious diseases. *Clin Lab Med.* 2004; 24:559-586, v.
10. From SARS to H7N9: Will history repeat itself? *Lancet.* 2013; 381:1333.
11. Penciner R. I am a SARS physician. *CJEM.* 2003; 5:281-282.
12. Wu EB, Sung JJ. Haemorrhagic-fever-like changes and normal chest radiograph in a doctor with SARS. *Lancet.* 2003; 361:1520-1521.
13. Lu S, Zheng Y, Li T, Hu Y, Liu X, Xi X, Chen Q, Wang Q, Cao Y, Wang Y, Zhou L, Lowrie D, Bao J. Clinical findings for early human cases of influenza A(H7N9) virus infection, Shanghai, China. *Emerg Infect Dis.* 2013; 19:1142-1146.
14. Gao HN, Lu HZ, Cao B, *et al.* Clinical findings in 111 cases of influenza A (H7N9) virus infection. *N Engl J Med.* 2013; 368:2277-2285.
15. World Health Organization. Avian influenza in humans. [http://www.who.int/influenza/human\\_animal\\_interface/avian\\_influenza/en/](http://www.who.int/influenza/human_animal_interface/avian_influenza/en/) (accessed on September 9, 2013)

(Received September 19, 2013; Revised October 1, 2013; Accepted October 3, 2013)

### Guide for Authors

#### 1. Scope of Articles

BioScience Trends is an international peer-reviewed journal. BioScience Trends devotes to publishing the latest and most exciting advances in scientific research. Articles cover fields of life science such as biochemistry, molecular biology, clinical research, public health, medical care system, and social science in order to encourage cooperation and exchange among scientists and clinical researchers.

#### 2. Submission Types

**Original Articles** should be well-documented, novel, and significant to the field as a whole. An Original Article should be arranged into the following sections: Title page, Abstract, Introduction, Materials and Methods, Results, Discussion, Acknowledgments, and References. Original articles should not exceed 5,000 words in length (excluding references) and should be limited to a maximum of 50 references. Articles may contain a maximum of 10 figures and/or tables.

**Brief Reports** definitively documenting either experimental results or informative clinical observations will be considered for publication in this category. Brief Reports are not intended for publication of incomplete or preliminary findings. Brief Reports should not exceed 3,000 words in length (excluding references) and should be limited to a maximum of 4 figures and/or tables and 30 references. A Brief Report contains the same sections as an Original Article, but the Results and Discussion sections should be combined.

**Reviews** should present a full and up-to-date account of recent developments within an area of research. Normally, reviews should not exceed 8,000 words in length (excluding references) and should be limited to a maximum of 100 references. Mini reviews are also accepted.

**Policy Forum** articles discuss research and policy issues in areas related to life science such as public health, the medical care system, and social science and may address governmental issues at district, national, and international levels of discourse. Policy Forum articles should not exceed 2,000 words in length (excluding references).

**Case Reports** should be detailed reports of the symptoms, signs, diagnosis, treatment, and follow-up of an individual patient. Case reports may contain a demographic profile of the patient but usually describe an unusual or novel occurrence. Unreported or unusual

side effects or adverse interactions involving medications will also be considered. Case Reports should not exceed 3,000 words in length (excluding references).

**News** articles should report the latest events in health sciences and medical research from around the world. News should not exceed 500 words in length.

**Letters** should present considered opinions in response to articles published in BioScience Trends in the last 6 months or issues of general interest. Letters should not exceed 800 words in length and may contain a maximum of 10 references.

#### 3. Editorial Policies

**Ethics:** BioScience Trends requires that authors of reports of investigations in humans or animals indicate that those studies were formally approved by a relevant ethics committee or review board.

**Conflict of Interest:** All authors are required to disclose any actual or potential conflict of interest including financial interests or relationships with other people or organizations that might raise questions of bias in the work reported. If no conflict of interest exists for each author, please state "There is no conflict of interest to disclose".

**Submission Declaration:** When a manuscript is considered for submission to BioScience Trends, the authors should confirm that 1) no part of this manuscript is currently under consideration for publication elsewhere; 2) this manuscript does not contain the same information in whole or in part as manuscripts that have been published, accepted, or are under review elsewhere, except in the form of an abstract, a letter to the editor, or part of a published lecture or academic thesis; 3) authorization for publication has been obtained from the authors' employer or institution; and 4) all contributing authors have agreed to submit this manuscript.

**Cover Letter:** The manuscript must be accompanied by a cover letter signed by the corresponding author on behalf of all authors. The letter should indicate the basic findings of the work and their significance. The letter should also include a statement affirming that all authors concur with the submission and that the material submitted for publication has not been published previously or is not under consideration for publication elsewhere. The cover letter should be submitted in PDF format. For example of Cover Letter, please visit <http://www.biosciencetrends.com/downcentre.php> (Download Centre).

**Copyright:** A signed JOURNAL PUBLISHING AGREEMENT (JPA) form must be provided by post, fax, or as a scanned file before acceptance of the article. Only forms with a hand-written signature are accepted. This copyright will ensure the widest possible dissemination of information. A form facilitating transfer of copyright can be downloaded by clicking the

appropriate link and can be returned to the e-mail address or fax number noted on the form (Please visit [Download Centre](#)). Please note that your manuscript will not proceed to the next step in publication until the JPA Form is received. In addition, if excerpts from other copyrighted works are included, the author(s) must obtain written permission from the copyright owners and credit the source(s) in the article.

**Suggested Reviewers:** A list of up to 3 reviewers who are qualified to assess the scientific merit of the study is welcomed. Reviewer information including names, affiliations, addresses, and e-mail should be provided at the same time the manuscript is submitted online. Please do not suggest reviewers with known conflicts of interest, including participants or anyone with a stake in the proposed research; anyone from the same institution; former students, advisors, or research collaborators (within the last three years); or close personal contacts. Please note that the Editor-in-Chief may accept one or more of the proposed reviewers or may request a review by other qualified persons.

**Language Editing:** Manuscripts prepared by authors whose native language is not English should have their work proofread by a native English speaker before submission. If not, this might delay the publication of your manuscript in BioScience Trends.

The Editing Support Organization can provide English proofreading, Japanese-English translation, and Chinese-English translation services to authors who want to publish in BioScience Trends and need assistance before submitting a manuscript. Authors can visit this organization directly at <http://www.iacmhr.com/iac-eso/support.php?lang=en>. IAC-ESO was established to facilitate manuscript preparation by researchers whose native language is not English and to help edit works intended for international academic journals.

#### 4. Manuscript Preparation

Manuscripts should be written in clear, grammatically correct English and submitted as a Microsoft Word file in a single-column format. Manuscripts must be paginated and typed in 12-point Times New Roman font with 24-point line spacing. Please do not embed figures in the text. Abbreviations should be used as little as possible and should be explained at first mention unless the term is a well-known abbreviation (e.g. DNA). Single words should not be abbreviated.

**Title Page:** The title page must include 1) the title of the paper (Please note the title should be short, informative, and contain the major key words); 2) full name(s) and affiliation(s) of the author(s), 3) abbreviated names of the author(s), 4) full name, mailing address, telephone/fax numbers, and e-mail address of the corresponding author; and 5) conflicts of interest (if you have an actual or potential conflict of interest to disclose, it must be included as a footnote on the title page of the manuscript; if no conflict of

interest exists for each author, please state "There is no conflict of interest to disclose"). Please visit [Download Centre](#) and refer to the title page of the manuscript sample.

**Abstract:** The abstract should briefly state the purpose of the study, methods, main findings, and conclusions. For article types including Original Article, Brief Report, Review, Policy Forum, and Case Report, a one-paragraph abstract consisting of no more than 250 words must be included in the manuscript. For News and Letters, a brief summary of main content in 150 words or fewer should be included in the manuscript. Abbreviations must be kept to a minimum and non-standard abbreviations explained in brackets at first mention. References should be avoided in the abstract. Key words or phrases that do not occur in the title should be included in the Abstract page.

**Introduction:** The introduction should be a concise statement of the basis for the study and its scientific context.

**Materials and Methods:** The description should be brief but with sufficient detail to enable others to reproduce the experiments. Procedures that have been published previously should not be described in detail but appropriate references should simply be cited. Only new and significant modifications of previously published procedures require complete description. Names of products and manufacturers with their locations (city and state/country) should be given and sources of animals and cell lines should always be indicated. All clinical investigations must have been conducted in accordance with Declaration of Helsinki principles. All human and animal studies must have been approved by the appropriate institutional review board(s) and a specific declaration of approval must be made within this section.

**Results:** The description of the experimental results should be succinct but in sufficient detail to allow the experiments to be analyzed and interpreted by an independent reader. If necessary, subheadings may be used for an orderly presentation. All figures and tables must be referred to in the text.

**Discussion:** The data should be interpreted concisely without repeating material already presented in the Results section. Speculation is permissible, but it must be well-founded, and discussion of the wider implications of the findings is encouraged. Conclusions derived from the study should be included in this section.

**Acknowledgments:** All funding sources should be credited in the Acknowledgments section. In addition, people who contributed to the work but who do not meet the criteria for authors should be listed along with their contributions.

**References:** References should be numbered in the order in which they appear in the text. Citing of unpublished results, personal communications, conference abstracts, and theses in the reference list is not recommended but these sources may be mentioned in the text. In the reference list,

cite the names of all authors when there are fifteen or fewer authors; if there are sixteen or more authors, list the first three followed by *et al.* Names of journals should be abbreviated in the style used in PubMed. Authors are responsible for the accuracy of the references. Examples are given below:

*Example 1* (Sample journal reference): Inagaki Y, Tang W, Zhang L, Du GH, Xu WF, Kokudo N. Novel aminopeptidase N (APN/CD13) inhibitor 24F can suppress invasion of hepatocellular carcinoma cells as well as angiogenesis. *Biosci Trends*. 2010; 4:56-60.

*Example 2* (Sample journal reference with more than 15 authors): Darby S, Hill D, Auvinen A, *et al.* Radon in homes and risk of lung cancer: Collaborative analysis of individual data from 13 European case-control studies. *BMJ*. 2005; 330:223.

*Example 3* (Sample book reference): Shalev AY. Post-traumatic stress disorder: diagnosis, history and life course. In: Post-traumatic Stress Disorder, Diagnosis, Management and Treatment (Nutt DJ, Davidson JR, Zohar J, eds.). Martin Dunitz, London, UK, 2000; pp. 1-15.

*Example 4* (Sample web page reference): Ministry of Health, Labour and Welfare of Japan. Dietary reference intakes for Japanese. <http://www.mhlw.go.jp/houdou/2004/11/h1122-2a.html> (accessed June 14, 2010).

**Tables:** All tables should be prepared in Microsoft Word or Excel and should be arranged at the end of the manuscript after the References section. Please note that tables should not be image format. All tables should have a concise title and should be numbered consecutively with Arabic numerals. If necessary, additional information should be given below the table.

**Figure Legend:** The figure legend should be typed on a separate page of the main manuscript and should include a short title and explanation. The legend should be concise but comprehensive and should be understood without referring to the text. Symbols used in figures must be explained.

**Figure Preparation:** All figures should be clear and cited in numerical order in the text. Figures must fit a one- or two-column format on the journal page: 8.3 cm (3.3 in.) wide for a single column, 17.3 cm (6.8 in.) wide for a double column; maximum height: 24.0 cm (9.5 in.). Please make sure that the symbols and numbers appeared in the figures should be clear. Please make sure that artwork files are in an acceptable format (TIFF or JPEG) at minimum resolution (600 dpi for illustrations, graphs, and annotated artwork, and 300 dpi for micrographs and photographs). Please provide all figures as separate files. Please note that low-resolution images are one of the leading causes of article resubmission and schedule delays. All color figures will be reproduced in full color in the online edition of the journal at no cost to authors.

**Units and Symbols:** Units and symbols

conforming to the International System of Units (SI) should be used for physicochemical quantities. Solidus notation (*e.g.* mg/kg, mg/mL, mol/mm<sup>2</sup>/min) should be used. Please refer to the SI Guide [www.bipm.org/en/si/](http://www.bipm.org/en/si/) for standard units.

**Supplemental data:** Supplemental data might be useful for supporting and enhancing your scientific research and BioScience Trends accepts the submission of these materials which will be only published online alongside the electronic version of your article. Supplemental files (figures, tables, and other text materials) should be prepared according to the above guidelines, numbered in Arabic numerals (*e.g.*, Figure S1, Figure S2, and Table S1, Table S2) and referred to in the text. All figures and tables should have titles and legends. All figure legends, tables and supplemental text materials should be placed at the end of the paper. Please note all of these supplemental data should be provided at the time of initial submission and note that the editors reserve the right to limit the size and length of Supplemental Data.

## 5. Submission Checklist

The Submission Checklist will be useful during the final checking of a manuscript prior to sending it to BioScience Trends for review. Please visit [Download Centre](#) and download the Submission Checklist file.

## 6. Online Submission

Manuscripts should be submitted to BioScience Trends online at <http://www.biosciencetrends.com>. The manuscript file should be smaller than 5 MB in size. If for any reason you are unable to submit a file online, please contact the Editorial Office by e-mail at [office@biosciencetrends.com](mailto:office@biosciencetrends.com).

## 7. Accepted Manuscripts

**Proofs:** Galley proofs in PDF format will be sent to the corresponding author via e-mail. Corrections must be returned to the editor ([proof-editing@biosciencetrends.com](mailto:proof-editing@biosciencetrends.com)) within 3 working days.

**Offprints:** Authors will be provided with electronic offprints of their article. Paper offprints can be ordered at prices quoted on the order form that accompanies the proofs.

**Page Charge:** Page charges will be levied on all manuscripts accepted for publication in BioScience Trends (\$140 per page for black white pages; \$340 per page for color pages). Under exceptional circumstances, the author(s) may apply to the editorial office for a waiver of the publication charges at the time of submission.

(Revised February 2013)

## Editorial and Head Office:

Pearl City Koishikawa 603  
2-4-5 Kasuga, Bunkyo-ku  
Tokyo 112-0003 Japan  
Tel: +81-3-5840-8764  
Fax: +81-3-5840-8765  
E-mail: [office@biosciencetrends.com](mailto:office@biosciencetrends.com)

---

### JOURNAL PUBLISHING AGREEMENT (JPA)

---

**Manuscript No.:**

**Title:**

**Corresponding Author:**

---

The International Advancement Center for Medicine & Health Research Co., Ltd. (IACMHR Co., Ltd.) is pleased to accept the above article for publication in BioScience Trends. The International Research and Cooperation Association for Bio & Socio-Sciences Advancement (IRCA-BSSA) reserves all rights to the published article. Your written acceptance of this JOURNAL PUBLISHING AGREEMENT is required before the article can be published. Please read this form carefully and sign it if you agree to its terms. The signed JOURNAL PUBLISHING AGREEMENT should be sent to the BioScience Trends office (Pearl City Koishikawa 603, 2-4-5 Kasuga, Bunkyo-ku, Tokyo 112-0003, Japan; E-mail: [office@biosciencetrends.com](mailto:office@biosciencetrends.com); Tel: +81-3-5840-8764; Fax: +81-3-5840-8765).

#### 1. Authorship Criteria

As the corresponding author, I certify on behalf of all of the authors that:

- 1) The article is an original work and does not involve fraud, fabrication, or plagiarism.
- 2) The article has not been published previously and is not currently under consideration for publication elsewhere. If accepted by BioScience Trends, the article will not be submitted for publication to any other journal.
- 3) The article contains no libelous or other unlawful statements and does not contain any materials that infringes upon individual privacy or proprietary rights or any statutory copyright.
- 4) I have obtained written permission from copyright owners for any excerpts from copyrighted works that are included and have credited the sources in my article.
- 5) All authors have made significant contributions to the study including the conception and design of this work, the analysis of the data, and the writing of the manuscript.
- 6) All authors have reviewed this manuscript and take responsibility for its content and approve its publication.
- 7) I have informed all of the authors of the terms of this publishing agreement and I am signing on their behalf as their agent.

#### 2. Copyright Transfer Agreement

I hereby assign and transfer to IACMHR Co., Ltd. all exclusive rights of copyright ownership to the above work in the journal BioScience Trends, including but not limited to the right 1) to publish, republish, derivate, distribute, transmit, sell, and otherwise use the work and other related material worldwide, in whole or in part, in all languages, in electronic, printed, or any other forms of media now known or hereafter developed and the right 2) to authorize or license third parties to do any of the above.

I understand that these exclusive rights will become the property of IACMHR Co., Ltd., from the date the article is accepted for publication in the journal BioScience Trends. I also understand that IACMHR Co., Ltd. as a copyright owner has sole authority to license and permit reproductions of the article.

I understand that except for copyright, other proprietary rights related to the Work (e.g. patent or other rights to any process or procedure) shall be retained by the authors. To reproduce any text, figures, tables, or illustrations from this Work in future works of their own, the authors must obtain written permission from IACMHR Co., Ltd.; such permission cannot be unreasonably withheld by IACMHR Co., Ltd.

#### 3. Conflict of Interest Disclosure

I confirm that all funding sources supporting the work and all institutions or people who contributed to the work but who do not meet the criteria for authors are acknowledged. I also confirm that all commercial affiliations, stock ownership, equity interests, or patent-licensing arrangements that could be considered to pose a financial conflict of interest in connection with the article have been disclosed.

---

**Corresponding Author's Name (Signature):**

**Date:**



